

UNCLASSIFIED

AD NUMBER
AD444624
NEW LIMITATION CHANGE
TO Approved for public release, distribution unlimited
FROM Distribution authorized to U.S. Gov't. agencies and their contractors; Administrative/Operational Use; JUN 1964. Other requests shall be referred to Research and Technology Laboratory, Attn: AFWL, Kirtland AFB, NM.
AUTHORITY
CFSTI, per AFWL ltr, 18 May 1966

THIS PAGE IS UNCLASSIFIED

UNCLASSIFIED

AD 4 4 4 6 2 4

DEFENSE DOCUMENTATION CENTER

FOR

SCIENTIFIC AND TECHNICAL INFORMATION

CAMERON STATION, ALEXANDRIA, VIRGINIA



UNCLASSIFIED

NOTICE: When government or other drawings, specifications or other data are used for any purpose other than in connection with a definitely related government procurement operation, the U. S. Government thereby incurs no responsibility, nor any obligation whatsoever; and the fact that the Government may have formulated, furnished, or in any way supplied the said drawings, specifications, or other data is not to be regarded by implication or otherwise as in any manner licensing the holder or any other person or corporation, or conveying any rights or permission to manufacture, use or sell any patented invention that may in any way be related thereto.

**Best
Available
Copy**

444624

RTD TDR-63-3096, Vol I

RTD
TDR
63-3096
Vol I

DESIGN PROCEDURES FOR SHOCK ISOLATION SYSTEMS
OF UNDERGROUND PROTECTIVE STRUCTURES

Volume I

Structure Interior Motions Due to Air Blast Induced Ground Shock

Final Report

June 1964

TECHNICAL DOCUMENTARY REPORT NO. RTD TDR-63-3096, Vol I



Research and Technology Division
AIR FORCE WEAPONS LABORATORY
Air Force Systems Command
Kirtland Air Force Base
New Mexico

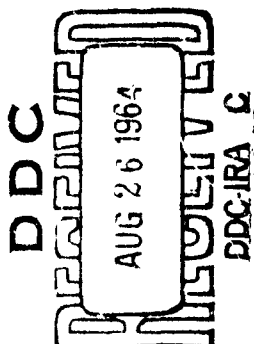
This research has been funded by the
Defense Atomic Support Agency under WEB No. 13.167.

Project No. 1080, Task No. 108005

(Prepared under Contract AF 29(601)-4565 by
Morrison, T., General American Transportation
Corporation, MRD Division, Niles, Illinois.)

CATALOGED BY DDC

AS



Research and Technology Division
Air Force Systems Command
AIR FORCE WEAPONS LABORATORY
Kirtland Air Force Base
New Mexico

When Government drawings, specifications, or other data are used for any purpose other than in connection with a definitely related Government procurement operation, the United States Government thereby incurs no responsibility nor any obligation whatsoever; and the fact that the Government may have formulated, furnished, or in any way supplied the said drawings, specifications, or other data, is not to be regarded by implication or otherwise as in any manner licensing the holder or any other person or corporation, or conveying any rights or permission to manufacture, use, or sell any patented invention that may in any way be related thereto.

This report is made available for study upon the understanding that the Government's proprietary interests in and relating thereto shall not be impaired. In case of apparent conflict between the Government's proprietary interests and those of others, notify the Staff Judge Advocate, Air Force Systems Command, Andrews AF Base, Washington 25, DC.

This report is published for the exchange and stimulation of ideas; it does not necessarily express the intent or policy of any higher headquarters.

DDC AVAILABILITY NOTICE

Qualified requesters may obtain copies of this report from DDC.

FOREWORD

This report is one of five volumes presenting the results of a series of studies carried out for the Air Force by General American Transportation Corporation and Newmark-Hansen Associates. The five volumes comprise RTD TDR-63-3096 and are organized as follows:

- Vol. I Structure Interior Motions Due to Air Blast Induced Ground Shock
- Vol. II Structure Interior Motions Due to Directly Transmitted Ground Shock
- Vol. III Response Spectra of Single-Degree-of-Freedom Elastic and Inelastic Systems
- Vol. IV Response Spectra of Two-Degree-of-Freedom Elastic and Inelastic Systems
- Vol. V Response Spectra of Multi-Degree-of-Freedom Elastic Systems

Volumes I and II are authored by General American Transportation Corporation. Volumes III, IV, and V are authored by Newmark-Hansen and Associates. Volumes II, IV, and V will be published early in 1965.

Acknowledgment is made to Captain H. Auld, Captain D. H. Merkle, and Lt J. F. Florey of AFWL for their continued cooperation during the course of the project and to Dr. S. Raynor of Northwestern University who serves as consultant to MRD of General American Transportation Corporation.

ABSTRACT

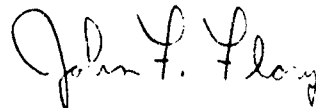
The primary purpose of this report is to provide guidance for designers of shock isolation systems during the initial phases of design. Volume I presents methods for estimating appropriate free field waveforms and the influence of soil-structure interaction upon interior structure motion. Volume III of RTD TDR-63-3096, prepared by Newmark-Hansen Associates, presents methods for synthesizing peak relative response spectra from the spectra characteristic of pulses of simple shape.

The inherent error in shock isolation design is at least ± 20 percent; to reduce this, much more soil test data than is now available will be required. Further, based on purely theoretical arguments, shock isolation per se can be eliminated for much equipment used in hard installations. If isolators are required they should be designed as low frequency systems that impose one g acceleration on the isolated equipment. Increase of the acceleration to be tolerated by the equipment will, in the great majority of instances, reduce neither the rattle space required nor the isolator cost.

Methods for making the necessary computations are given.

PUBLICATION REVIEW

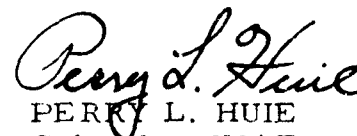
This report has been reviewed and is approved.



JOHN F. FLORY
2Lt USAF
Project Officer



THOMAS J. LOWRY, JR.
Colonel USAF
Chief, Civil Engineering Branch



PERRY L. HUIE
Colonel USAF
Chief, Research Division

TABLE OF CONTENTS

<u>Section</u>		<u>Page</u>
1	INTRODUCTION: GENERAL DISCUSSION OF PROBLEM.....	1
	1.1 Normal Modes, Damping and Coupling.....	10
	1.1.1 Undamped Modes.....	10
	1.1.2 Damping and Coupling.....	12
	1.2 Shock Spectrum.....	18
	1.3 Equivalent Drop Method.....	21
2	CONCLUSIONS AND RECOMMENDATIONS.....	24
	2.1 Conclusions.....	24
	2.2 Recommendations to Shock Isolation Designers.....	27
	2.3 Research Recommendations.....	28
3	INHERENT ACCURACY OPTIMUM SYSTEM CHARACTERISTICS.....	30
	3.1 Wave Reflection in Real Soils.....	30
	3.2 Suspension Frequency Range.....	40
	3.3 Available Accuracy.....	48
4	DETERMINATION OF FREE FIELD INPUT.....	55
	4.1 The Input Wave Estimate.....	59
	4.1.1 The Overpressure Wave.....	60
	4.1.2 Wave Velocities.....	62
	4.1.3 Compression Wave Attenuation.....	74
	4.1.4 The Input Wave.....	86
	4.1.5 Vertical and Horizontal Free Field Inputs..	108

TABLE OF CONTENTS (CONTINUED)

<u>Section</u>		<u>Page</u>
	4.2 Approximate Estimates of Input.....	110
5	SOIL-STRUCTURE INTERACTION.....	112
	5.1 Summary of Interaction Theory.....	114
	5.2 Simplification of Interaction Procedure.....	117
	5.3 Simplified Design Method.....	125
6	NONLINEAR SYSTEMS.....	128
	6.1 Conservative Nonlinear Systems.....	130
	6.2 Nonconservative Nonlinear Systems.....	142
	6.3 General Consideration of Nonlinear Isolation Systems: Their Advantages and Disadvantages.....	146
	6.4 Negative Spring Isolators.....	148
7	ISOLATOR ELIMINATION.....	153
8	DETERMINATION OF INPUT PARAMETERS.....	160
	8.1 Simplified Structure Frequency Formulas.....	160
	8.1.1 Domes.....	160
	8.1.2 Circular Cylinders.....	161
	8.1.3 Circular Arches.....	161
	8.1.4 Rectangular Slabs.....	162
	8.2 Normal Mode Geometry.....	162
	8.3 Soil Parameters.....	162
	8.3.1 Bedrock Elevation and Material.....	162
	8.3.2 Stress-Strain Parameters.....	163
	8.3.3 Percyclic Damping Factors for Real Soils.....	163

TABLE OF CONTENTS (CONTINUED)

<u>Section</u>	<u>Page</u>
APPENDIX A DEVELOPMENT OF MOTION-TIME METHOD FOR DISTRIBUTED SYSTEMS.	A-1
A.1 Statement of the Problem; Method of Approach.....	A-1
A.2 The Differential Equation.....	A-1
A.2.1 Physical Meaning of Terms of Fundamental Equations.....	A-18
A.2.2 Range of Applicability of the Basic Equations...	A-19
A.3 Formal Solution of the Fundamental Equations.....	A-26
A.4 Evaluation of Generalized Forcing Functions.....	A-33
A.5 Coupled Modes... ..	A-46
A.6 Natural Frequency.. ..	A-50
APPENDIX B A NUMERICAL METHOD OF SOLUTION OF THE RESPONSE EQUATION...	B-1
REFERENCES	B-5
DISTRIBUTION	C-1

LIST OF FIGURES

<u>Figure No.</u>		<u>Page</u>
1.1	Block Diagrams of Nuclear Ground Shock Isolation Problem....	5
1.2	Block Diagram Tacitly Followed for Some Shock Isolation Schemes.....	7
1.3	Elementary Coupled Linear System.....	14
1.4	Comparison of Peak Relative Response Spectra Due to Velocity Jump and Exponential Pulse.....	20
3.1	Propagation of Vertical Wave Into Soil.....	35
3.2	Stress-Strain Curve of Hypothetical Nonlinear Elastic Soil..	39
3.3	Surface Displacement Induced by Conversion of Soil Kinetic Energy to Potential Energy.....	39
4.1	Overpressure Decay Rate.....	61
4.2	Approximation of Blast Wave by Exponential Increments.....	63
4.3	Confined Compression Stress Versus Strain.....	64
4.4	Variation of Soil Stress-Strain Curve.....	67
4.5	Concave Stress-Strain Curve.....	69
4.6	Damping of Rectangular Pulse.....	76
4.7	Decaying Amplitude of Rectangular Pulse.....	77
4.8	Propagation of Damped Longitudinal Pulse.....	78
4.9	Damping of Triangular Pulse.....	79
4.10	Decay of Triangular Pulse According to Percyclic Damping Law.....	80
4.11	Approximate Triangular and Long Wave Length Components of Blast Wave.....	82
4.12	Damping of Triangular Pulse.....	85

LIST OF FIGURES (CONTINUED)

<u>Figure No.</u>		<u>Page</u>
4.13	Soil Stress-Strain Curve.....	87
4.14	Overpressure Wave.....	88
4.15	Sum of Pressures at Structure.....	93
4.16	Estimated Stress-Strain Curve.....	95
4.17	Overpressure-Time.....	97
4.18	Ratio of Secant Shock Velocity To c_0 Versus Stress.....	99
4.19	Overpressure Versus $c_0 t$	101
4.20	Stress Versus t^*	103
4.21	Stress Versus Shock Wave Propagation Distance	104
4.22	Waveforms at Different Values of t^*	105
4.23	$\frac{1}{\rho} \left(\frac{\partial p}{\partial x} \right)$ Versus t^*	107
6.1	Schematic of Conservative Nonlinear System.....	131
6.2	Energy-Stroke Diagram of Isolator.....	131
6.3	Force-Stroke Diagram of Isolator.....	131
6.4	Comparison of Equilibrium Energy of Two Nonlinear Systems...	133
6.5	Rattle Space Required by Nonlinear System.....	137
6.6	Rattle Space Required by Nonlinear System; Rise Time Correction.....	140
6.7	Isolator Energy Curves.....	141
6.8	Schematic of Nonconservative Nonlinear System.....	143
6.9	Toggle Negative Spring Characteristics.....	149
6.10	Schematic of Cam Operated Negative Spring.....	150
6.11	Negative Spring Isolation System.....	151

LIST OF FIGURES (CONTINUED)

<u>Figure No.</u>		<u>Page</u>
7.1	Equivalent Drop Height Vs. Peak Surface Overpressure $\bar{C} = 1000$ Ft/Sec $\gamma = 110$ lbs/ft ³	157
7.2	Equivalent Drop Height Vs. Peak Surface Overpressure $\bar{C} = 2000$ Ft/Sec $\gamma = 110$ lbs/ft ³	158
7.3	Equivalent Drop Height Vs. Peak Surface Overpressure $\bar{C} = 3000$ Ft/Sec $\gamma = 110$ lbs/ft ³	159
A.1	Vector Representation of Velocity Induced Forces.....	A-17
A.2	Ground Waves Induced by Blast Wave and Bedrock.....	A-35
A.3	Resolution of Vector Normal Mode Motions.....	A-38
A.4	Pressures Induced by Plane Compression Wave.....	A-40
A.5	Pressures Induced by Plane Shear Wave.....	A-42
A.6	No Title.....	A-43

LIST OF SYMBOLS

Note: See separate list for symbols used in Appendix A. All vectors are given in the appendix list of symbols.

A	=	structure surface area	N_i	=	Norm, ith mode
c	=	wave propagation velocity	n	=	acceleration in gravity units
\bar{c}	=	average compression wave propagation velocity	n	=	pulse propagation distance in initial pulse widths
c_c	=	sonic velocity of shell material	n	=	subscript, nth mode.
D	=	depth to bedrock	P	=	pressure
D	=	flexural rigidity	P_o	=	peak overpressure
E	=	Young's modulus	R	=	structure radius
E_k	=	kinetic energy	r	=	pulse decay ratio
E_p	=	potential energy	s	=	pulse coordinate in initial pulse widths
ΔE_m	=	potential energy increment	$T_i(t)$	=	response amplitude of ith mode
F	=	Spring force	t	=	time
f	=	frequency, cycles per second	t_d	=	duration of wave
g	=	acceleration of gravity	t_r	=	rise time
h	=	shell thickness	t_r	=	period, rigid mode
I	=	impulse	t_s	=	subtangent duration
i	=	subscript, ith mode	t_d	=	period, deformational mode
K	=	soil resistance factor	t^*	=	time required for peak pressure to attenuate to a given level
k	=	Spring constant	U	=	soil or air shock velocity
L	=	wave path length	V	=	structure volume
L_s	=	subtangent wave length	v	=	velocity
M	=	mass	w	=	weight
m	=	shell unit mass			

LIST OF SYMBOLS' (CONTINUED)

x, y, z	=	displacements, as defined in text
α	=	acceleration
β	=	factor defined in text
γ	=	soil density.
δ	=	percyclic damping constant
δ	=	damping factor
ϵ	=	unit strain
λ	=	a characteristic length for shells
ν	=	Poisson's Ratio
ρ	=	soil unit mass
$\tau_i(t)$	=	forcing function for ith mode
Ω_i	=	natural frequency of ith mode in soil
ω_i	=	natural frequency of ith mode in vacuum
ξ, η, ζ	=	rectangular coordinate system

Particular values of various quantities are denoted by subscripts,
asterisks, and carats as defined in the text.

LIST OF SYMBOLS FOR APPENDIX A

Scalars

A	=	structure area	δ_i	=	damping constant for ith mode
A_i	=	amplitude constant of ith mode	θ_i	=	arbitrary phase angle for ith mode
C	=	constants defined in Table B.1	ν	=	Poisson's Ratio
c	=	wave propagation velocity	ρ	=	soil mass density
c_1	=	compression seismic velocity	$\tau_i(t)$	=	forcing function for ith mode
c_2	=	shear seismic velocity	Ω_i	=	natural frequency of ith mode in soil
D	=	proportionality constant	ω_i	=	natural frequency of ith mode in vacuum
D	=	flexural rigidity			
E	=	Young's Modulus			
h	=	shell thickness			
i	=	modal index			
j	=	modal index			
K, k	=	soil resistance factors			
m	=	unit mass of shell			
n	=	modal index			
N_i	=	modal norm			
\hat{R}	=	ratio of soil deformation pressure to structure deformation pressure			
$S_r(t)$	=	rigid body mode amplitude function			
$T_i(t)$	=	modal amplitude function			
V	=	structure volume			
β	=	defined in Figure A.1			

LIST OF SYMBOLS FOR APPENDIX A (CONTINUED)

Vectors

\bar{l}	=	tangential unit vector
\bar{n}	=	normal unit vector
\bar{p}	=	pressure
\bar{p}_1	=	input pressure
\bar{u}	=	absolute structure displacement
\bar{w}	=	relative structure displacement
\bar{z}	=	absolute free field displacement
$\bar{\phi}_i$	=	normal mode
$\dot{\bar{\psi}}_u$	=	vector defined in text
$\dot{\bar{\psi}}_z$	=	vector defined in text

Misc.

$L()$	=	linear vector operator of spacial variables
$B_n()$	=	boundary conditions
∇^2	=	Laplacian operator
\bar{p}	=	free field pressure tensor

missile have been established. The inside diameter of the silo within which the missile will be housed may depend more strongly on the rattle space required by the missile and its isolation system than upon any other single factor save missile envelope diameter. The cost of the missile silo and associated door and operating equipment varies somewhere between the square and the cube of the silo diameter, other factors being equal. Therefore the shock isolation designer is placed in the difficult position of having to establish space requirements that are adequate for isolation but held to a minimum in order to keep costs down at a time when he has little detailed information upon which to base his estimates. The primary purpose of this report is to provide methods that will assist the shock isolation designer in arriving at conclusions to this and similar problems.

Two general avenues of approach were open at the outset of the work herein reported:

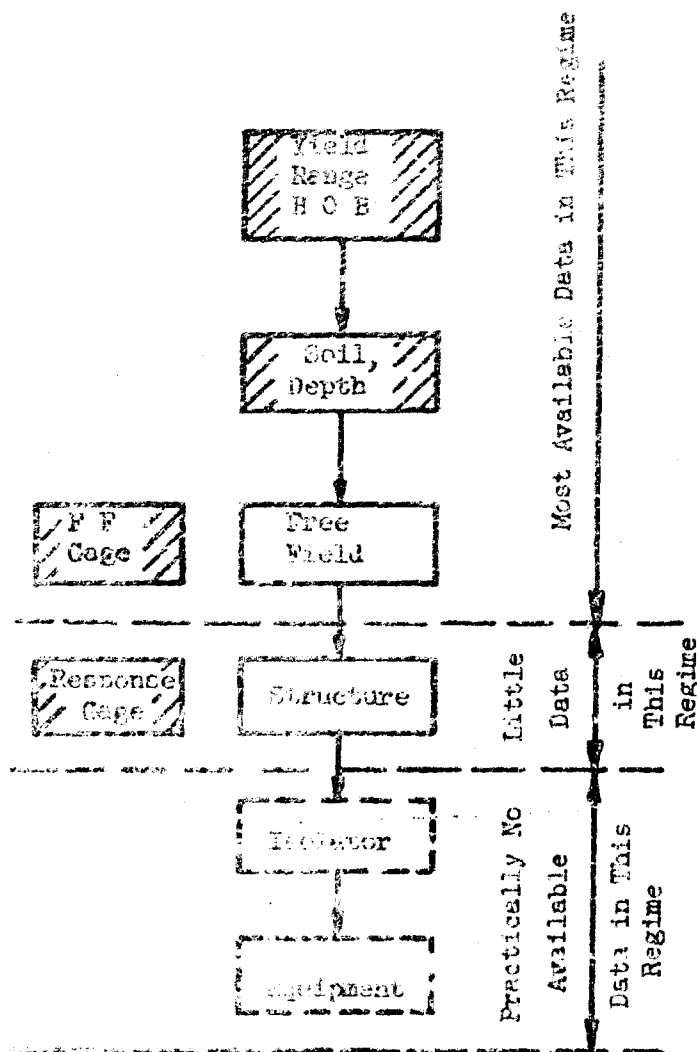
1. Formulas and the necessary associated compendium of data could be prepared so that any problem likely to face a designer would have been considered and graphs presented covering suitable ranges of the various parameters.
2. Methods could be developed the use of which would enable the designer to consider the particular problem he faced from basic principles and to expeditiously carry out the design without reliance upon a compendium of previously computed data.

Both approaches were considered on the project but it became evident that the latter approach was by far the more desirable. Shock isolation design for the suspension system of a large liquid fueled missile and the design of isolators for a ruggedized item of electronic equipment mounted on a wall bracket have little in common other than the name "shock isolation" and the fundamental laws of mechanics governing the design. The compendium required for the first approach would have been truly massive. Further, it developed that, within engineering accuracy, the second method became quite practical.

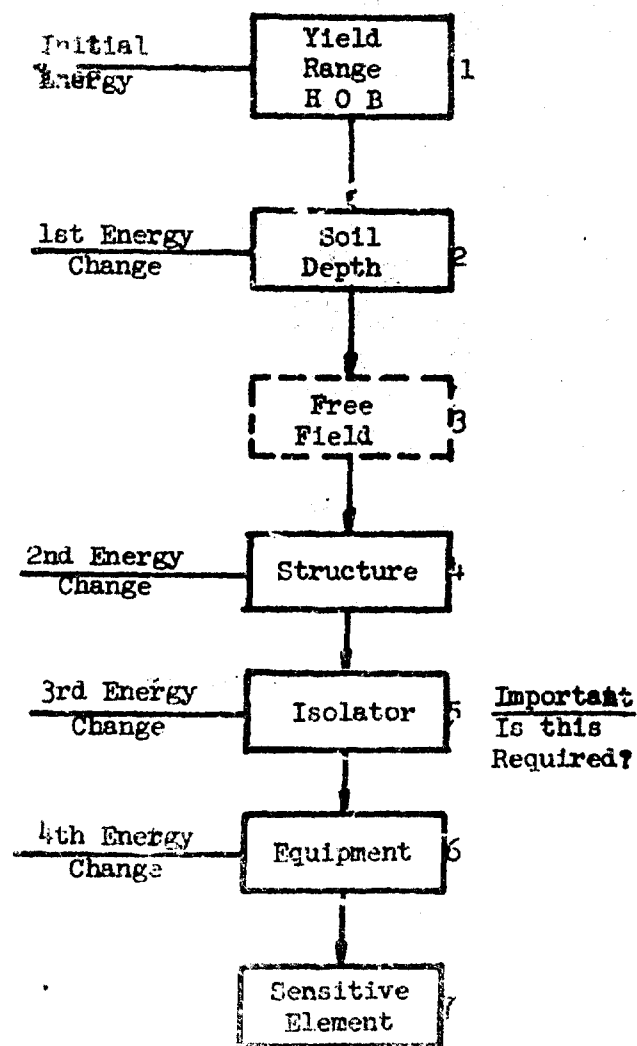
The vague concept "shock sensitivity of equipment" in the past has received considerable attention. Nevertheless at the present time it is practically impossible to clearly define the shock sensitivity of an individual item of equipment let alone to formulate a general sensitivity criterion with sufficient accuracy and mathematical precision to enable deduction of shock isolation criteria. The complexities of equipment used are so great and so varied that efforts in this direction have been unavailing. However, at least one precise statement fundamental to shock sensitivity can be made: damage to an equipment element is induced when either the total energy communicated to the element or the rate of flow of energy delivered to the element exceeds certain critical values. Often, of course, it is a practical impossibility to distinguish the critical energy component and/or its critical level. Knowing, however, that the damaging agent ultimately is energy, regardless of how described, we can gain considerable insight into the overall shock isolation problem by considering the path followed by the energy leaving an exploding weapon and ultimately arriving at a sensitive element of equipment.

Figure 1.1 shows two block diagrams representing, in a general way, the propagation of energy originating at the detonation of a nuclear weapon through the blast environment to shock sensitive equipment. One block diagram represents the conditions for which we have data obtained at the nuclear weapons test sites; the second represents the situation at a proposed installation site. Consider, first, the test site. Eight blocks are shown. Of these we have factual information for three blocks; yield, the detonation parameters, range and height of burst; the free field gage outputs and, in a few instances, response gage outputs. We have partial information for a fourth block, the soil characteristics and depth at which measurements were taken. It should be observed that the output of the free field gage is not what might be termed the true free field underground blast motion condition. It is the output of a gage which, by its very presence, modifies the free field that would exist in its immediate vicinity if the gage were not there. Further, it is the output measured over a relatively small area, perhaps that of a cylinder a few inches in diameter or less. Portions of the gage output would be substantially the same if the gage were moved significant distances, with range, soil parameters and depth held constant. Other portions of its output, however, would vary markedly if the gage were moved only a few feet or even, in some cases, a few inches. These latter portions can be accounted for in any design procedure only on a statistical basis, if they are indeed significant.

At a weapons system installation, it should be noted, the energy released by detonation of the bomb is modified at least four times before reaching the portion of the equipment subject to damage. The energy is first converted from



At a Weapons System Installation Site



At a Weapons System Installation Site

NUCLEAR GROUND SHOCK ISOLATION PROBLEM

Best Available Copy

the pressure-volume and kinetic energy of the bomb fragments and air-soil environment into the energy that we term the free field pressure. This, in turn, may or may not be markedly modified by any structure buried in the free field. Then the energy is further greatly modified by any isolator provided within the structure between the structure itself and the equipment mounted therein. It is to gain this modification that the isolator is provided. Finally, in coursing through the equipment, that portion of the energy passing through the isolator is again further modified significantly before reaching the particular element of the equipment at which damage might be caused. Our problem is to deduce from the limited information represented by the shaded blocks in the test site block diagram a series of criteria, theories, and design formulas which will enable us, within an acceptable degree of accuracy, to follow the energy through the block diagram representing conditions at an installation site and arrive at meaningful criteria for the design of isolators of minimum size and cost but adequate mechanical properties to insure that the equipment mounted therein survives the blast.

Since the energy successively passes through some four major modifications before arriving at the point at which it can cause damage, it is evident that neglect of one of the four can introduce more error in our overall design procedure than might be eliminated by refined design of any of the other energy conversions. In particular, the block diagram shown in Figure 1.2 which has tacitly been assumed for some hard structure shock isolation designs, can be a poor representation of the overall problem. The methods of extrapolating test site gage records to conditions at an installation site are questionable for large structures.

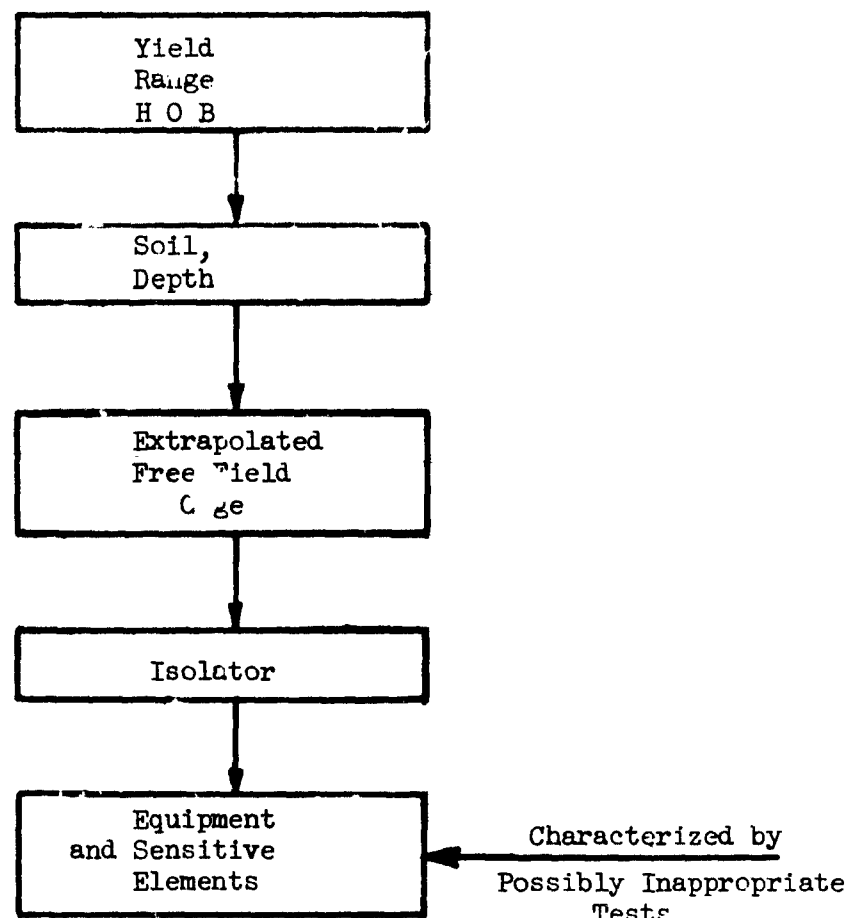


Figure 1.2 BLOCK DIAGRAM TACITLY FOLLOWED FOR
SOME SHOCK ISOLATION SCHEMES

The point of departure for the project reported herein was Block 3, the free field motion history of Figure 1.1. The energy chain from the bomb burst to free field is an extremely complex area that is receiving a great deal of effort by a number of investigators at the present time. For this project we have made use of information presently available to describe generally the free field motion history that would exist under any particular set of circumstances. However, we have not imposed the requirement that the free field data be of any particular form or characterizable by any specific mathematical expression. Thus, as further information is developed on the nature of the free field this can be fit into the shock isolation design scheme presented.

A substantial portion of the effort carried out on the project is concerned with the second energy change represented by block 4 of Figure 1.1, the soil structure interaction. Even though a structure buried in soil remains substantially rigid during ground motion its presence has a significant effect on the total energy available to the isolator and isolated equipment and possibly even more influence on the rate of delivery of this energy. The natural vehicle for carrying out these computations is the normal mode method which is discussed in considerable detail in Appendix A of this report.

In the following subsections particular aspects of the isolation problem are discussed in nonmathematical terms.

1.1 Normal Modes, Damping and Coupling

1.1.1 Undamped Modes

The vibration of an undamped linear system, that is a system in which all displacements are proportional to the loads, free of damping, always can be expressed as an infinite series of vibrations of certain special configurations termed "normal modes". This is true no matter how complex the overall system of vibration is and is independent of whether the vibration is free or forced; indeed for free vibration each modal motion consists of a particular geometric configuration, each point of which oscillates harmonically in phase with all other points at a specific frequency characteristic of the mode. Such a vibration would continue indefinitely. The total energy of each mode would be independent of time, and there would be no interchange of energy between the various excited modes. It is this energy independence quality that ultimately defines the various modal configurations. At the maximum displacement of a mode all of its energy would be potential, stored in the system elements. A quarter period later all of the energy would be kinetic. For this reason this energy is termed the relating energy of the mode.

When the mathematics are carried out the amplitude of the free vibration of a normal mode is found to satisfy the same equation as a simple mass-spring system, i.e.,

$$\ddot{x}_n + \omega_n^2 x_n = 0 \quad (1.1)$$

where

x_n is the amplitude of the nth mode, a function of time

ω_n is the natural frequency of the nth mode.

If a distributed system of forces is applied to the structure, vibration again will consist of the infinite series of normal modes. However, in this instance each mode will not vibrate harmonically, rather the modal amplitude will be given by solution of Equation (1.2).

$$\ddot{x}_n + \omega_n^2 x_n = f_n \quad (1.2)$$

This equation is seen to be analogous to the equation of forced motion for a mass-spring system where the function f_n fills the role of forcing function. It will be found that f_n is equal to the rate of energy delivery to the nth mode by the distributed forces applied to the structure and multiplied by a constant characteristic of the mode.

Since the energy delivered to a particular mode by a forcing function generally is inversely proportional to a power of the modal frequency on the order of 2-to-3 the significance of the high frequency modes decreases rapidly. Therefore, though mathematically accurate solution of the problem requires consideration of an infinite number of modes, engineering accuracy generally can be obtained by considering two or three, and often times only the fundamental mode is of real significance. An exception to this situation occurs when a resonance effect takes place; however, for the transient response that is of principal importance for nuclear blast induced shock, resonance plays a secondary role because the forcing function (ground shock wave) does not last a sufficient number of periods to build up a strong resonance.

An aspect of normal mode theory that is unfortunately frequently glossed over in the literature deserves specific attention. Most of the elementary problems discussed in texts on vibration, e.g., strings, beams, membranes, and plates possess a characteristic that simplifies analysis but is not intrinsic to the general problem: The displacements of all points of the structures mentioned are parallel to each other, i.e., all displacements of the string and the beam are perpendicular to the axes of these members; the displacement of all points on the surface of the plate and membrane are perpendicular to the rest planes of these elements. In general, this situation is not true. Thus the displacements of the circular cylinder vibrating in its bending modes consists of a radial component and a simultaneous lateral component tangent to the surface of the cylinder. Though the motion of any particular point on the surface of the cylinder is along a straight line, the lines at different points on the structure are not parallel. Further, for the cylinder there is no point at which the scalar magnitude of the motion is zero in a manner analogous to the nodal points of vibration of strings and beams or the nodal curves of membranes and plates.

1.1.2 Damping and Coupling

It can be shown mathematically that the normal mode solution exists for a damped structure if the equations of motion can be put in the form of Sturm-Liouville problem. Within this limitation the only case which is of physical significance and which may be, from a practical standpoint, solved mathematically is the case where the damping force is proportional to velocity at every point of the system and has the same direction as the displacement vector at every point of the system. Furthermore, the scalar proportionality constant, i.e., the

damping constant relating the damping force vector and the velocity vector, must be constant for the entire system. Most real systems do not comply with this criterion. However, it often can be used as a fair approximation to the real system though it must be appreciated that the major reason for making the approximation is not physical but mathematical; the problem is much simpler to solve if velocity proportionate damping is assumed.

If the damping of the system is not velocity proportionate the normal mode method of solution can be employed though in this case it loses some of its physical reality and becomes essentially a mathematical tool of some complexity that will, however, give results to any desired degree of accuracy if sufficient computations are carried out.

The influence of non-velocity proportionate damping can have serious consequences to design; therefore, its effects will be discussed at some length from the physical standpoint so that the designer may gain some feel as to what might actually take place in a particular isolation system. The crux of the matter is that substantial motions, other than those anticipated by an elementary application of the normal mode theory, may develop after passage of the ground shock wave. These might require considerable additional rattle space and substantial modification of the suspension mechanism over those required if the system were truly undamped in the mathematical sense.

The physical reasons for this situation can most easily be observed by considering the simplest of multi-degree of freedom systems, a pair of masses and springs in series. In Figure 1.3 we have shown two masses in series with two springs but only one dashpot connecting the two masses. Evidently the

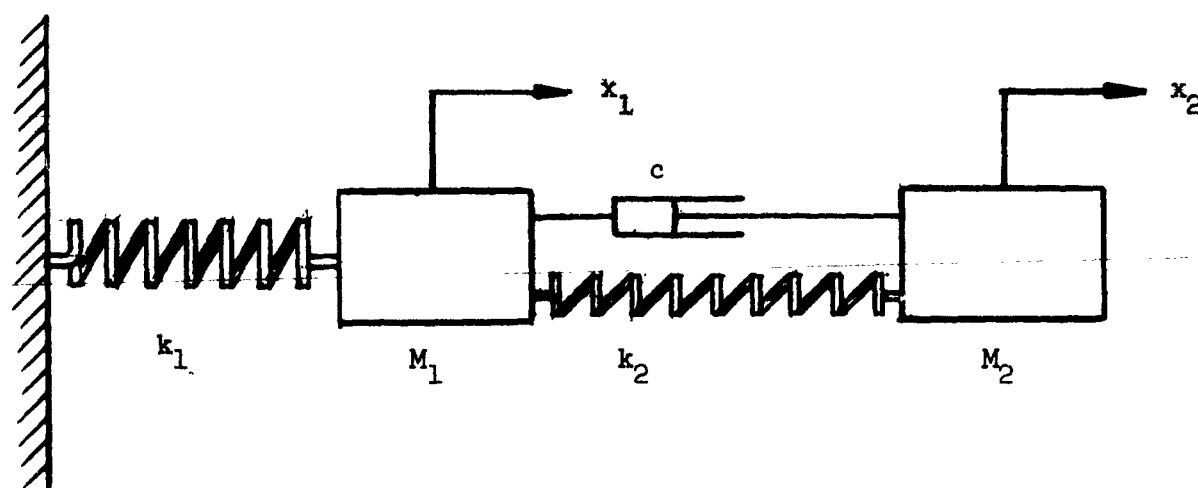


Figure 1.3 ELEMENTARY COUPLED LINEAR SYSTEM

requirement that the proportionality constant for damping be the same for all elements is not met by the system shown in Figure 1.3. Now if the dashpot were eliminated the system shown would have two normal modes. For each mode, the contribution to the displacements x_1 and x_2 would always be proportional though the proportionality constants for the two modes would differ. With the dashpot in place, however, during motion of the masses a force is developed by the dashpot which is proportional to the difference between the velocity of mass 2 and mass 1. The energy dissipated is equal to the integral of the product of this dashpot force and the differential relative displacement of the masses. However, the dashpot force is applied to both masses. Therefore, if we assume that the gross motion of the dashpot is to the right the dashpot system will remove energy from the M_2, k_2 system and add energy to the M_1, k_1 system. In other words, in addition to dissipating energy as heat, the damping element transmits energy from one spring-mass element to the other, depending on motions of the elements connected.

In Appendix A of this report the analysis of the general system is presented. There it is found that for nonvelocity proportionate damping the damping factors for all modes couple energy into all other modes. Thus, to return to Figure 1.3 if one mode only were to be excited the dashpot immediately would begin to remove energy from this mode and transmit it to the mode that was not initially excited. Of course, while doing this it also would dissipate some energy as heat. If the vibration continued for a long enough period of time, ultimately all of the energy initially supplied to the excited mode would have been dissipated as heat or coupled to the mode that was not initially excited. In general, this transfer of energy requires a great many periods of vibration. Therefore, the effect is most

pronounced when the amount of damping is small so that only a small portion of the energy is dissipated as heat during each period of vibration and the system continues to vibrate long enough for the damping elements to transfer the energy from the excited to the unexcited mode. These are precisely the conditions that exist in a real system that we normally consider undamped.

The several modes for real systems may differ markedly from each other in their geometry and directions of motions. For instance, a pendulum supported on springs has not only the obvious pendulum motion in two directions and the gross vertical and lateral motions of the support but also a rotation about the axis of the pendulum. If a suspension system, such as used for some missiles, consisting essentially of a pendulous cage containing the missile and supported by springs at the top of the silo were not sufficiently damped, the energy communicated to the pendulum by the ground shock wave might, after a period of time, appear as a rotary motion of the entire suspension system about a vertical axis, a situation that could induce severe damage to the missile and its suspension system if not provided for in the design. Further even if the torsional mode were not significantly excited, coupling of even a small amount of the energy of vertical oscillation to the horizontal pendulum mode can be serious because a small amount of circulating energy can represent a wide swing for a long pendulum.

The modes of a system having nonvelocity proportionate damping, as discussed in the previous paragraphs, are accurately described as coupled modes. The damping couples energy from one mode to the other. Unfortunately, the term "coupled modes" is sometimes applied to an entirely different motion configuration. This may be explained as follows. The vibration of a general system is a vector quantity, i.e.,

for a given mode, motion at different parts of the system may take place in different directions even though the motions are at all times in phase with each other. For any particular vector mode, this motion can be resolved into scalar components in any suitably chosen set of coordinate directions. The scalar components are sometimes referred to as coupled modes. These cannot exist independently of each other and individually do not have the simple energy relations characterizing true modes. In this report when modal components are considered they are so identified.

If any damping at all is present, during each cycle of vibration a certain fraction of the circulating energy is removed from each mode. Normally, damping is considered to be a conversion of the mechanical circulating energy into heat by one mechanism or another, dashpots, internal friction, etc. A more general definition of damping is any mechanism that removes some of the circulating energy from the system during the course of a period of vibration. Under this definition the divergent wave of energy emanating from a structure vibrating in a material medium is a form of damping. The energy carried by the wave does not return to the structure. For instance, a missile silo vibrating in soil will radiate a substantial energy wave. The energy carried by this wave does not return to the silo. Therefore, this aspect of soil structure interaction introduces a significant amount of damping. In Appendix A it is shown that for the lower order modes of reasonably proportioned structures the damping is greater than critical. Therefore, for these modes there is negligible coupling of energy between modes induced by departure of the real damping from velocity proportionality and approximations can be made for computational purposes without thereby neglecting significant motion components.

1.2 Shock Spectrum

The peak relative response spectrum provides a useful tool for shock isolation design under certain circumstances. The companion volume of this report, prepared by Newmark-Hansen & Associates is devoted exclusively to the several aspects of shock spectra as they are generally termed. Here we point out simply the general ideas behind the shock spectrum approach and call to the attention of the reader how certain information developed by use of the techniques presented in this report can be used as a starting point for application of the Newmark-Hansen report.

A shock spectrum is simply a plot of peak displacement, peak velocity, or peak acceleration of a mass-spring system against the system's natural frequency for a specific forcing function. If one has available a shock spectrum for a forcing function input of interest then the peak amplitude of each of the modes of any linear vibrating system characterizable by normal modes and subjected to the forcing function can be taken from the spectrum if the frequencies of vibration of the modes can be estimated. Further, if the damping of the system of interest is sufficiently small so that each cycle of vibration is approximately sinusoidal, the modal motions, displacement, acceleration, and a so-called pseudo velocity, that very nearly matches actual peak velocity can all be taken from the same graph, if it is plotted on quadruple coordinate logarithmic paper.

Since the spectrum is merely a plot of peak values of response of mass-spring systems versus frequency, it is applicable strictly only to linear, uncoupled systems. Further, if damping is to be considered, the percentage of critical damping used in development of the spectrum must be the same as the

percentage of damping of the equipment to be designed with the aid of the spectrum. Also, in the mathematical sense the peak relative response spectrum is not applicable to couple systems or to nonlinear systems. In actual practice the errors introduced by employing spectra to design systems for which they are not strictly applicable often are small enough to neglect.

In this report methods are developed for determining the motion on the interior of a protective structure in terms of the free-field motion. For large structures there can be considerable divergence between these. The Newmark-Hansen report presents approximate, but quite accurate, methods for constructing spectra from certain cardinal characteristics of the input motion. Thus, by a two-step process, developing first the interior structure motion and then the spectrum it is possible to construct a peak relative response spectrum for the design of shock isolators, reflecting in the spectrum the soil-structure interaction, structure orientation and free-field ground shock wave characteristics.

The shock spectrum also provides a useful tool for evaluation of the effects introduced by simplifications of an analysis. Figure 1.4 shows a comparison of the spectra resulting from a step function velocity input, and a decaying exponential velocity input of the same peak amplitude. A glance at the spectra is all that is required to show that if the decay constant, α , has a numerical magnitude of 1 sec^{-1} or greater, no more than 10 percent error is introduced by a step wave approximation at isolator frequencies of 5 cps or greater.

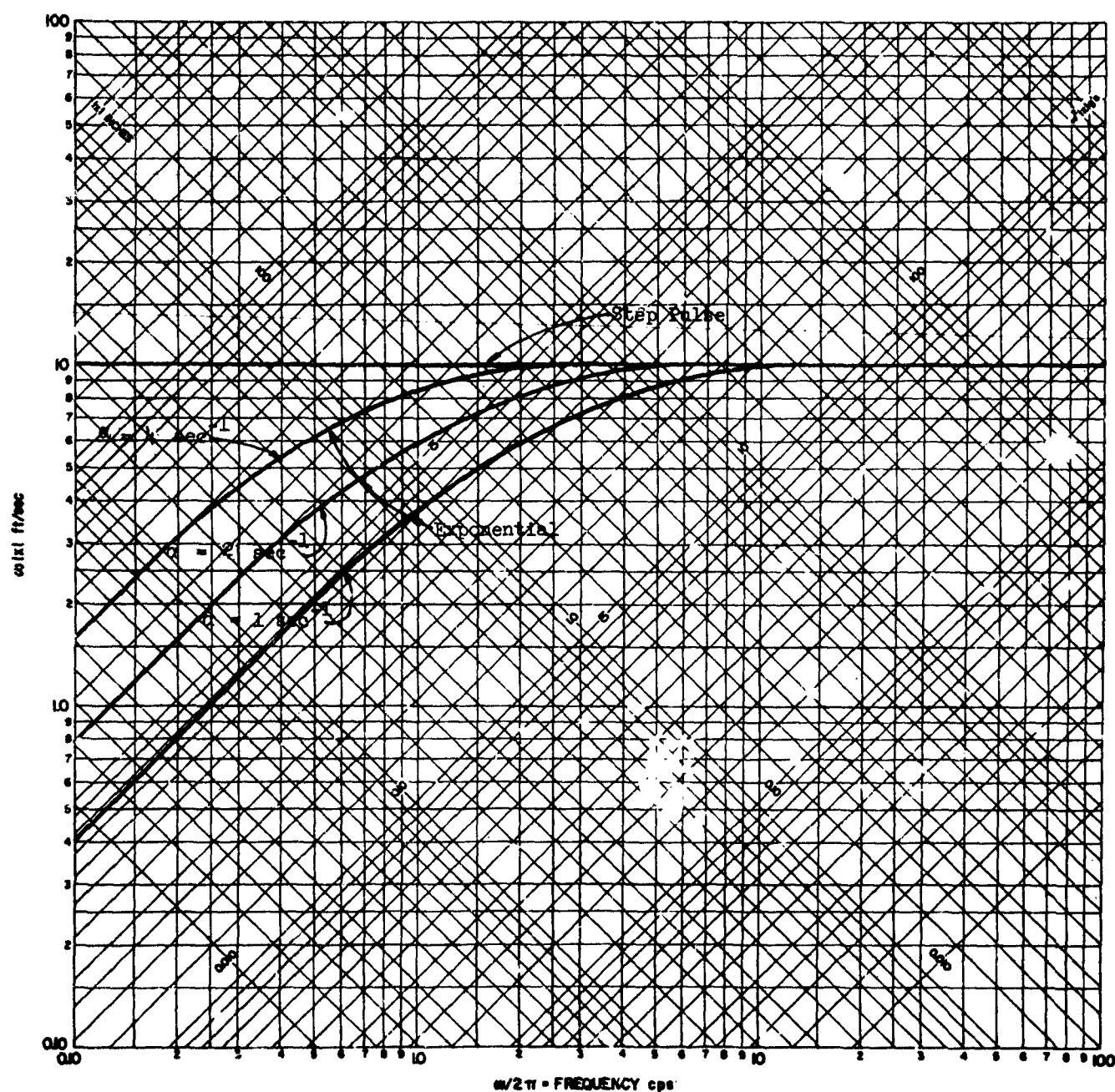
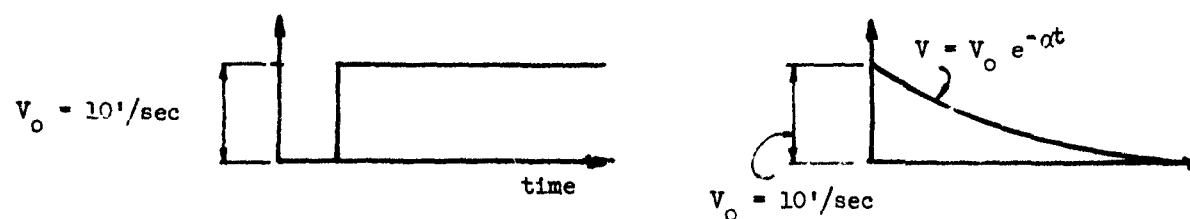


Figure 1.4 COMPARISON OF PEAK RELATIVE RESPONSE
 SPECTRA DUE TO VELOCITY JUMP AND EXPONENTIAL PULSE

1.3 Equivalent Drop Method

The equivalent drop method is particularly useful during the early stages of design for making upper limit estimates of rattle space requirements and establishing for a considerable variety of equipment whether or not shock isolators will be necessary.

The soil particle motion at depth in real soils, due to detonation of a large nuclear weapon may be quite complex; it will have at least two mutually perpendicular components of motion and possibly three. However, in particulate soils subjected to air blast the vertical component of motion generally is considerably larger than either of the horizontal components. For the remainder of this discussion, we will focus our attention on the vertical motion component only, realizing that the conclusions drawn apply to the smaller horizontal components also.

In general, when engulfed by the ground shock wave the soil particle vertical velocity component very rapidly increases from zero to some peak value and then much more slowly decreases back to zero. In the subseismic region, generally below the 100 psi overpressure level for particulate soils, the vertical particle velocity may oscillate to some degree. Further, even in the superseismic region if bedrock is near the surface subjected to air blast, the ground shock wave reflected upward from bedrock may impart a small oscillatory component to the vertical particle velocity though generally this is of not more than one-half period duration. The area under the particle velocity versus time curve gives the net vertical displacement of the soil particle.

These complex motions can be conservatively idealized by considering the vertical particle velocity to be a step-wave. If it were not for the reflection from bedrock a surface particle, under this assumption, would continue to move downward indefinitely. However, if the reflected wave proceeding upward from bedrock is assumed to be equal in amplitude to the incident wave, the downward motion of the surface particle would be stopped at the instant of arrival of the reflected wave, though the permanent displacement of the surface thereby obtained would be considerably greater than the permanent displacement actually resulting from detonation of a real bomb. Evidently, this idealization may considerably over-estimate soil particle motion. However, a step function of particle velocity, or velocity jump as it is generally termed, enables very rapid estimates of rattle space and shock input to equipment.

The peak relative response spectrum of a velocity jump when drawn on the conventional four coordinate logarithmic paper is just a horizontal line at pseudo-velocity equal to the velocity jump (see Figure 1.4). Now, if an object were suspended a certain distance above an absolutely unyielding floor and the bottom surface of the object parallel to the floor were made of absolutely unyielding material, and the object then allowed to drop and impact against the floor the shock delivered to the object would be equivalent to a velocity jump equal in magnitude to the velocity obtained by the object falling under gravity just at the instant of impact. The shock spectrum of this impact then is an upper envelope of all shock spectra having peak values on the velocity axis equal to the velocity jump. Thus, from the standpoint of shock damage to equipment it is possible to conservatively equate overpressure levels, bedrock depth, and soil parameters to an equivalent drop of the equipment to a hard surface.

(The horizontal component of shock can be similarly handled except that the equipment should be envisioned as turned sideways when dropped.) Though the method is obviously crude it has the important advantage that the somewhat intangible quantities significant to more sophisticated shock isolation analysis are converted into a parameter for which engineers have considerable intuitive feel. Further, the numerical values of the equivalent drop and velocity jump are surprisingly small. Thus, at the 100 psi overpressure level, in soft soil having a modulus of elasticity of only 20,000 psi at the 100 psi level, the equivalent drop is only 4 inches. It could be concluded therefore, that most machinery and ruggedized electronic equipment would require no shock isolation for these conditions. Only very sensitive elements, e.g., a liquid fueled missile, would be unable to resist a 4 inch drop under gravity to a hard surface.

Even for a sensitive missile isolated by a spring system, the equivalent drop provides a useful index for approximate determination of the relations between rattle space, suspension frequency, and acceleration.

The development of the formulas for the equivalent drop approach, including a relaxation of the step function form of the particle velocity to forms more nearly duplicating actual conditions are contained in Reference 1.

Graphs of the equivalent drop versus input parameters are included in Section 7.

SECTION 2

CONCLUSIONS AND RECOMMENDATIONS

2.1 Conclusions

2.1.1 At the present state of knowledge highly refined shock isolation design is not justified.

2.1.2 The inherent error, due to soil parameter uncertainties, in determination of rattle space for a shock isolation system is at least ± 20 percent and in some instances may be as great as ± 50 percent.

2.1.3 The largest source of inherent error in shock isolation calculations is due to uncertainty in the stress-strain behavior of real soils at the over-pressure levels of interest. Uncertainties in the values of the propagation velocities of compression waves, which ultimately hinge on the stress-strain behavior of soil, contribute the greatest inherent errors to computed rattle space requirements.

2.1.4 Theoretical deductions indicate that at "typical" real sites the second largest source of inherent error results from uncertainty (or neglect) of bedrock elevation. (For some conditions this is the largest error.)

2.1.5 Theoretical deductions indicate that field tests carried out at Frenchman Flat and on the Pacific Proving Ground cannot provide significant information on the influence of bedrock at more typical sites. This is due to the peculiar geology at these test sites.

2.1.6 The third most important source of inherent error is due to uncertainties in energy dissipation (wave attenuation) characteristics of soil.

2.1.7 A hard structure functions as an effective filter of high frequency ground shock components regardless of assumed soil characteristics. The maximum frequency that can be transmitted to the interior is the larger of:

1. The rigid body frequency in soil.
2. The first deformational mode frequency in soil.

(Note: The second of these may be much higher than the first deformational frequency in vacuum.)

2.1.8 To within less error than the inherent error of the free field motion, the interior structure motion can be considered to be the sum of two components:

1. A rigid body motion equal to the free field particle motion having a rise modified to reflect soil-structure interaction;
2. A deformational motion quasi-statically computed but having a rise modified to reflect soil-structure interaction; the quasi-static deformation is equivalent to the deformation the structure would undergo at any instant if the ground shock wave were statically applied to the soil-structure complex. This motion is a function of time but, since it is computed quasi-statically, it is independent of soil and structure inertia.

2.1.9 Theoretical considerations, not known to have been verified experimentally, indicate that shock isolators can be omitted for much equipment in hard shelters, even at high (1000 psi) overpressure levels.

2.1.10 If shock isolation is required the minimum energy (and generally minimum cost) vertical system will result if the frequency is chosen so that one gravity unit acceleration is applied by the system to the isolated equipment at maximum departure of the equipment from equilibrium.

2.1.11 The reduction in rattle space achieved by manipulation of suspension frequency and increase of tolerable equipment acceleration is only a fraction of the error inherent in determination of rattle space.

2.1.12 It is believed that negative spring systems having natural frequencies two or three orders of magnitude lower than conventional (~ 1 cps) systems can be developed. A negative spring is defined as any device having a negative force versus displacement characteristic. The main problem to be overcome in systems using negative springs is adjustability under varying magnitude and distribution of static load to maintain constant static deflection. Such systems would be substantially independent of cross coupling effects between modes, would not ring significantly after excitation, and would have only slightly greater energy capacity, for given stroke, than linear spring systems.

2.1.13 Air springs and similar systems having concave upward force versus displacement curves at a given stroke will either

1. Have much larger energy capacity than a linear spring system of the same stroke and peak acceleration, or

2. Subject the equipment to a considerably greater acceleration than a linear spring system of the same stroke and energy capacity.

2.1.14 Theoretical considerations indicate that sharp, short pulses of stress having rise times measured in microseconds can be generated within structure and equipment by tension and compression waves propagating through materials having concave stress strain curves. These pulses can damage small, delicate elements such as vacuum tube heaters and filaments. They can be prevented from reaching equipment by mounting the equipment on plates or brackets in such a way that all energy propagated through the bracket must appear at some point as a bending wave (as opposed to a direct tension or compression wave).

2.1.15 Peak relative response spectra for interior structure motion can be synthesized approximately by combination of spectra due to simple pulses. The errors introduced by the approximations are considerably smaller than the errors inherent in the input (ground motion) data.

2.1.16 Shear waves can be neglected in shock isolation design without introduction of significant error. Neglect of the shear waves is slightly conservative.

2.2 Recommendations to Shock Isolation Designers

2.2.1 The input motion to the isolator will be the least accurately known data used in the design. Accordingly, this aspect of the problem deserves as much meaningful refinement as can be carried out. (See Section 4)

2.2.2 If equipment must be isolated to a few g then the minimum energy, and probably minimum cost, vertical system will result if the frequency is chosen so that \pm one g acceleration is developed at maximum stroke. For these and other low frequency systems peak displacement only need be computed. (See Section 4)

The concept of the "shock response spectrum" is a useful one in the design of shock isolation equipment. For a detailed discussion of its applicability as an index of equipment shock damage the reader is referred to Reference 7.

2.2.3 A small component of circulating energy represents a wide swing for a long pendulum. The circulating energy of a vertical system will be equal to the product of maximum stroke and equipment weight. Thus, if even a small fraction of this is coupled to the pendulum the latter can be excited to destructive amplitudes. Therefore, both systems should be damped using Coulomb (not viscous) dampers and the ratio of vertical to pendulum frequency should be as large as practical, greater than three and an irrational number. Even frequency multiples should be avoided, particularly 2. An accurate nonlinear analysis of the resulting system should be carried out.

2.2.4 In many installations isolators can be omitted from much equipment. Section 7 gives a simple method for determination of a convenient conservative criterion (equivalent drop distance) for determination of whether isolators are necessary.

2.3 Research Recommendations

Though the complex problems of wave propagation and soil-structure interaction are as yet not understood completely, it is evident that existing approximate

techniques introduce much less error into shock isolation calculations than does the present dearth of knowledge of the stress-strain behavior of real soils at high pressure levels. Even static test data at 500 to 1000 psi is extremely scarce.

Conceding at the outset that dynamic effects may modify static data somewhat and further that the almost infinite variety of soils will preclude ever obtaining a compendium of precise data it still can be argued that practically any factual data would place the designer in a better position than he now occupies.

If a designer had available a series of stress-strain curves with numbers for real soils he could at least use some judgement in estimating a curve for other soils and have a degree of confidence in the values of the slope of his approximation at pressures varying between zero and peak overpressure.

Accordingly, it is strongly recommended that the following data be obtained from static and laboratory dynamic tests for a variety of real soils:

2.3.1 Stress versus strain curves from confined compression tests in the range between zero and 500 psi.

2.3.2 Slopes of the hysteresis loops across the entire range of pressures.

2.3.3 Percyclic (or other) damping factors for single high pressure pulses.

SECTION 3

INHERENT ACCURACY OPTIMUM SYSTEM CHARACTERISTICS

If all of the input parameters of a shock isolation system design were known with three figure accuracy, sophisticated analysis and optimization could be carried out and nicely engineered suspension systems developed. Regardless of the accuracy that might be desirable however, the inherent uncertainties in input parameter values limit the accuracy that can be obtained.

In this section the problems of input error and system optimization will be examined. These will be used to establish limiting accuracy to be striven for and to delineate the mathematical complexity necessary to achieve this accuracy.

3.1 Wave Reflection in Real Soils

At most locations within the bounds of continental United States, bedrock occurs within one or two hundred feet of the surface, though actual depths at specific locations may vary from zero at Limestone, Maine to several hundred feet in parts of North Dakota.

If bedrock lies below the surface a distance on the order of one hundred feet, theory predicts that a strong reflected wave will be developed in the particulate overburden and that neglect or consideration of the reflected wave introduces an uncertainty factor greater at the lower overpressures than that of any other parameter even including the square of the wave propagation velocity.

Considerable evidence has been presented however that the predictions of elastic theory do not appear to occur in real soils. Sauer (Reference 9) points out that experimental data obtained from nuclear field tests do not exhibit significant reflections of stress waves. Newmark and Halmiwanger (Reference 6) state further that laboratory tests on soil with differences in seismic velocity and density of adjacent layers have yielded similar results. The authors of Reference 7 have concluded, based on the data presented by Muskat and Meres (Reference 4), that the energy carried by reflected waves is relatively unimportant, on the order of 11 to 15 percent of the incident wave energy. Thus in spite of the predictions of elementary elastic theory the tendency in shock isolation design has been to ignore reflections as being a theoretical complication of considerable magnitude yet one that influences results well below the inherent error in the problem and one that has not been evidenced in actual test data.

In spite of the evidence the author of this report does not agree with this philosophy and has not adopted it in preparation of the report.

In Nevada ground motion data have been obtained for only KT weapons. At the overpressure levels of interest (> 100 psi) the positive phase duration is on the order of 1/10 second and the compression wave propagation velocity is about 1500 ft per second. Thus, neglecting all attenuation factors the wave length of the entire positive phase is on the order of 150 feet.

At the Nevada Test Site bedrock occurs at a depth of 650 feet. The bedrock seismic velocity is about 10,000 ft. per second. Above the bedrock is an approximately 450 foot layer of sand and gravel having an average seismic velocity on the order of 3000 to 3500 ft. per second; above this is a 200 foot layer of

loess having an average seismic velocity of about 2000 feet per second. Since the ratio of acoustic impedances of the regions above and below the minus 200 ft. elevation is less than two, a sizeable reflection at the interface, even if well defined, is not expected. Thus the only sizeable reflection that could be expected in Nevada is that from bedrock. But the bedrock reflection must travel a distance of about 9 or 10 initial wavelengths. Thus even a conservative estimate of attenuation indicates that the reflected wave would have an amplitude less than 2 percent of the initial amplitude.

It is not surprising that no bedrock reflected wave is observed in Nevada; none should be expected.

In the Pacific the surface layer, not more than about 20 feet thick has a seismic velocity varying from 800 to 4000 ft. per second at water level. Below the water level a layer about 2500 feet thick has a average seismic velocity of about 800 ft. per second. Then below this is a layer 5 to 10 thousand feet thick having a seismic velocity of about 11,000 ft. per second.

At the 100 psi level the positive phase duration of a multi-megaton bomb is on the order of 2 seconds. At higher overpressures the positive phase duration increases but the time from peak overpressure to 10 percent of peak overpressure decrease. For these large durations the 20 foot surface layer is just a skin separating the aero-shock from the ground shock wave in the 800 ft/second layer. Thus the wave length of the entire positive phase in the 2500 ft. thick "surface" layer is about 1600 feet; the initial wave length of the portion of a 500 psi wave between 500 and 50 psi would be only about 500 ft. for a multi-megaton bomb.

Thus the reflected waves must travel a distance between three and ten initial wave lengths before appearing near the surface. The low seismic velocity exhibited is due primarily to the structured, porous nature of the coral island, and therefore the inelastic damping of the material is very high. If geometric attenuation and a percyclic damping factor of 0.5 are assumed, even at three initial wave lengths propagation the reflected wave will be attenuated to about 10 percent of its initial peak value and will arrive at the surface at least six seconds after blast wave arrival.

We conclude therefore that at the Pacific Proving Ground evidence of "bedrock" reflected waves should not be expected, particularly at the higher overpressures.

The Muskat, Meres paper cannot be taken as evidence that significant bedrock reflections will not occur; these authors did not consider that problem. Muskat and Meres have limited their data to an interface acoustic impedance ratio of 2.6 ($\bar{\gamma} \bar{\alpha}$ in their paper). The elementary one dimensional elastic theory indicates a reflection having only 20 percent of the incident wave energy at this ratio. At a soil rock interface occurring within one to two hundred feet of the surface the ratio would be more nearly seven to ten. At an acoustic impedance ratio of 7 the reflected energy is 55 percent of the incident energy. Further, the reflected pressure is 75 percent of the incident pressure. Surface displacement is proportional to the pressure.

Another argument against reflections in soil that is sometimes advanced is that the interface between particulate soil and rock generally is not sharp but consists of a five or ten foot layer of irregular rock surface, boulders, cemented soil, etc. The transition region presents formidable difficulties to analysis

so it may safely have imputed to it any set of mystical properties desired. The reflected wave above the transition region consists of the sum of an infinite set of multiple reflections and refractions taking place within the transition.

Here we will make no attempt to consider the problem mathematically but will present a simple physical discussion that clearly illustrates that the physical effect we generally choose to characterize as a mathematical reflection must occur in real soils and will have significant influence on surface motions.

Figure 3.1 shows schematically a column of real soil resting upon a relatively rigid bedrock. Between the two is a relatively thin but finite transition region.

If a pressure is applied to the surface of the soil and maintained, a wave is propagated into the soil column. Physically, the wave represents the distance within the soil column that is under compression, though the latter need not be constant within the wave. The compression causes the column to shorten and the surface pressure delivers energy to the soil equivalent to the product of surface pressure and surface displacement. The compression of any element of soil causes all elements above to move downward. Since the process is continuous all elements of soil acquire a velocity (particle velocity) which need not be equal for the various elements. The particle velocity results in the soil column acquiring kinetic energy.

In most real soils compression of the soil induces some heat. The sum of heat energy, kinetic energy and strain energy in the column at any instant is just equal to the energy delivered by the surface pressure acting through the distance the surface has displaced at that instant.

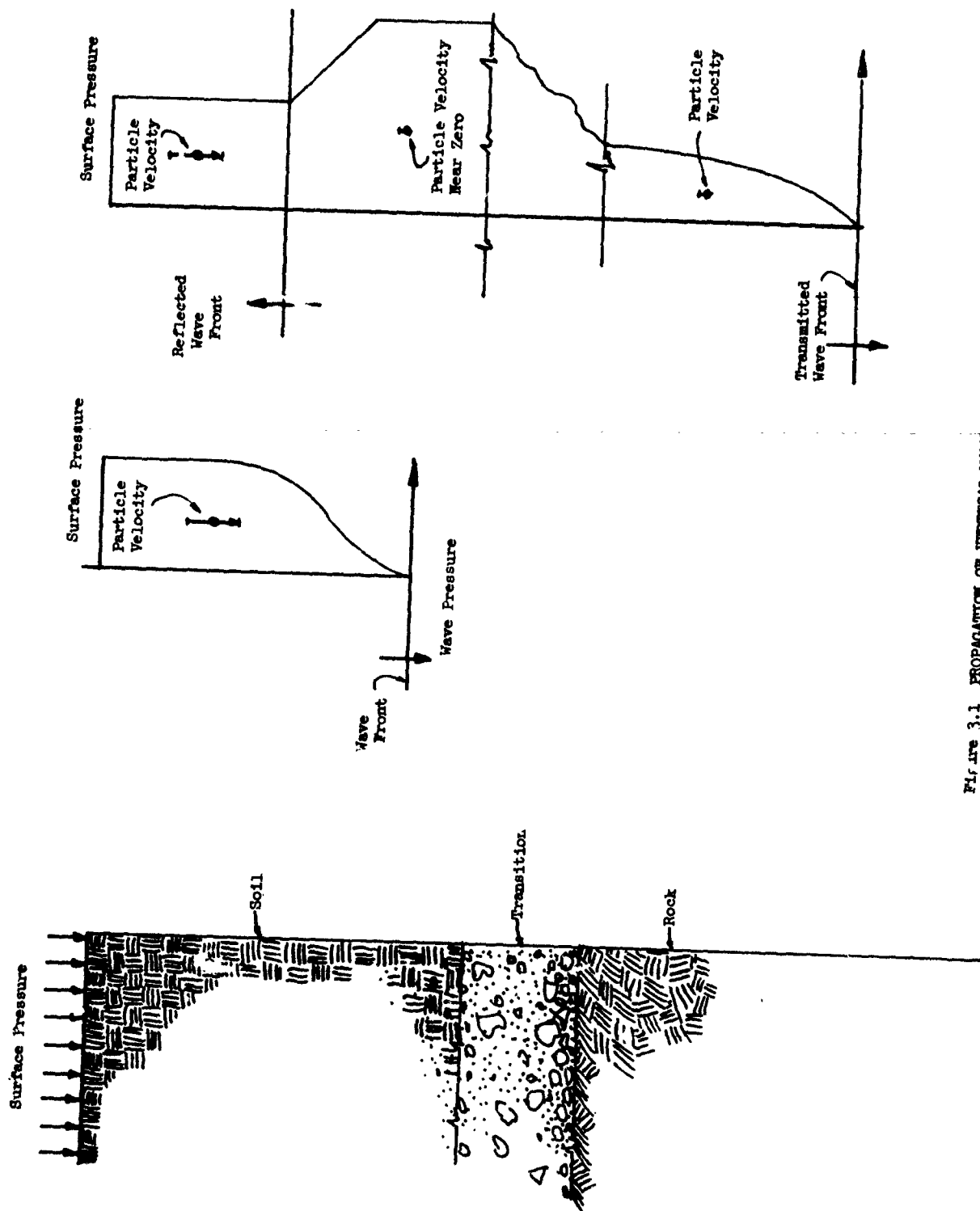


Figure 3.1 PROPAGATION OF VERTICAL WAVE INTO SOIL

When the wave front passes through the transition region into the bedrock a number of things can happen. Here we are concerned only with the fact that some wave does propagate into the rock. The pressure associated with this wave can be either higher or lower than the applied surface pressure. However, we have postulated that the rock be stiffer than the soil; therefore at a given unit strain a unit volume of rock contains more strain energy than an equivalent volume of soil. Thus if a unit volume of rock compressed as much as the soil above had been compressed, energy would be created, an impossibility. We conclude therefore that regardless of the detailed characteristics of soil and rock if the latter is stiffer than the soil the unit compression will be less than in the soil. This argument is independent of the rock-soil transition characteristics.

Now if the unit compression in the rock is less than that in the soil the velocity gained by the rock is less than that already established in the soil. The result is that the soil piles up against the rock, the pileup commencing at the interface and proceeding to the surface. (This is the reflected wave). During the pileup the soil particle velocity is reduced to the rock surface (particle) velocity and the difference in kinetic energy is converted into soil strain energy and heat. The additional strain in the soil induced by the pileup causes the surface to further displace and allows the applied pressure to deliver more energy to the column. However, the stress induced in the soil is greater than the applied pressure so when the pileup reaches the surface it immediately moves upward the surface on which the pressure is applied, causing the soil column to expand and the surface to receive an upward motion component.

At this point the surface pressure is insufficient to maintain the compression in the pile so the latter relaxes starting at the surface and proceeding downward. This is the surface reflected tension wave.

Now, it should be evident that a finite transition region between the rock and soil can affect only the initial details of the process but not the gross results.

If the rock were so stiff that it could be considered with tolerable error to be infinitely rigid then nearly all of the kinetic energy in the soil would be converted into strain energy and heat. The "nearly" qualification is used because for the most real materials all of the particles in the soil would not simultaneously be reduced to zero velocity. Evidently however, from physical reasoning, the residual velocities remaining in particles after engulfment by the reflected wave must be small. Thus for a first estimate, the surface displacement induced by the reflected wave would be equal to the displacement necessary to accommodate as strain energy the algebraic sum of three energy components:

1. The kinetic energy left in the soil by passage of the initial compression wave (positive),
2. The energy delivered to the soil by the surface pressure acting through the additional surface displacement induced by the reflected wave (positive),
3. The energy lost as heat (negative).

The real blast wave decays with time and consequently detailed analysis becomes quite complex. However, we can make a fair estimate of the additional

surface displacement by considering the stress strain curve of the soil. In order to simplify the discussion a nonlinear elastic soil will be considered, i.e., one that does not generate heat during compression. (Such a soil probably does not exist.) Since the heat generating process (hysteresis) produces permanent displacement this restriction will not impose unrealistic results.

Figure 3.2 schematically shows the stress strain curve of a hypothetical nonlinear elastic soil. If pressure and velocity variations are not too great the same curve can be taken as a reasonable approximation of the average stress versus average strain in a finite column of soil.

Now, consider a column of soil loaded at a constant pressure, p . The displacement of the surface is proportional to the soil strain. Thus in Figure 3.3 the abscissa noted is proportional to the initial surface displacement for a soil column of fixed length.

The energy delivered to the column by the surface pressure is equal to the product of pressure and displacement. This is proportional to the area of rectangle OADE in Figure 3.3. Now the strain energy in the soil is proportional to the area under the curve ODA. Therefore, since there is no heat loss in the nonlinear elastic soil the kinetic energy in the column is proportional to the shaded area ODE. We emphasize again that these relations would be strictly true only if the pressure pulse traveling in the soil were a step wave having a clean shock front. Then the compression would be constant within the loaded column of soil and the relations described here would be valid. In fact, however, a step pulse is not conserved in a nonlinear elastic soil. Therefore these relations are at best reasonable approximations to the true conditions within the soil.

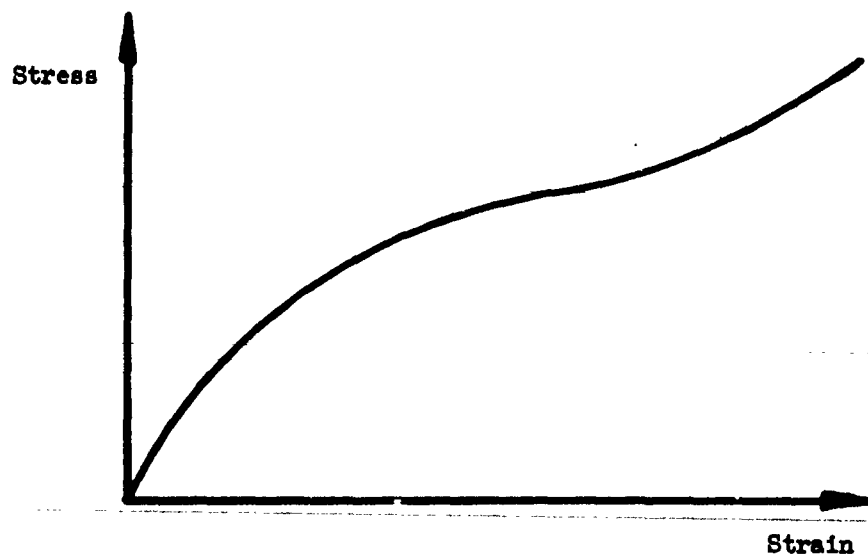


Figure 3.2 STRESS-STRAIN CURVE OF
HYPOTHETICAL NONLINEAR ELASTIC SOIL

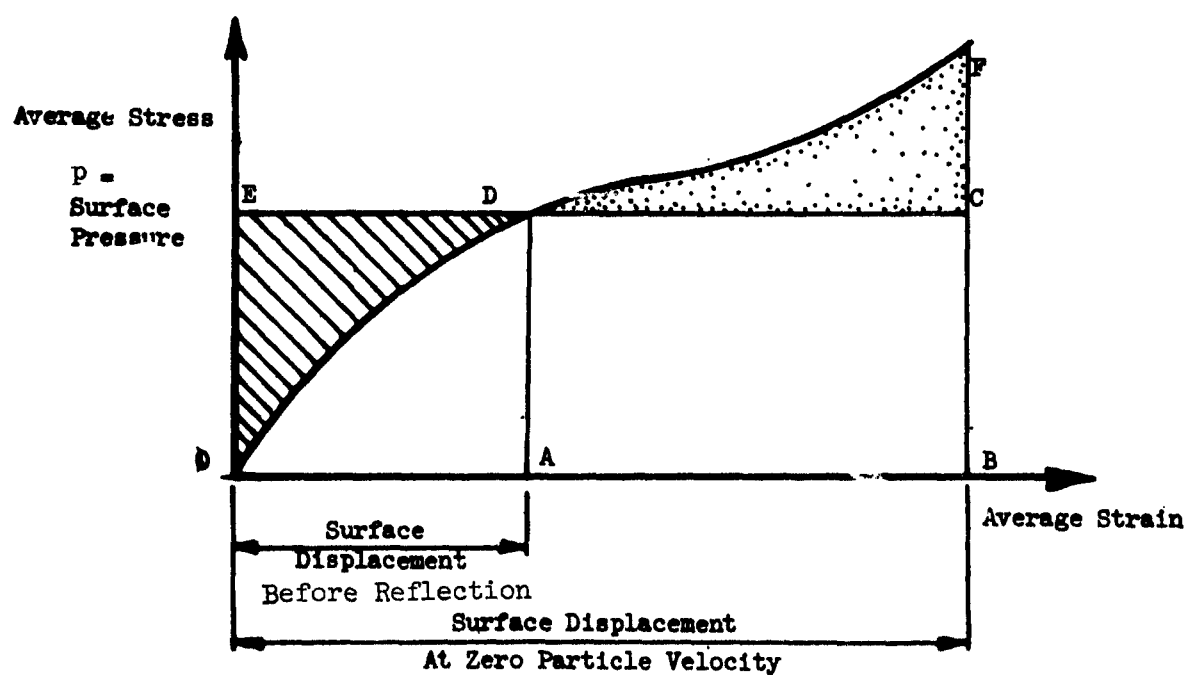


Figure 3.3 SURFACE DISPLACEMENT INDUCED BY
CONVERSION OF SOIL KINETIC ENERGY TO POTENTIAL ENERGY

Upon reflection, the kinetic energy is converted into strain energy causing the surface to displace an additional amount AB , and the total energy delivered to the column by surface pressure is then proportional to the area of rectangle $OBCE$. If the velocities of all particles simultaneously become zero then this energy would have to be equivalent to the strain energy proportional to the area $ODFCBA$. Thus, for these conditions the shaded area ODE would have to be equal to the stippled area DCF , and the ratio of reflection induced surface displacement to the primary wave induced surface displacement would be equal to the ratio $\frac{AB}{OA}$.

For a linear elastic medium this ratio is just unity. Evidently however, for the hypothetical soil illustrated in Figure 3.3 this ratio can be considerably greater than unity. For other stress strain curves it might be less. Computations are further complicated in a real case because some heat may be developed, a portion of this heat being reversible and the remainder irreversible. Neglect of the heat, however, is conservative for design because its neglect implies greater kinetic and strain energy than actually occur.

There is no doubt that when a decaying surface pressure wave, hysteretic medium and geometric attenuation are considered, the ratio of reflected wave induced to primary wave induced surface motion can vary widely from the oversimplified conditions of Figure 3.3. Our point is that whatever the "exact" value of the ratio, neglect of this factor in many real instances would introduce an error or uncertainty greater than the uncertainty in any other parameter influencing the ground motion problem.

3.2 Suspension Frequency Range

Consider the principal characteristic of the vertical motion of a particle in the free field. The particle is motionless until the wave front of the ground

shock wave arrives. Then, due to the rise time of the wave the particle experiences a rapid increase in velocity to a peak value. The time required for this to occur is on the order of a few milliseconds. Subsequently the wave continues to bedrock and reflects, the reflected wave ultimately engulfing the particle. If the wave had a flat top and reflection at bedrock approached that of perfect reflection from an infinitely rigid surface, the velocity of the particle would remain constant during this interval. Then at engulfment by the reflected wave the velocity of the particle would decrease to zero.

because of the departure of real soils from the idealized elastic assumptions, the imperfect reflection at bedrock, the decay of the wave subsequent to peak pressure, dissipation of the wave energy as it travels, and the fact that not one wave but a series of waves are actually involved, the general character of the particle velocity history is somewhat modified. But its overall character can be represented by

1. A rapid rise of a few milliseconds.
2. A nearly constant plateau followed by a slow decay, the total occupying a time period on the order of $1/4$ second for large bombs, and deep (100-200 feet) bedrock.
3. A rapid decay through zero to a small negative value.
4. A decaying negative velocity of long duration.

The directly transmitted ground shock component is superimposed on this.

It should be appreciated that the motion of the selected particle is physically due to the compression of the soil between the particle and bedrock plus any bedrock motion. Thus since a uniform wave advancing at nearly constant

velocity compresses the soil at a uniform rate the velocity of any selected particle above such a wave would be nearly constant.

From the above we can see that the simplest approximation to free field particle velocity is a velocity step function. This can be made more realistic by imposing a short rise time, a decay rate dependent on bomb size and possibly soil characteristics, and finally terminating the velocity pulse at the time required for the ground shock wave to make the round trip from particle to bedrock and back to particle. (These assumptions would imply permanent displacement of the surface.)

If a structure of finite size were immersed in the soil the motions observed at a point on the structure interior would differ from those in the free field. A reasonably proportioned structure (even very unreasonably heavy structures) will be lighter than the soil displaced; therefore it may be regarded as a captive bubble in the soil. When engulfed by the ground shock wave the bubble deforms and reflected waves are radiated from its surface. Depending on structure rigidity as compared with soil rigidity the reflected waves may either increase or decrease the interface pressure.

Now it should be evident that at some time subsequent to engulfment the captive bubble will be "riding" with the surrounding free field. Thus the net overall effect of soil-structure interaction is to increase the rise time of structure interior velocity. Roughly, this rise time increase is equal to the time required for the wave to engulf the structure, a few milliseconds for silos and one to two tenths of a second for large command centers. Evidently, from the

standpoint of shock isolation the soil-structure interaction becomes more important with increasing structure size.

Consider now the basic problems to be faced in designing an isolator. We will not complicate the discussion by considering damping, inelastic effects, etc. .

The first and possibly most important questions to be answered are "Is any shock isolation required; does the structure provide enough for this equipment?" These questions, we will find, can be the most difficult to answer; here we assume that isolation is required.

The ultimate isolator would have zero natural frequency thus supporting the suspended equipment in an absolutely motionless state while allowing the supporting structure to move around it. At the present state of technology such isolators are very nearly achievable at not unreasonable cost. However, the rattle space required by such an isolator is the maximum occupied by a reasonable design (an unreasonable design could increase it). If some acceleration of the suspended equipment could be tolerated the rattle space could be decreased. Since decrease of rattle space may be reflected as savings in cost of the entire installation a knowledge of the tradeoff between isolator rattle space required and acceleration of equipment to be tolerated can be very useful.

The tradeoff criteria need not be highly accurate. Decrease of rattle space from 12 inches to 11 inches would not ultimately appear as a dollar savings; decrease from 12 inches to 6 inches however might justify a reduction in structure size and be reflected as a real dollar value.

The peak relative response spectrum of the forcing function described above fairly closely follows the conventional trapezoidal spectrum used in missile

shock isolation design. On the left hand, or displacement leg of the spectrum, changes in isolation frequency will vary the acceleration suffered by the suspended equipment but the rattle space required would remain invariant. On the horizontal, or velocity branch of the spectrum, the product of displacement and acceleration remains invariant with changes of frequency.

Reference to Figures 2.17 to 2.22 of the Newmark-Hansen report shows that the "velocity plateau" of spectra for simple pulses of duration t_d and having the general character of the ground shock induced velocity extends across the range of $t_d f$ between about 0.4 to 1.0 and has a maximum pseudo velocity about 1-1/2 times the maximum velocity of the input pulse.

Thus if rattle space is to be decreased by employing a stiffer isolation system the minimum isolator frequency that could be used would be on the order of

$$f_{\min} \approx \frac{0.4}{t_d} \text{ cycles per second} \quad (3.1)$$

The peak absolute acceleration, α , in gravity units would be given by

$$\alpha = \frac{4\pi^2}{g} z_{\max} f_{\min}^2 \quad (3.2)$$

where z_{\max} is peak relative displacement.

Now peak soil particle velocity is given by

$$V = \frac{P_O}{\rho c} \quad (3.3)$$

where

P_O is peak overpressure and

ρc is the average acoustic impedance of the soil.

The maximum relative displacement, z_{\max} , is equal to the maximum soil displacement for the conditions being considered. Thus

$$z_{\max} = \beta V t_d = \frac{\beta p_o t_d}{\rho c} \quad (3.4)$$

where β is a factor, somewhat less than one, so chosen that $\beta V t_d$ equals the area under the velocity curve.

Also, the duration, t_d , is given approximately by

$$t_d \approx \frac{2D}{c} \quad (3.5)$$

where D is the depth of soil between the isolator and bedrock.

Combining these approximations yields

$$\alpha(g) = \frac{450 \beta [p_o(\text{psi})]}{[\gamma(\text{pcf})] [D(\text{ft})]} \quad (3.6)$$

where γ , the unit weight of the soil has been substituted for ρg .

Now, it should be noted that the three parameters remaining in Equation (3.6) are those most accurately known, the wave velocity, c , having cancelled out. Therefore Equation (3.6) gives an excellent estimate of the minimum acceleration that must be withstood if designs are to be made on the horizontal branch of the shock spectrum.

If we take

$$\begin{aligned} \gamma &= 110 \text{ lbs/ft}^3 \\ D &= 100 \text{ ft} \\ \beta &= 0.85 \end{aligned}$$

we obtain

p_o	100 psi	300 psi	500 psi	1000 psi
α	3.5 g	10.5 g	17.4 g	34.8 g

We conclude immediately that the experience already obtained on hard installations, which indicates that shock isolation systems are almost universally designed for frequencies on the displacement leg of the spectrum, is indicative of design conditions for future higher pressure installations. Only small ruggedized equipment is likely to be installed at the higher g levels. Thus for most work we will have to use low frequency systems designed for rattle space equal to the entire soil motion.

Accepting that the systems used will have to be low frequency maximum input displacement systems, we ask ourselves if there is an optimum frequency on the displacement leg of the spectrum. It is fairly simple to show that there is.

For a first order estimate the cost of a spring suspension system is proportional to the weight of the springs provided. The weight of the springs in turn is proportional to their energy capacity.

Now the energy capacity of linear springs is equal to one half the product of the total stroke of the springs and the force developed at total stroke. The total stroke is equal to the equilibrium stroke ("static deflection", or distance the spring compresses when the equipment to be isolated is placed upon it) plus the working stroke.

At the equilibrium position the force exerted by the springs is equal to the suspended weight, i.e., in proportion to one g acceleration; at total stroke the force is proportional to ng acceleration, n being the maximum design acceleration of the system including gravity.

Denote

U	=	total spring energy
x	=	equilibrium stroke
z	=	working stroke
w	=	weight of isolated equipment
F_t	=	spring force due to total stroke
F_x	=	spring force due to equilibrium stroke
k	=	spring constant

Then

$$W = F_x = kx \quad (3.7)$$

$$F_t = k(x + z) \quad (3.8)$$

$$\frac{F_t}{F_x} = n = \frac{x + z}{x} \quad (3.9)$$

$$U = \frac{1}{2} F_t (x + z) = \frac{1}{2} k (x + z)^2 \quad (3.10)$$

$$U = \frac{1}{2} wxn^2 \quad (3.11)$$

Now, for a given system w and z are invariant but x depends on the value of n chosen. Then for minimum energy

$$\frac{dU}{dx} = 0 = \frac{1}{2} w \left[\hat{n}^2 + 2nx \frac{dn}{dx} \right] \quad (3.12)$$

$$0 = \hat{n} + 2 \frac{dn}{dx} \hat{x} \quad (3.13)$$

where

\hat{n} is the value of n

and \hat{x} is the value of x satisfying Equation (3.13).

From Equation (3.9)

$$\frac{dn}{dx} = \frac{1}{x} - \frac{(x+z)}{x^2} \quad (3.14)$$

Substituting Equations (3.9) and (3.14) into (3.13)

$$0 = \frac{\hat{x} + z}{\hat{x}} + 2 - 2 \frac{(\hat{x} + z)}{\hat{x}} \quad (3.15)$$

Solving yields

$$\hat{x} = z \quad (3.16)$$

$$\text{and} \quad \hat{n} = 2 \quad (3.17)$$

Thus the minimum energy vertical linear spring system will be obtained if the spring constant is chosen so that the equilibrium stroke is equal to the working stroke. The total acceleration including gravity on the isolated equipment during passage of the blast wave then will vary between 0 and 2 g.

Since the equilibrium energy of a lateral isolation system can be made zero the energy capacity of the lateral system can be made indefinitely low by decreasing the system frequency, and cost will be purely a function of the mechanical devices elected by the designer.

3.3 Available Accuracy

The uncertainty in input parameters limits the accuracy with which shock isolation computations can be carried out.

If criteria are available for establishing the limits of accuracy available they can be used to establish the degree of complexity that will be meaningful in carrying out the computations.

It is shown in Section 3.2 that, if isolators are required, in the majority of instances low frequency systems are indicated. In fact, the minimum energy (and probably minimum cost) systems have the natural frequency of oscillation so chosen that the active stroke of the isolator is equal to the equilibrium stroke.

The period of vibration of a linear mass spring system, T , is given by

$$T = 2\pi\sqrt{\frac{x}{g}} \quad (3.18)$$

where x is the equilibrium stroke, i.e., the static displacement.

For the one g system having equilibrium stroke equal to working stroke

$$x = z_{\max} \quad (3.19)$$

Substituting Equation (3.5) into (3.4) yields

$$x = z_{\max} = \frac{2\beta p_{\sigma} D}{\rho c^2} \quad (3.20)$$

Therefore

$$T = \frac{2\pi}{c} \sqrt{\frac{2\beta p_{\sigma} D}{\gamma}} \quad (3.21)$$

Dividing this by the approximate duration of the velocity pulse, Equation (3.5)

$$\frac{T}{t_d} = \pi \sqrt{\frac{2\beta p_{\sigma}}{\gamma D}} \quad (3.22)$$

We note that again the more inaccurate parameters have cancelled out and that Equation (3.22) therefore gives an excellent estimate of the ratio T/t_d .

Choosing

$$\begin{aligned} \beta &= 0.85 \\ \gamma &= 110 \text{ lbs/ft}^3 \\ D &= 100 \text{ ft, } 200 \text{ ft} \end{aligned}$$

for

	P_{σ}	100 psi	300 psi	500 psi	1000 psi
$\frac{T}{t_d}$	D = 100 ft	4.9	8.5	11	15.4
	D = 200 ft	3.5	6	7.7	12

We conclude that most systems will be designed by impulse methods requiring for their input only the peak displacement of the soil. The exceptions would occur at the lower overpressure levels, systems in structures large enough to considerably modify the input motion by soil-structure interaction and possibly systems in which isolation devices were omitted.

Therefore the limiting accuracy available for design of most isolation systems can be determined by considering the accuracy with which the peak input displacement can be determined.

First consider the approximate Equation 3.20.

$$z_{\max} = \frac{2\beta p_{\sigma} D}{\rho c^2} \quad (3.20)$$

The relative error $\Delta z/z$ is given by

$$\frac{\Delta z}{z} = \frac{\Delta \beta}{\beta} + \frac{\Delta D}{D} - \frac{\Delta \rho}{\rho} - \frac{2\Delta c}{c} \quad (3.23)$$

Now the average value of ρ will be known to within two or three percent accuracy if soil samples are taken. The depth D can be measured to within a couple of feet by seismic means but most likely will vary from point to point at a particular site resulting in a larger average error. Probably, if the average value could be determined to ± 5 percent (100 ft ± 5 ft) we would have to be satisfied.

The average wave velocity, c , reflects the nonlinearities of the stress-strain curve of the soil, the soil hysteresis, and in Equation 3.20 all of the other approximations to the "elastic constants" of soil. (We note that the denominator of Equation 3.20 is equivalent to the modulus of elasticity of the soil, possibly the least accurately determinable soil characteristic.) One is hard put to make even a good estimate of the accuracy with which c can be determined. However, the seismic velocity, c_1 , can be measured to two significant figures. Wilson (Reference 12) suggests that the velocity of the peak pressure be taken as $1/2$ to $3/4$ of the vertical seismic velocity. Accepting Wilson's estimate we could take for the compression wave velocity $5/8 \pm 1/8$ of the seismic velocity of the soil, an inherent error of ± 20 percent.

If the overpressure level is in the vicinity of the plateau of the soil stress strain curve the reflected wave will travel faster than the incident wave due to the precompression induced by the incident wave. Because of the large inherent error it does not seem reasonable to attempt to distinguish between these velocities in computation. Therefore it is suggested that, lacking actual test data the average compression wave velocity be taken as equal to 66 ± 15 percent of the uphole seismic velocity recognizing that the error given is approximate.

In circumstances where the reflected wave does not add to the incident wave it is suggested that, lacking test data, the compression wave velocity be taken as 60 ± 20 percent of the uphole seismic velocity.

At the high overpressure levels (≥ 1000 psi) some accuracy in the calculations can be gained by making use of the fact that by the time the reflected wave arrives the overpressure will have decayed to a small fraction of its peak value.

Maximum surface displacement will occur at the instant of peak reflected pressure arrival except in the rare instances where soil attenuation is so great that a point is reached where rate of attenuation of pressure just balances the rate of increase of impulse delivered to the soil by the aeroshock wave.

Excepting the latter condition the maximum displacement is given by

$$x = \frac{I_d}{\rho c} \quad (3.24)$$

where

x is the peak displacement

ρ is the average soil density

c is the average compression wave velocity

I_d is the impulse given by

$$I_d = \int_0^{\frac{2D}{c}} p(t) dt \quad (3.25)$$

D is the distance from structure to bedrock

and $p(t)$ is the pressure in the soil including the effects of attenuation with distance traveled.

Now if $2D/c$ is a time sufficiently long that it represents a major fraction of the positive phase duration the impulse I_d will be very insensitive to D and c . From the elementary differentiation formulas the relative error in x is given by

$$\frac{\Delta x}{x} = - \left(\frac{\Delta c}{c} + \frac{\Delta \rho}{\rho} \right), \quad (3.26)$$

I_d being presumed accurately known when formula 3.24 is used.

Now the density of a soil is probably its most accurately known quantity; the ratio $\Delta\rho/\rho$ usually can be taken as no more than 5 percent if the soil at the site is known. The wave propagation velocity however is known with considerably less accuracy, particularly at higher overpressures and for the more inelastic soils. Indeed, for real soils it can only be an approximate, average estimate of a variable quantity of considerable complexity. An estimate of ± 20 percent for $\Delta c/c$ generally would be quite good.

Thus the percent error in displacement resulting from use of the simple formula and inherent input data error is on the order of ± 25 percent.

Some engineers might question the accuracy of the formula because it is based on elastic theory and is being used, with appropriate parameter approximations, for an inelastic medium. They might argue, and quite reasonably, that for the inelastic medium there is not justification for taking

$$E = \rho c^2 \quad (3.27)$$

which is done in the development of Equation 3.24. Instead, they might prefer to use

$$x = \frac{I_d c}{E} \quad (3.28)$$

which is more primitive than Equation 3.24, and estimate an average effective value of E independent of propagation velocity.

The relative error in x resulting from Equation 3.28 is

$$\frac{\Delta x}{x} = \frac{\Delta c}{c} - \frac{\Delta E}{E} \quad (3.29)$$

Now there is probably no more difficult quantity to measure and estimate for an inelastic soil than the effective modulus of elasticity. Even with laboratory tests accuracy better than about ± 20 percent is unlikely. Thus by the use of Equation 3.28 the error in x would be ± 40 percent, 50 percent higher than would be obtained by use of Equation 3.24.

SECTION 4

DETERMINATION OF FREE FIELD INPUT

In Section 3 it is shown that an error on the order of ± 20 percent must be tolerated in the determination of input to shock isolation systems. Indeed, in many real situations even this accuracy could be obtained only with the aid of an extensive field and laboratory test program.

It also is pointed out in Section 3 that if shock isolation systems are used they will be low frequency systems. In relatively small structures the influence of soil-structure interaction on system design will be nominal with a low frequency system. In subsequent sections of this report it is shown that the accuracy obtainable with existing simplified soil-structure interaction theories is considerably better than the input error that must be tolerated.

Now, since the actual design of an isolator to resist an established input can be carried out with scientific precision, if desired, the principal source of error in the entire design problem is the error in the input.

Inasmuch as errors on the order of ± 20 to 30 percent will be involved in a shock isolator design, a strong case could be made for adopting some simple convention and be done with it. It can be argued, quite reasonably, that if we must guess the input we may as well guess the result.

Two counter arguments can be advanced:

1. As a consequence the possibility that shock isolation can be eliminated from a particular system could not be considered.

2. Such an approach would effectively stop further progress in the field of nuclear shock isolation.

Therefore it is believed to be necessary for this report to present methods that are rational and as accurate as practical within the present state of the art for determination of the free field ground shock input characteristics. Since the accuracy level of a given design will reflect the accuracy of the input, this phase of the shock isolation design problem deserves a greater portion of the designer's time than any other aspect of the overall problem.

A considerable program in the general area of nuclear blast induced ground motions is currently being carried out by a number of government agencies and contractors. Already a substantial literature on the subject has developed. However, to date a single consistent theory covering the several elements of ground motion and real soils has not been forthcoming. Even a digest of the theoretical and experimental data already developed would be of substantial volume and, because of gaps in the data and internal contradictions would be of limited value to designers.

In view of this situation the estimation procedures contained in this section must be regarded as tentative, to be replaced with more accurate procedures as the results of research effort become available. However it is believed that since a substantial error must be tolerated in any event, a single internally consistent approach that covers the major influences significant to the shock isolation problem is desirable. In particular, if the effects of soil-structure interaction and the possibility that isolators might be omitted are to be considered in any detail, ground shock input wave forms are required. Since

practically all of the published methods for making ground shock estimates are directed solely toward estimation of the three numerical input parameters required for construction of a trapezoidal shock spectrum, considerable departure from these methods has been necessary.

The difficulties inherent in the theoretical prediction of ground waves in real soils ultimately hinge on the nonlinear, inelastic behavior of the soils. Propagation velocity, energy attenuation, wave diffusion, and permanent displacement all are primarily influenced by these characteristics.

A procedure for determining the significant characteristics of the input wave that requires a minimum of soil data is presented subsequently. Data required are

1. the stress-strain curve of the soil (confined compression test)
2. the seismic velocities of the soil
3. the soil density
4. the pericyclic damping factor
5. bedrock depth.

It is assumed that the dissipation process conforms with the pericyclic damping theory. This theory postulates that a sinusoidal wave decays exponentially at a certain rate per cycle. Thus the fraction of the amplitude that remains after propagating through a distance of one wave length, as compared with the initial amplitude of the wave, is a constant and is denoted by $e^{-\delta}$. The theory assumes that the speed of propagation and the pericyclic decay rate for sinusoidal waves are independent of wave frequency and stress level and dependent only on material properties. For a waveform that is not sinusoidal, the waveform is

represented by a Fourier integral of sinusoidal components, each of which is assumed to obey the pericyclic damping law independently. Each component, having a different wave length, decays a different amount in traveling a given distance because it travels a different number of wavelengths. The waveform at any later time is represented by a Fourier integral of the decaying sinusoidal components.

The pericyclic damping theory, though based on artificial assumptions, is found to agree well with experimental data and has found acceptance by leading investigators in the field of stress wave propagation. Values of the logarithmic detriment, δ , ranging approximately from 0.2 to 0.5 have been reported for granular media. Some typical values are given in Section 8.

The design procedure has been simplified somewhat by making the assumption that bedrock is infinitely rigid and perfectly reflecting. The combined effects of these assumptions is slightly conservative. That is, the motions predicted are somewhat greater than would be predicted if the exact physical characteristics of the bedrock were taken into account.

Regardless of the energy dissipation characteristics of the soil, the momentum of the ground shock wave is conserved as it proceeds through the soil. Ultimately all of the momentum enters the underlying bedrock. If the effects of geometric dispersion of the wave are neglected, the displacement of the bedrock due to the momentum can be computed from the formula

$$y = \frac{I}{\rho c} \quad (4.1)$$

where

y is the bedrock displacement

I is the impulse of the ground wave.

Though the waveform may be considerably changed by passage through the soil and rock, since its momentum is conserved its impulse is conserved and is equal to the impulse of the overpressure wave.

At the 1000 psi level, for a bedrock weighing 160 pounds per cubic ft. and having a seismic velocity of 10,000 ft per second, a one megaton bomb would produce a rock surface displacement of about 1.9 inches, geometric dispersion being neglected; a 20 megaton bomb would produce a rock surface displacement of about 5.2 inches.

However, in the bedrock the wavelength of the positive phase from the one megaton bomb would be greater than 12,000 feet. The initial root of the product of the two principal radii of curvature of the shock front at the 1000 psi region would be about 7,000 feet, dependent on the soil wave propagation velocity. Therefore, geometric attenuation would reduce the surface displacement to about $1/4$ of the value computed above, or about $1/2$ inch for the one megaton bomb and $1-1/2$ inches for the 20 megaton bomb. These figures are very small fractions of the total displacement of soil surface with respect to bedrock. Further, the soil displacement computed as a consequence of assumed 100 percent reflection from bedrock more than compensates for these small errors.

4.1 The Input Wave Estimate

Determination of the input waves is carried out in 5 steps:

1. The overpressure wave is estimated.
2. The compression wave propagation velocity is estimated.
3. The attenuation of the compression wave is estimated.

4. The compound wave resulting from addition of primary wave and bedrock reflection is estimated.
5. The vertical and horizontal free field input waves are estimated.

The above steps are considered in order in Sections 4.1.1 through 4.1.5. Where desirable a brief discussion of the theory is included though in the main the theory has been described in the references and is not repeated.

The reader is cautioned that the methods presented here are approximate. Studies now under way will provide more accurate data on subsurface waveforms. Because of the importance of input data accuracy these data should be used for applicable conditions when they become available.

4.1.1 The Overpressure Wave

In a series of classified reports Brode has presented theoretically determined overpressure waveforms resulting from a surface burst. In Reference 2 Brode presents overpressure data in unclassified form. Figure 4.1 was constructed from the unclassified data, some extrapolation being necessary at the very high overpressure levels. The curves on Figure 4.1 enable a 5 point fit of the overpressure wave between the limits of peak overpressure and 10 percent of peak overpressure.

The dashed curve gives the subtangent duration, the time at which the overpressure has decayed to $1/e$ times peak overpressure. If the initial portion of the blast wave were a true exponential, the subtangent duration would be equal to the time interval subtended by the tangent to the overpressure curve at peak overpressure.

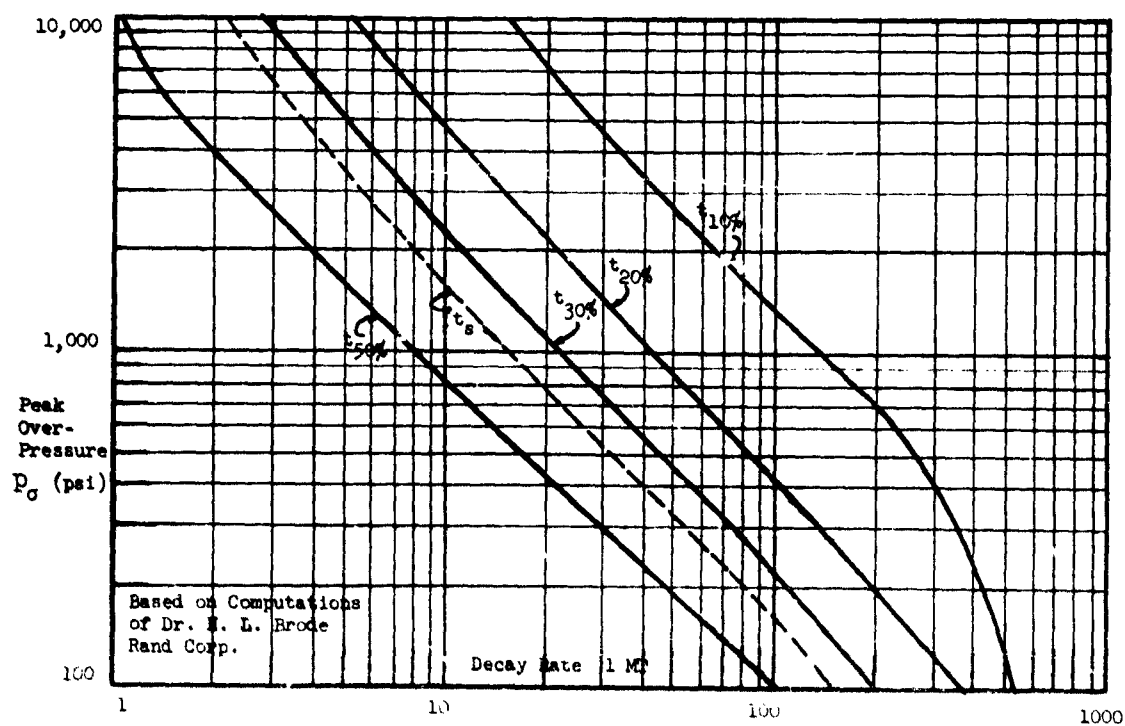
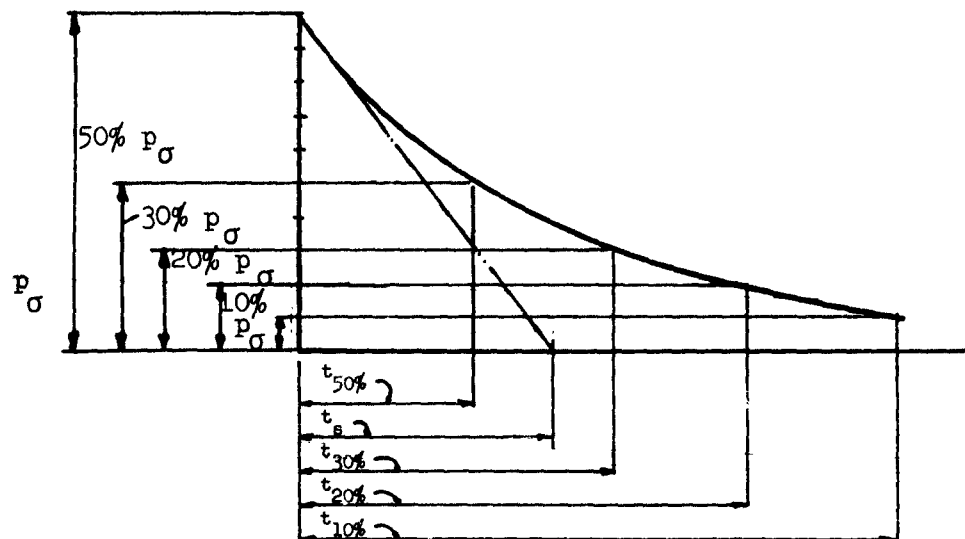


Figure 4.1 OVERPRESSURE DECAY RATE

Within the intervals between the points given in Figure 4.1 the waveform can be taken as an exponential, the decay constants differing from interval to interval. The notation and formulas are given in Figure 4.2.

It should be noted that the first derivative of the approximate curve jumps at the transition points. Therefore accelerations should not be computed from the approximation.

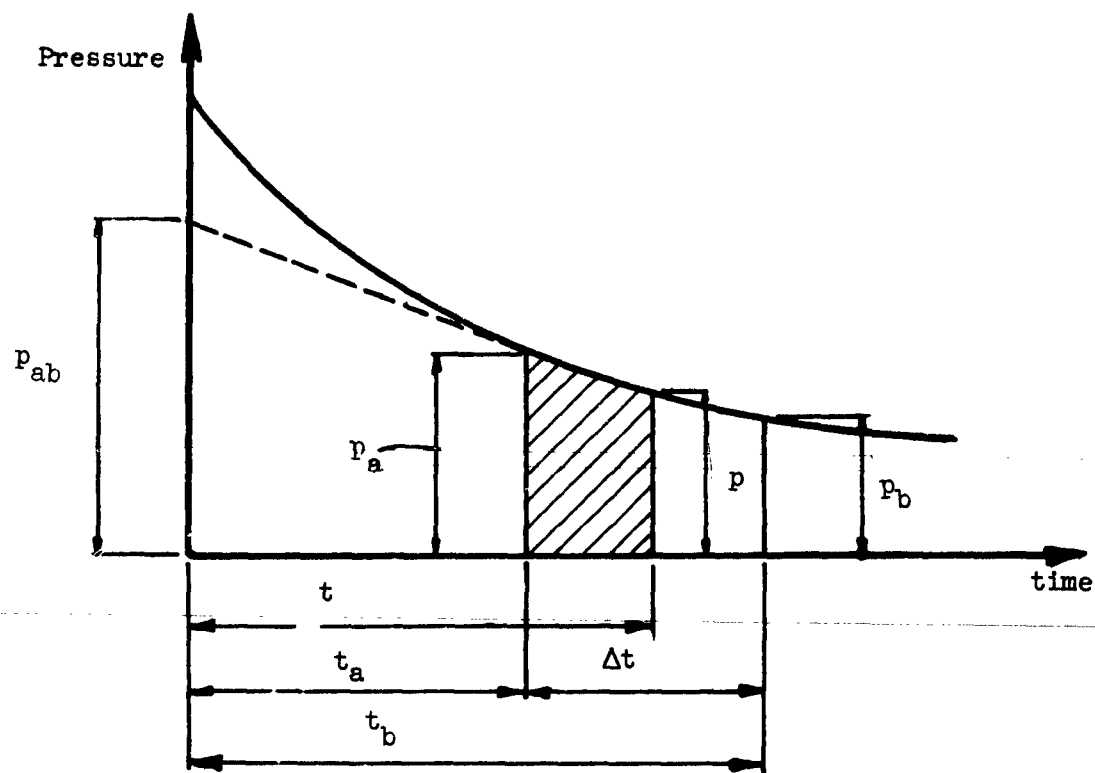
4.1.2 Wave Velocities

The average modulus of elasticity and, equivalently, average wave velocities of a real soil contribute the greatest factor of uncertainty to shock isolation design. The material in this section is presented in an effort to enable the designer to improve his estimates. It is emphasized however that no tests have been conducted to prove or disprove the method though data reported for other purposes do not contradict the approach.

In order to carry out the estimation procedure the data previously listed are required.

Even if these data are only estimates themselves some improvement in the accuracy of the input can be achieved over that obtainable by simply taking the compression wave velocity as $1/2$ to $3/4$ of an estimated seismic velocity.

Figure 4.3a schematically shows a stress-strain curve for a sandy soil. Now, a pressure wave initially of the same waveform as the overpressure wave would be dispersed in propagating through the medium, that is the peak would be attenuated and would lag behind the "toe" of the wave which would be of zero amplitude and propagate at seismic velocity c_1 . Between the toe of the wave and



$$p = p_{ab} e^{-\alpha_{ab} t}$$

$$\alpha_{ab} = \frac{1}{\Delta t} \log_e \frac{p_a}{p_b}$$

$$p = p_a \left(\frac{p_b}{p_a} \right)^{\frac{t - t_a}{\Delta t}}$$

$$I_{ab} = \text{Impulse in interval } \Delta t$$

$$I_{ab} = \frac{p_a - p_b}{\alpha_{ab}} = \frac{(p_a - p_b) \Delta t}{\log_e \frac{p_a}{p_b}}$$

$$I_{at} = \text{Impulse of shaded area}$$

$$I_{at} = \frac{p_a}{\alpha_{ab}} \left[1 - \left(\frac{p_b}{p_a} \right)^{\frac{t - t_a}{\Delta t}} \right]$$

Figure 4.2 APPROXIMATION OF BLAST WAVE BY EXPONENTIAL INCREMENTS

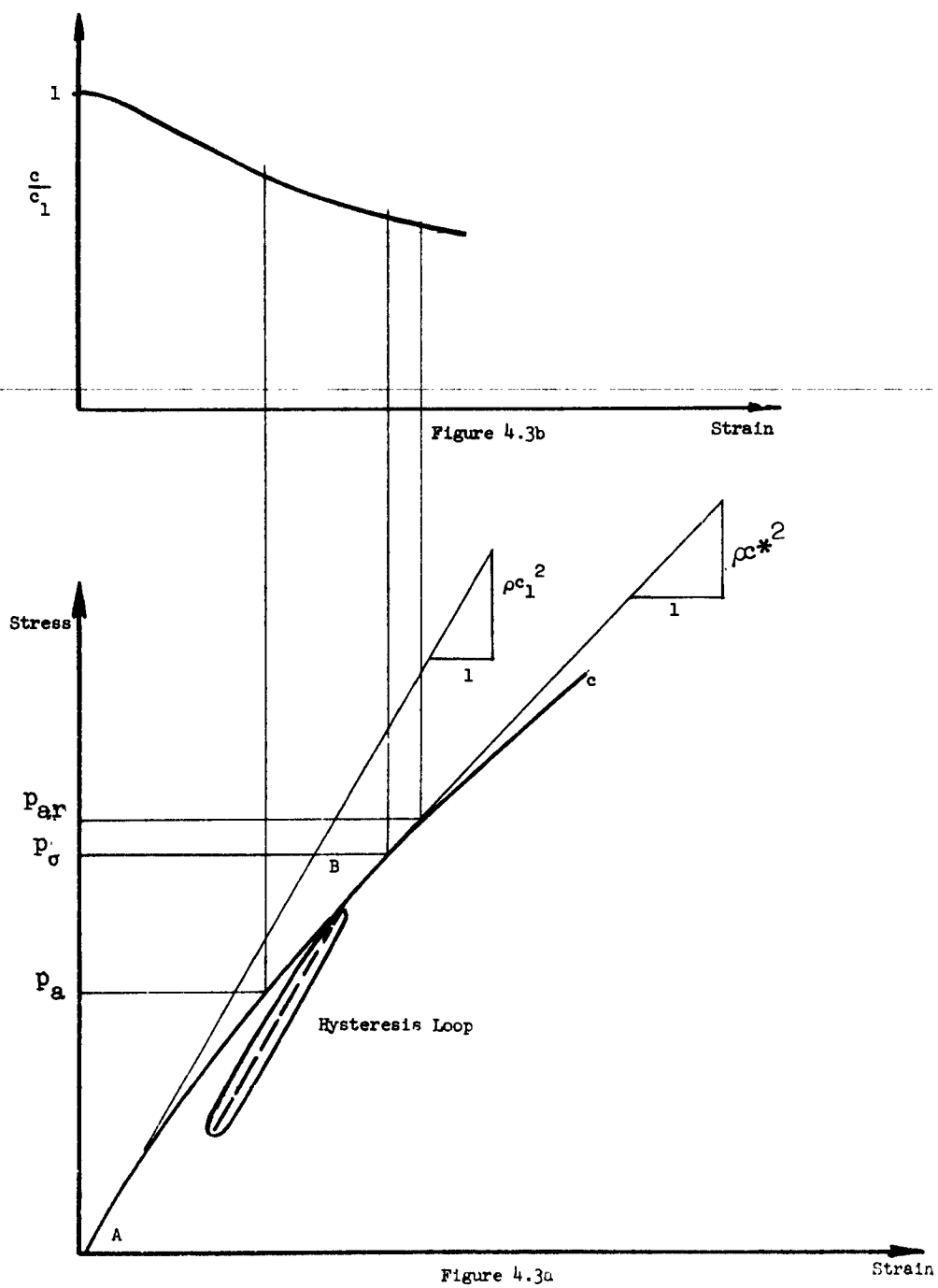


Figure 4.3 CONFINED COMPRESSION STRESS VERSUS STRAIN

the maximum the pressure would be continually increasing. Therefore, each element of the rise would propagate at the instantaneous velocity c^* defined as shown in Figure 4.3a.

The relation between instantaneous wave propagation velocity, stress, strain, and density is given as follows:

$$c^{*2} = \frac{1}{\rho_0} \frac{d\sigma}{d\epsilon} \quad (4.2)$$

where

- c^* = infinitesimal disturbance propagation velocity with respect to particle motion at a pressure
- ρ_0 = density at zero stress
- σ = stress
- ϵ = engineering strain

This is derived from continuity and momentum conservation only and is independent of stress strain laws. It is valid everywhere except at a finite discontinuity of stress, i.e., a shock front. It should be noted that c^* is the propagation velocity measured in a coordinate system moving at the local particle velocity. Therefore, to obtain the wavefront velocity in a fixed coordinate system the particle velocity, v , should be added. This quantity is given by

$$v = \int_0^\sigma \frac{d\sigma}{\rho c^*} \quad (4.3)$$

where

- ρ = density at stress σ
- c^* = wave velocity with respect to particle velocity at stress σ

Evidently, the particle velocity computation is lengthy for a nonlinear soil.

Since it is small in comparison with c^* , less than 5 percent generally, the computation of c can be greatly simplified with tolerable error by approximating $c = c^*$.

Evidently, since the pressure peak is continuously attenuated it will propagate at varying velocity. For the conditions shown in Figure 4.3a the peak would propagate with continuously increasing velocity. It should be noted that although the peak of the wave is continuously attenuated as it propagates through the ground, at any given point in the soil the pressure continuously rises to the peak without going through a hysteresis loop. Therefore, the peak of pressure always propagates at the velocity defined by the stress-strain curve envelope ABC.

A plot of the ratio c/c_1 can be constructed by measuring the slopes of the stress-strain curve and taking the square roots of the ratios of these to the slope at the origin. Since the slopes only are measured and the plotted results represent the roots of these, the error in the ratio c/c_1 thus obtained is less than half of the error in stress at a given strain as given by the stress-strain curve. The dashed curve ADF of Figure 4.4 would yield a velocity ratio curve practically identical with that resulting from curve ABC.

Since the seismic wave velocity can be measured to within ± 5 percent or better accuracy the compression wave velocity can be estimated by this technique to within considerably better limits than the ± 20 percent resulting by taking an average ratio.

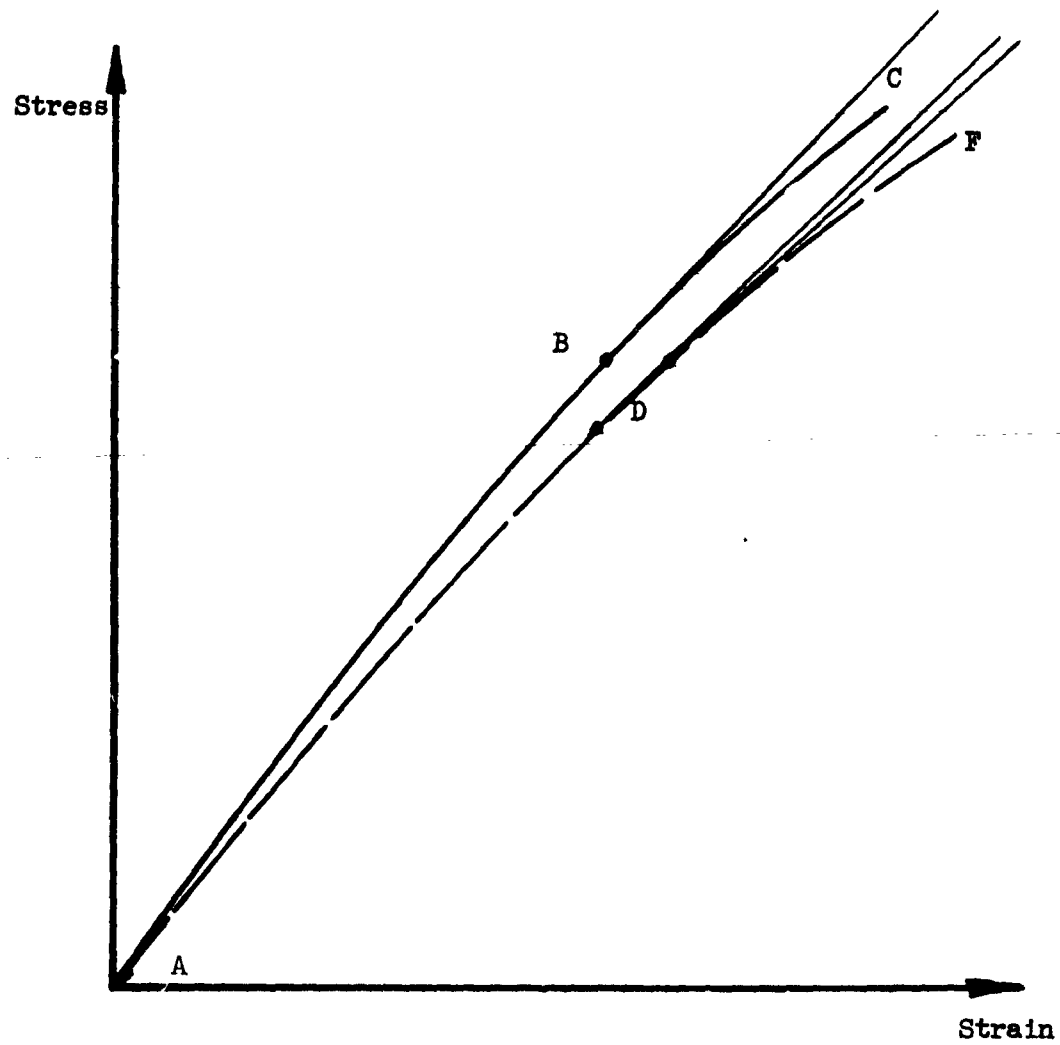


Figure 4.4 VARIATION OF SOIL STRESS-STRAIN CURVE

Three pressures are identified in Figure 4.3a:

1. p_o the peak overpressure,
2. p_a peak attenuated pressure at a buried structure,
3. p_{ar} peak attenuated reflected pressure arriving at the structure.

When these three pressure values have been estimated the corresponding instantaneous compression wave velocities can be taken from a graph similar to Figure 4.3b. An average value then can be chosen for computation purposes.

In order to estimate wave attenuation by the method of Section 4.1.3 the compression wave propagation velocity is required. Thus the method becomes one of guess and check. An original guess corrected once should be sufficient to arrive at consistent propagation velocity and wave attenuation factors.

The arguments leading to the estimation procedure given above are valid as long as the entire ground shock wave lies on a portion of the soil stress-strain curve that is everywhere convex upward.

If the stress-strain curve of the soil is concave upward the propagation phenomena are qualitatively changed. Inasmuch as all soils exhibit a concave stress strain curve at high enough pressure this problem merits some consideration.

Figure 4.5 illustrates schematically a generalized stress-strain curve ABCDEF. The curve is convex from A to the point of inflection, D, and concave beyond D.

In general we should expect that if a wave of amplitude p_h were propagating into such a material a shock front would quickly form. If the pressure maximum were preceded by a rising pressure the stresses within the interval of the rise

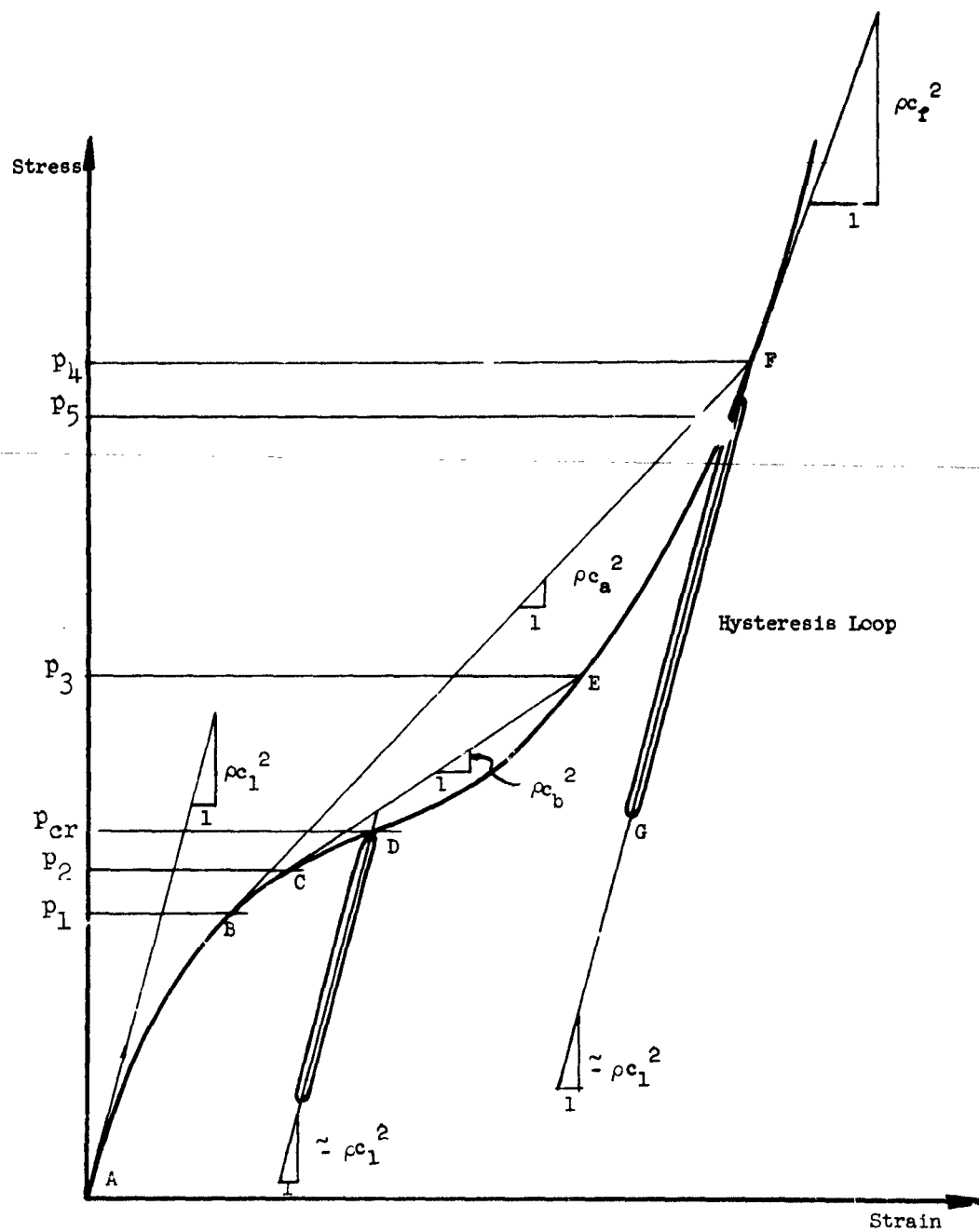


Figure 4.5 CONCAVE STRESS-STRAIN CURVE

time would travel at lower velocities than that at the peak and quickly be overtaken. Since the overpressure wave has an abrupt rise at the higher overpressures we conclude that the sharp rise is conserved in soil if the air induced ground pressure is above the point of inflection D. We repeat that all real soils exhibit a concave region similar to DEF at pressures above some critical level.

Looking at curve ABCDEF one is tempted to conclude that a decaying wave having a sharp rise would be stretched out in propagating through such a soil e.g. pressure p_5 in Figure 4.5 closely following peak pressure p_4 would move at a slower speed and therefore the interval p_4-p_5 would grow with time. However, the decay of the wave also propagates according to the peculiar laws of such stress-strain curves and actual physical results differ greatly from this intuitive conclusion.

Kolsky (Reference 3) and others have investigated the phenomena. The results of these investigations predict wave behavior that differ markedly from the intuitively anticipated behavior presented in the previous paragraph.

The principal physical effects that result in the qualitative peculiarities of the propagated wave are two:

1. The velocity of propagation of a shock front is not given by Equation (4.2); the derivative is meaningless at the shock front discontinuity.
2. The velocity of propagation of the decaying portion of the wave following the shock front is given by Equation (4.2) but the derivative $\frac{d\sigma}{d\epsilon}$ should be taken on a hysteresis loop (FG of Figure 4.5) rather than on the envelope.

The accurate analysis of these phenomena is exceedingly complex and is still under study by a number of investigators. However, if two simplifying assumptions are made a method for closely estimating resulting waveforms is forthcoming. One simplifying assumption reasonably matches reality. It is

1. The hysteresis loops are shrunk to their centerlines and their centerlines are all parallel to the tangent at zero stress and strain. Therefore the propagation velocity on a hysteresis loop is equal to the seismic compression velocity.

The second assumption may depart considerably from reality. It is

2. The stress-strain curve (ABCDEF of Figure 4.5) is the Hugoniot of the soil. At very high pressures this assumption has been found to be grossly in error for materials having definite, definable properties. The error decreases as the pressure is lowered.

The influence of the second assumption will be considered first.

An elementary manipulation of the continuity and momentum conservation equations results in Equation 4.4 for propagation of a shock front, if a shock front exists.

$$U^2 = \frac{(1-\epsilon_2)^2}{\rho_0} \frac{(\sigma_2 - \sigma_1)}{(\epsilon_2 - \epsilon_1)} \quad (4.4)$$

where

σ_2 and σ_1 are the stresses on the high and low pressure sides of the shock front respectively,

ϵ_2 and ϵ_1 are the engineering strains on the high and low pressure sides of the shock front, respectively,
 ρ_0 is the density at zero stress,
 and U^* is the shock velocity measured in a coordinate system moving with the particle velocity ahead of the shock.

Again, only a small error is introduced if the shock velocity measured in a fixed system is approximated by U^* . Further, the term $(1-\epsilon_2)^2$ generally can be considered unity without serious error. Actually, this term is equivalent to

$\frac{\rho_0}{\rho_2}$ and is equal to 1 if changes in soil density due to pressure are small enough to be neglected. Thus a slightly inaccurate but reasonable approximation for the shock velocity is given by

reasonable approximation for the shock velocity is given by

$$U^2 = \frac{1}{\rho_0} \frac{(\sigma_2 - \sigma_1)}{(\epsilon_2 - \epsilon_1)} \quad (4.5)$$

Now, an arbitrary curve can not be taken as the locus of all points (σ_0, ϵ_0) , (σ_1, ϵ_1) , (σ_2, ϵ_2) for which Equation 4.4 is satisfied. The correct curve, termed the Hugoniot, along with Equation 4.4 is satisfied also satisfies the equation of conservation of energy. If no heat were generated by the passage of the shock front the static stress strain curve and the Hugoniot would be identical. However, in any real material heat is generated by passage of a shock front. Therefore, for real materials, the curves differ.

However, beyond the near crater region the heat generated by passage of the ground shock wave is small. Therefore, the assumption that the stress strain curve is the Hugoniot is not unreasonable. The reader should not be deluded into believing that this convenient argument indicates that differences between stress strain curves and the Hugoniot actually are negligible. Possibly the best counter argument is that dynamic stress strain curves lie between the static curve and the Hugoniot. Nevertheless, it is a far better approximation of a real soil than the homogenous, isotropic, elastic medium of the theory of elasticity.

Now consider a wave having an abrupt rise in pressure from p_1 to p_4 (see Figure 4.5). In view of Equation 4.5 the propagation velocity of the discontinuity (shock front) would be c_a not c_f . Also we note that portions of the wave at pressures below p_1 would be propagating faster than the shock front. This brings out the first qualitative peculiarity of wave propagation through a medium having a concave stress strain curve. A shock front is conservative but is preceded by an ever increasing precursor. Also we note that if the shock front decayed (to, say, p_3 of Figure 4.5) the maximum amplitude of the precursor would increase. If the pressure decreased to p_{cr} precursor and post shock wave would merge and the shock would vanish.

Now consider the decaying portion of the wave behind the shock front. It follows a hysteresis loop and therefore is moving at higher velocity. Thus the decaying of the wave overtakes the shock front and the latter is continuously attenuated. A consequence of the assumption that the wave velocity on any hysteresis loop is equal to the seismic velocity is that the rarefaction wave

behind the shock front moves at constant, seismic velocity regardless of the position of the shock front on the stress strain (Hugoniot) curve. Actually, laboratory tests show that the seismic velocity does not remain constant as confining pressure is increased. Generally, the seismic velocity increases (e.g. Reference 11, page 57).

In Section 4.1.3 it is shown that the higher velocity rarefaction wave rapidly attenuates peak pressure. Therefore the error introduced by setting the "hysteresis velocity" equal to the seismic velocity has the net result of decreasing predicted attenuation, an error on the side of safety.

In summary, the shock propagation velocity in a soil having a concave upward stress strain curve should be as determined from the slope of the secant drawn on the stress strain curve between the pre-shock and post shock stresses, analogous to line BF and velocity c_a of Figure 4.5. Since the peak stress is attenuated by the rarefaction wave the value of propagation velocity will vary with time.

4.1.3 Compression Wave Attenuation

The percyclic damping theory is based on artificial theoretical assumptions. Its three salient virtues are:

1. It checks experimentally obtained data with excellent accuracy.
2. It is simple to apply, to both theoretical and practical problems.
3. The damping constants for at least a few real soils have been measured and reported in the geophysical literature. (These are given in Section 8.)

The writer of this report believes that designers will agree with him that number 3 above is the theory's most sterling virtue.

The elements of the theory are given in Section 4.0 of this report.

Weiner (Reference 10) has investigated the influence of the theory on the one dimensional propagation of simple pulses. The data he reports are directly applicable to the ground shock problem. Figures 4.6 through 4.9 are taken from Reference 10. In these figures "n" is the number of initial pulse widths propagated.

The dimensionless equation for pulse form after propagation of n initial pulse widths given by Weiner for the initially triangular pulse is

$$r(s,n) = \frac{1}{\pi} (1+2s) \tan^{-1} \frac{2 \frac{\delta n}{\pi}}{\left(\frac{\delta n}{\pi}\right)^2 + (4s^2-1)} + \frac{\delta n}{2\pi^2} \log_e \frac{\left(\frac{\delta n}{\pi}\right)^2 + (2s-1)^2}{\left(\frac{\delta n}{\pi}\right)^2 + (2s+1)^2} \quad (4.6)$$

In the above formula

- s = distance from center of pulse measured in initial pulse widths
- n = pulse propagation distance in initial pulse widths
- δ = percycle damping constant (per cycle)
- $r(s,n)$ = dimensionless ratio of wave amplitude to initial amplitude at centerline

A plot of the ratio of peak amplitude to initial peak amplitude as a function of pulse propagation distance is given in Figure 4.10.

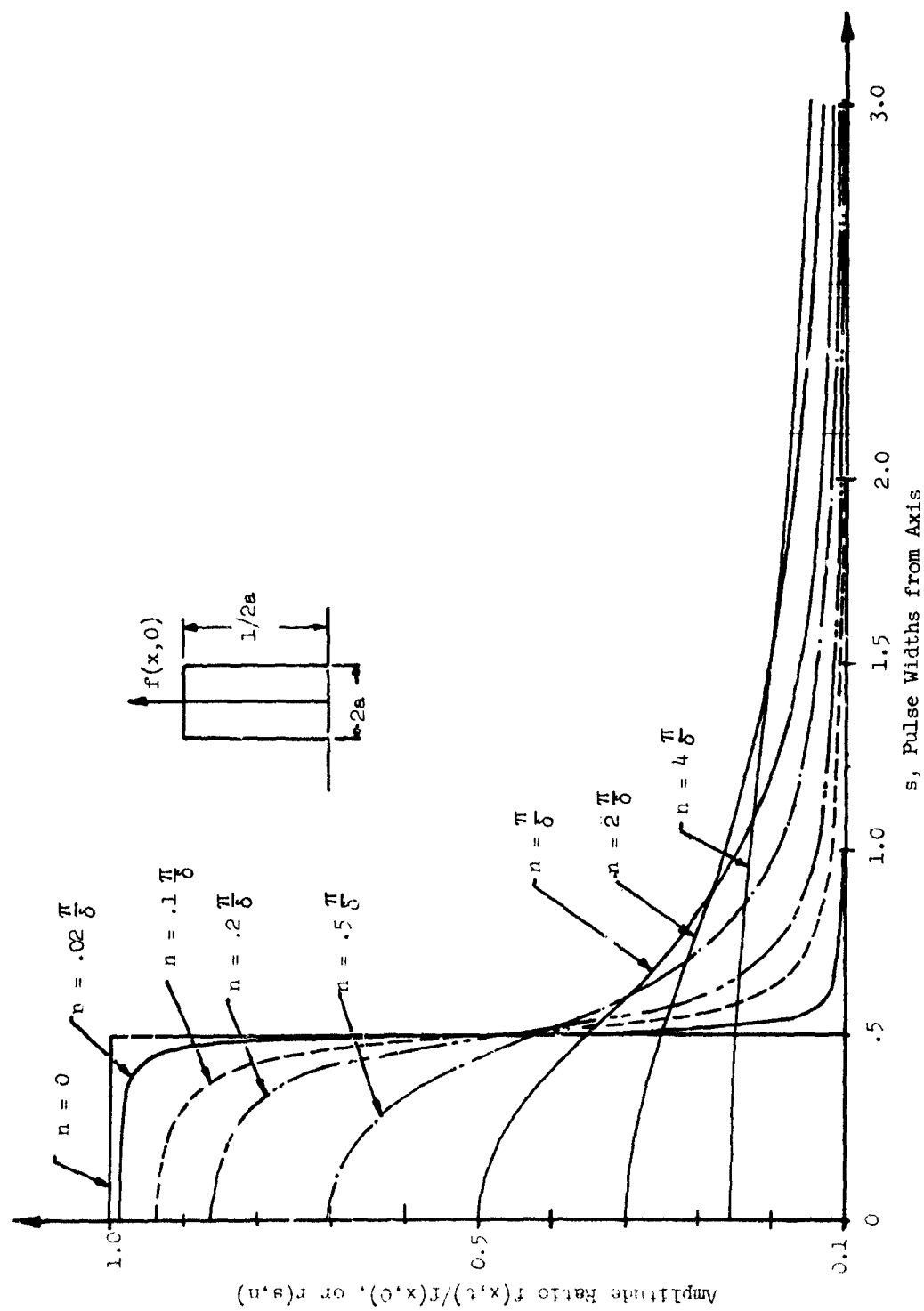


Figure 4.6 DAMPING OF RECTANGULAR PULSE

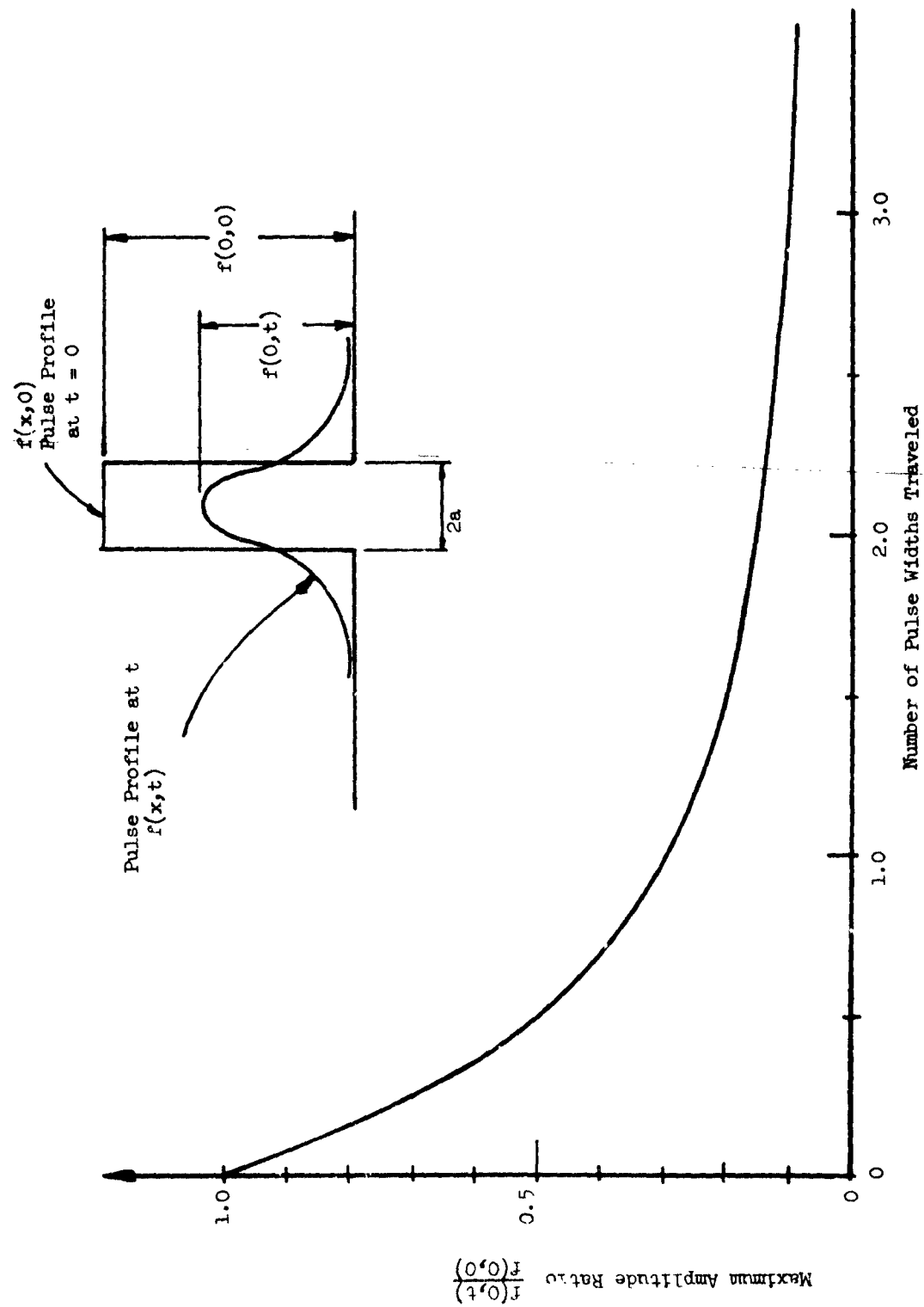


Figure 4.7 DECAYING AMPLITUDE OF RECTANGULAR PULSE

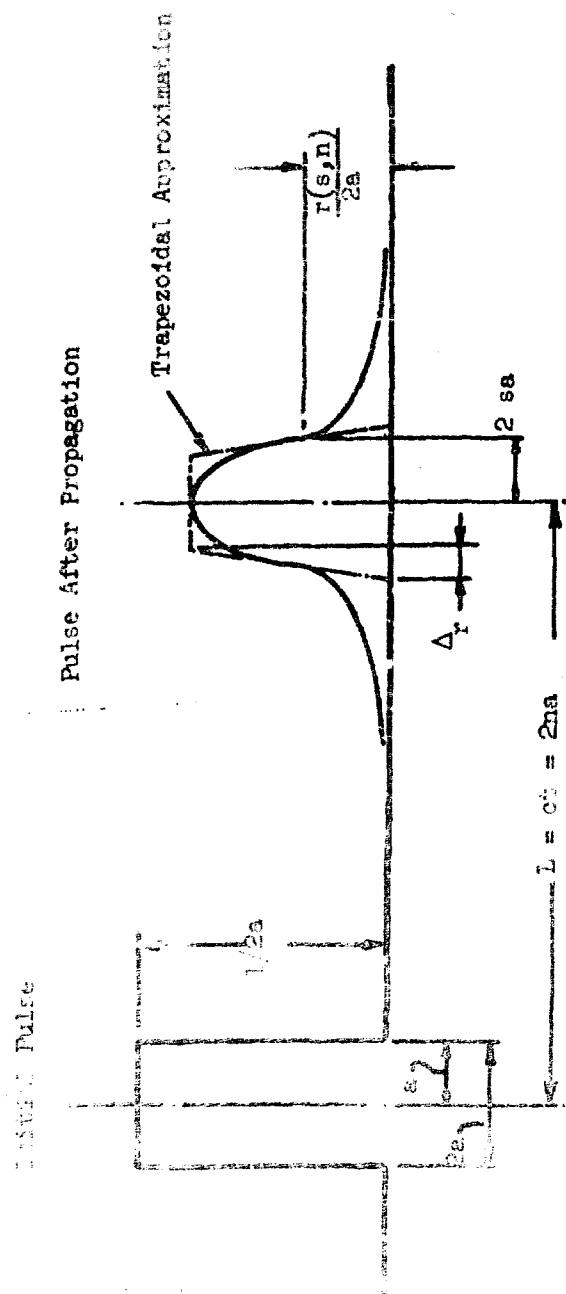


Figure 2 PROPAGATION OF DAMPED LONGITUDINAL PULSE

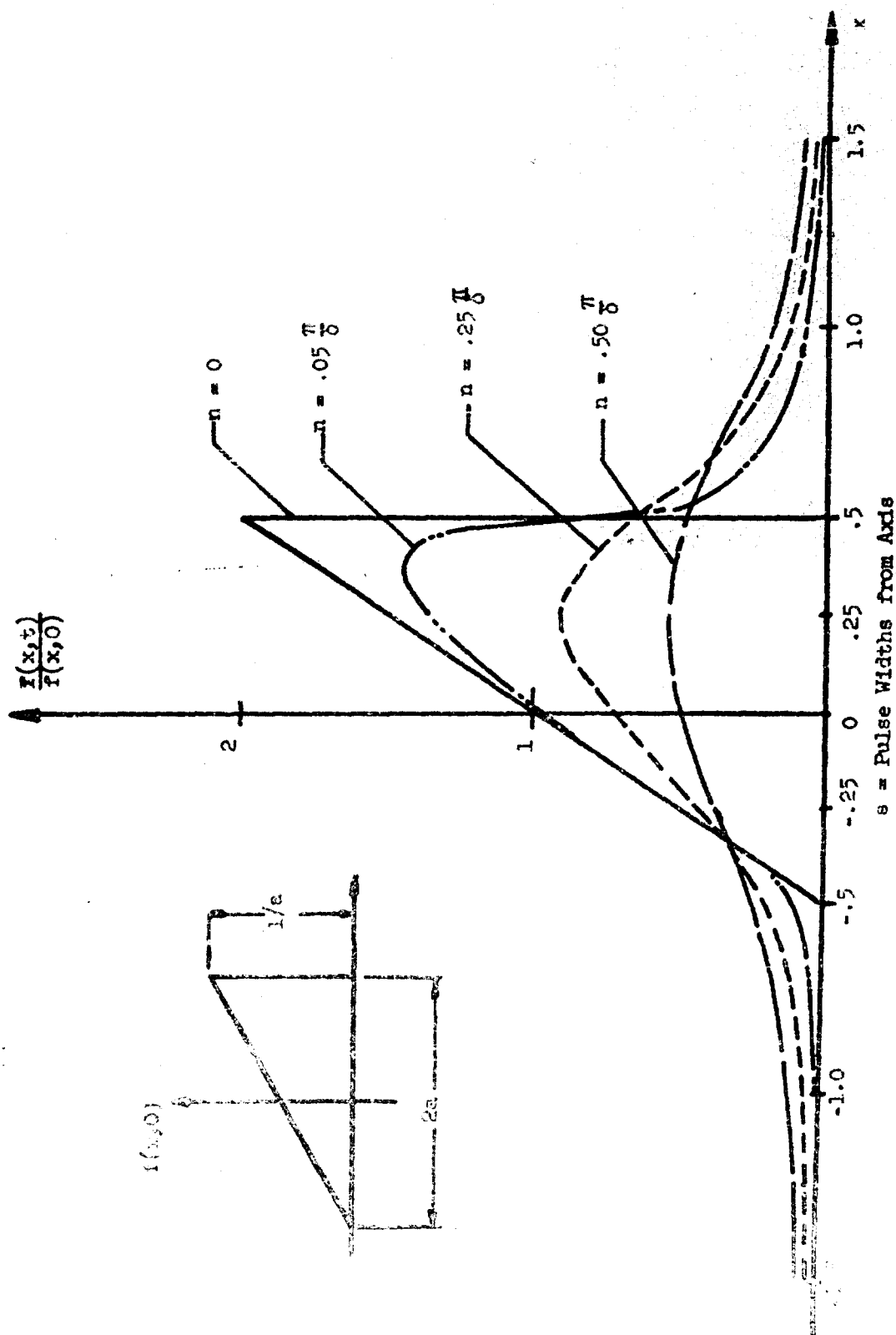
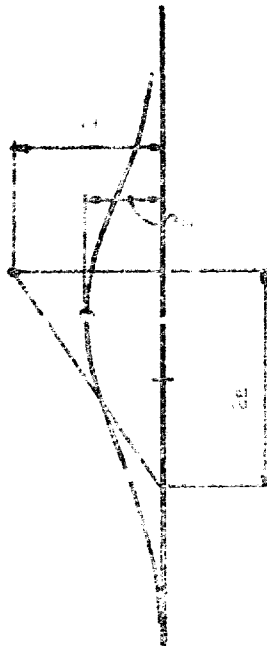


Figure 4.9 DAMPING OF TRIANGULAR PULSE



$a = \frac{\text{distance propagated}}{2a}$

$\delta = \text{percyclic damping constant}$

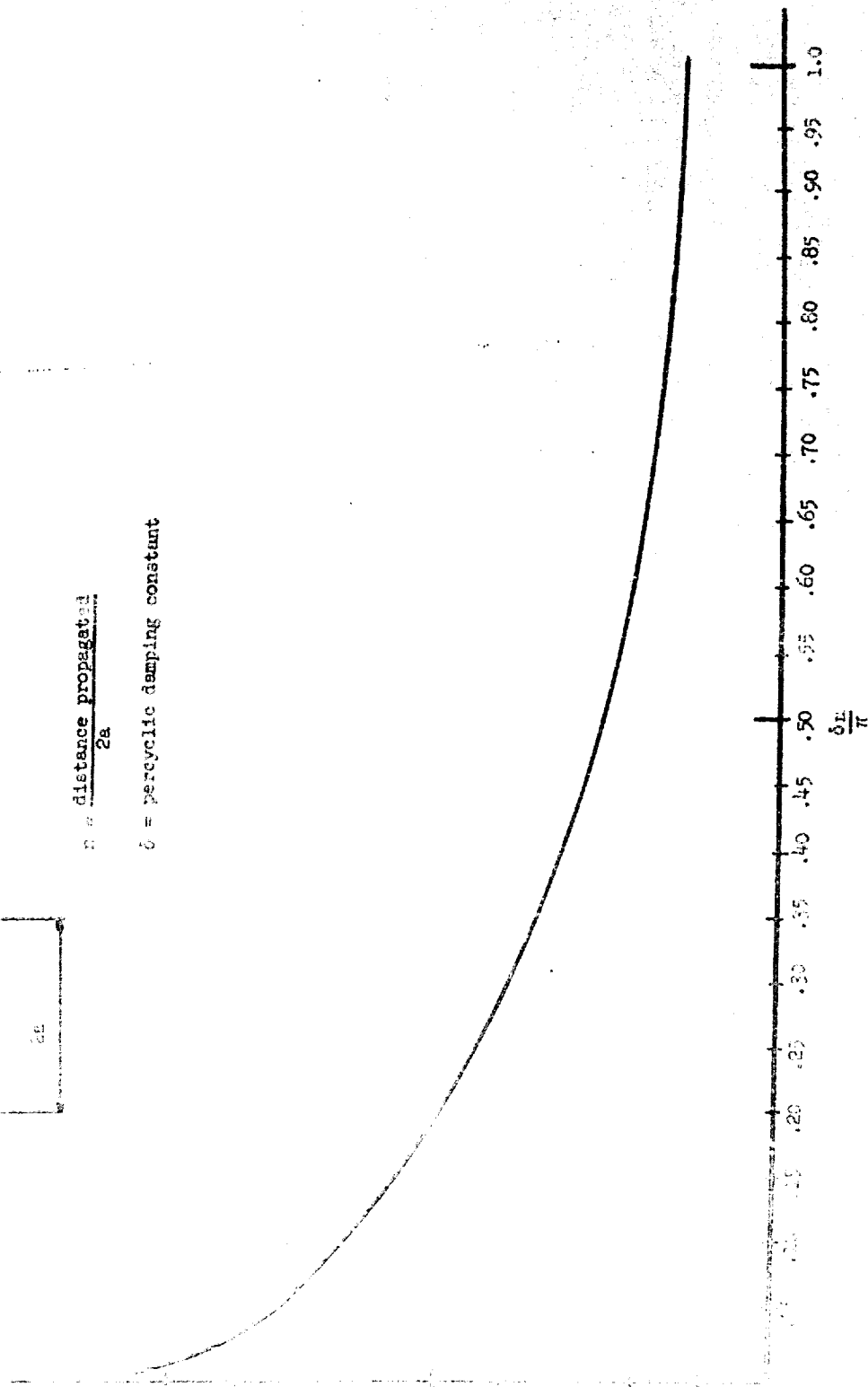


FIGURE 4.10 DELAY OF TRIANGULAR PULSE ACCORDING TO PERCYCLIC DAMPING LAW

Now, we note that the perycyclic damping theory is developed for materials having a constant wave propagation velocity and we intend to apply it to nonlinear media having variable propagation velocities. Objections certainly can be raised but we point out:

1. A more applicable theory of comparable simplicity does not appear to be available.
2. The perycyclic damping theory has given good results in geophysical work where the media also are nonlinear.

In the following paragraphs a method for estimating compression wave attenuation for soils having convex upward stress strain curves is developed, based on the perycyclic damping theory. The attenuation of peak pressure in soils ~~having concave upward stress strain curves~~ is so rapid that a separate damping computation would add no accuracy to the waveform determination.

Figure 4.11 shows a typical overpressure wave constructed from Figure 4.1. (A 1 MT bomb and 500 psi have been used for the construction). The wave is equivalent to the sum of the triangular wave and the "difference" wave shown. Now the difference wave is of long wave length and any high frequency Fourier components which it contains are of low amplitude. Therefore it will be attenuated only slightly in passing through the soil and the attenuation that does occur will affect only the point where the trailing edge of the triangular wave joins it. The triangular wave, on the other hand, has a short wave length, and contains a large portion of its energy in high frequency components. Therefore it will be attenuated rapidly. We make the approximation that all of the attenuation occurs in the triangular component of the wave.

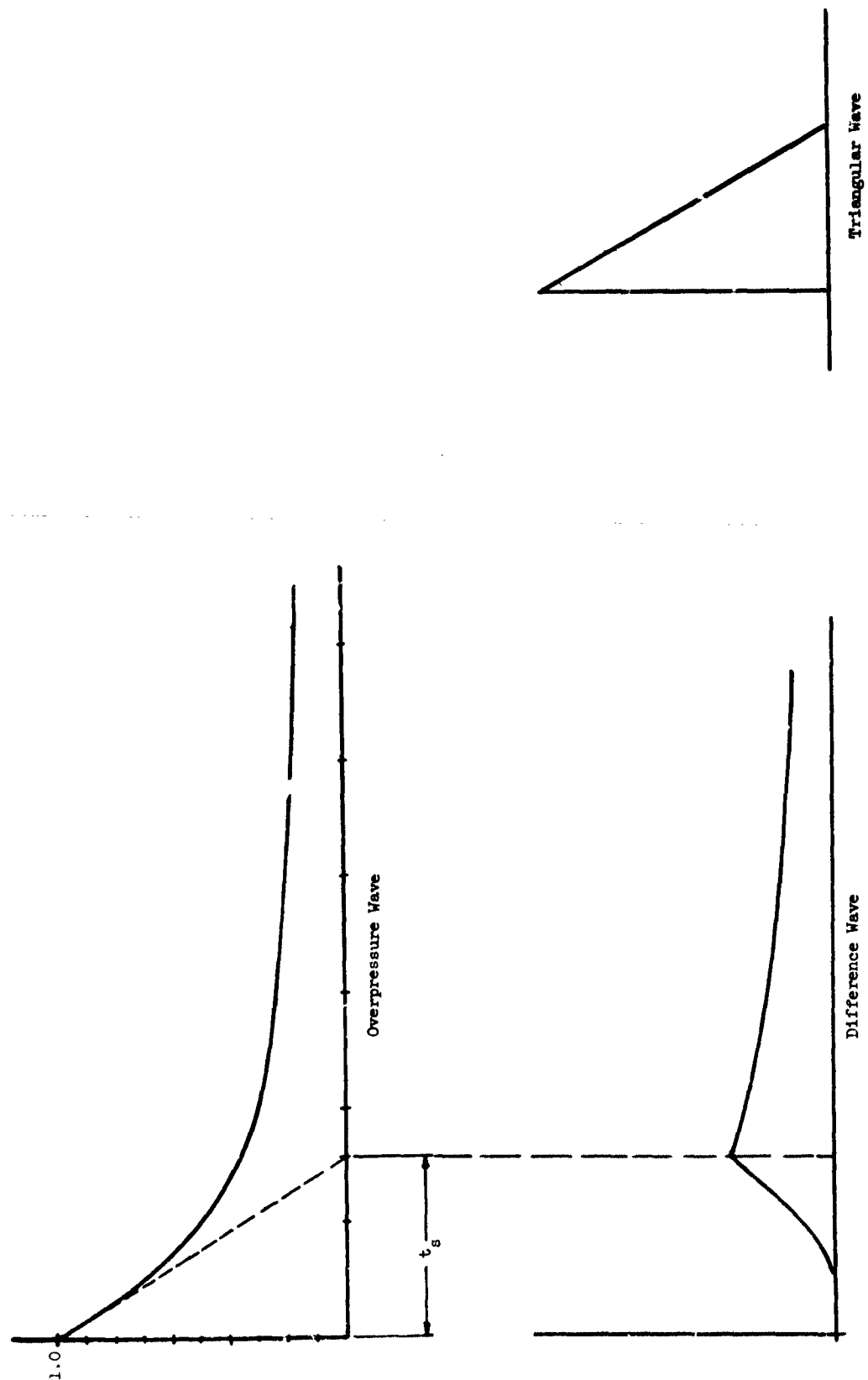


Figure 4.11 APPROXIMATE TRIANGULAR AND LONG WAVE LENGTH COMPONENTS OF BLAST WAVE

The duration of the triangular wave has been set arbitrarily. However, the value chosen makes the central angle of the peak of the triangle equal to the central angle of the peak of the blast wave. Since the high frequency components of the peak are most strongly attenuated the subtangent duration appears to be the best choice for the triangular base.

To apply the theory:

1. Determine wave path length from surface to structure and surface to bedrock to structure. The angle between the paths and vertical is equal to the Mach angle of the compression wave.
2. Determine the percyclic damping constant. Test data should be used if available; otherwise estimate with the aid of data in Section 8.
3. Determine the subtangent duration of the overpressure wave from Figure 4.1.
4. Determine the subtangent length by multiplying the subtangent duration by the compression wave velocity. (This will be a guess and check procedure in connection with determination of the compression wave velocity per Section 4.1.2).
5. Determine n for the direct path and the reflected path.
6. Compute $\frac{\delta n}{\pi}$ for direct path and reflected path and obtain attenuation factors from Figure 4.10.
7. Determine the rise time by computing delay from time of arrival of toe of wave (moving at velocity c_1) to time of

arrival of peak (moving at velocity c). If L is the path length and t_r the rise time

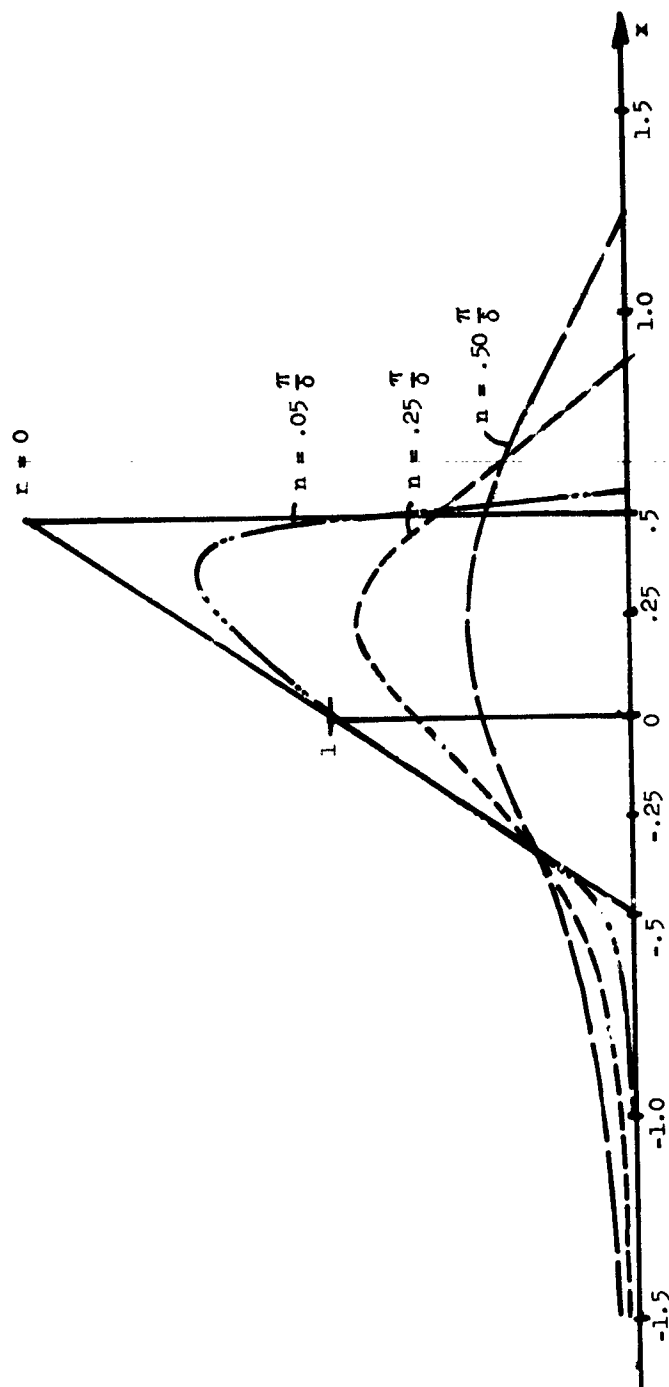
$$t_r = L\left(\frac{1}{c} - \frac{1}{c_1}\right)$$

The curve of the rise can be interpolated between the curves of Figure 4.12 (Figure 4.12 has been constructed from Figure 4.9 by continuing the maximum slope of Figure 4.9 curves to the "s" axis).

According to the elastic theory lateral motion of a soil particle should stop shortly after engulfment by the shear wave. Field test records obtained in Nevada however do not exhibit this abrupt termination of the horizontal velocity.

This behavior can be rationalized if it is assumed that the rate of energy dissipation of shear waves is considerably higher than that of compression waves. According to the elastic theory the shear wave stress is considerably lower than the compression wave stress in the superseismic region. Thus, if the shear wave were attenuated at a greater rate than the compression wave its intensity rapidly would be reduced below the level of the wave anomalies introduced by the nonlinear characteristics of the soil and the argument based on elastic theory loses its force.

Now, precise numbers are not available, but it is known that shearing distortion of particulate soil dissipates energy much more rapidly than pure compression. Thus, though the Nevada test site can hardly be considered typical the weight of evidence indicates that, lacking test data to the contrary, the shear waves can be neglected in shock isolation design.



s = Pulse Widths from Axis

Figure 4.12 DAMPING OF TRIANGULAR PULSE

4.1.4 The Input Wave

The input wave determination for convex and concave stress strain diagrams are considered separately. Specific examples are used to illustrate the methods.

Case I Stress Strain Curve Convex Problem

A structure is to be placed 35 feet below surface; bedrock is 120 feet below surface. The design overpressure is 300 psi and the design bomb size is 10 MT. The seismic velocity is

$$c_1 = 2700 \text{ ft/sec.}$$

The average soil density is 120 lbs/ft³. The soil is a lightly cemented sand. The percyclic damping factor is estimated (Section 8) to be 0.20.

The average stress-strain curve of the soil is estimated to be as shown in Figure 4.13. [The soil chosen for this example might almost be classified as a soft rock. It has been chosen to illustrate how a slightly curved stress-strain curve can modify ideal elastic results.]

Develop the estimated pressure time curves at the structure for both incident and reflected waves.

Step 1 - Construct the overpressure-time curve (Figure 4.14)

From Figure 4.1

At 300 psi and 1 MT

$$P = 150 \text{ psi} \quad t_{50} = 31 \text{ ms}$$

$$P = 110 \text{ psi} \quad t_s = 55$$

At 300 psi and 10 MT

$$t_{50} = 67 \text{ ms}$$

$$t_s = 118$$

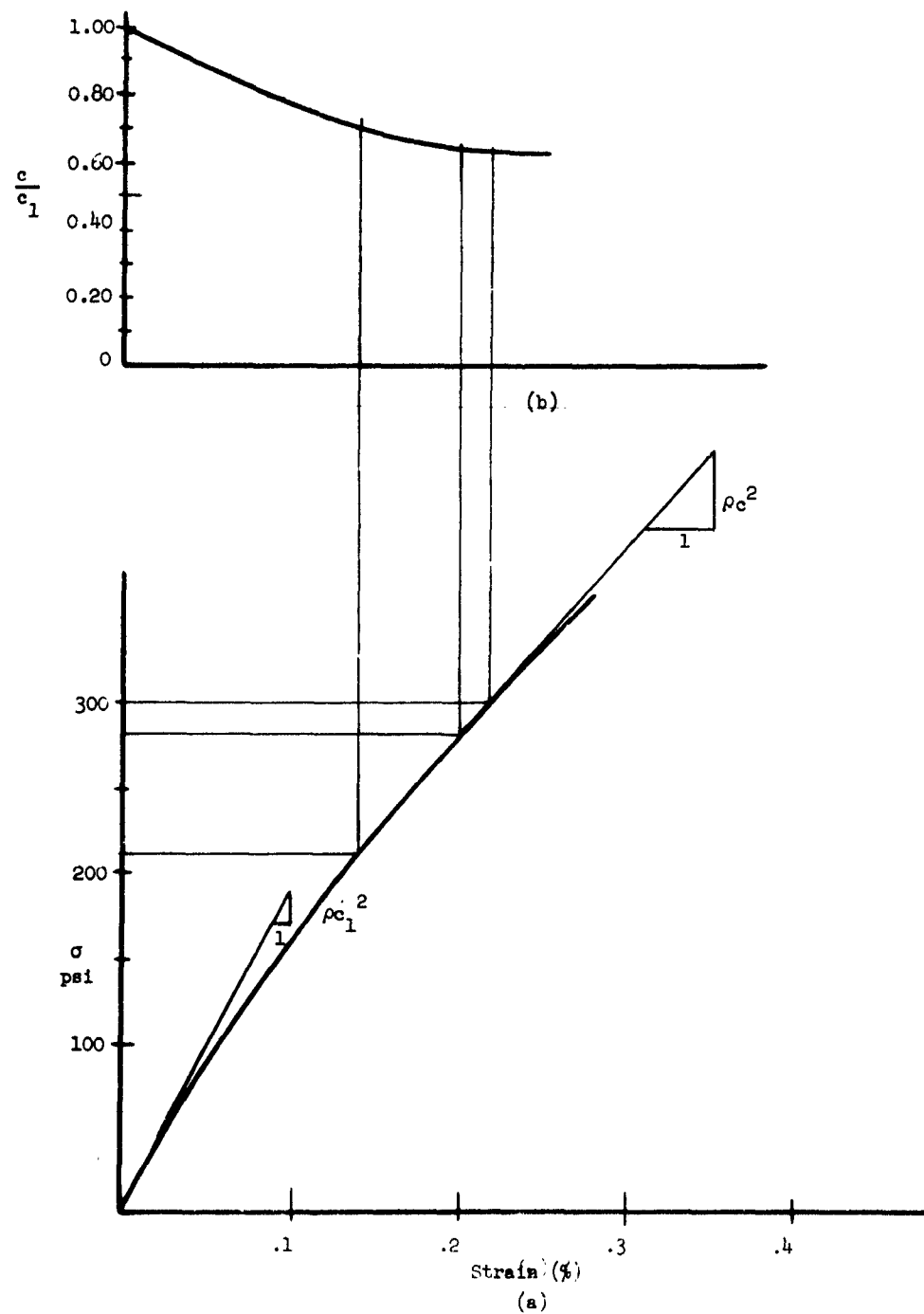


Figure 4.13 SOIL STRESS-STRAIN CURVE

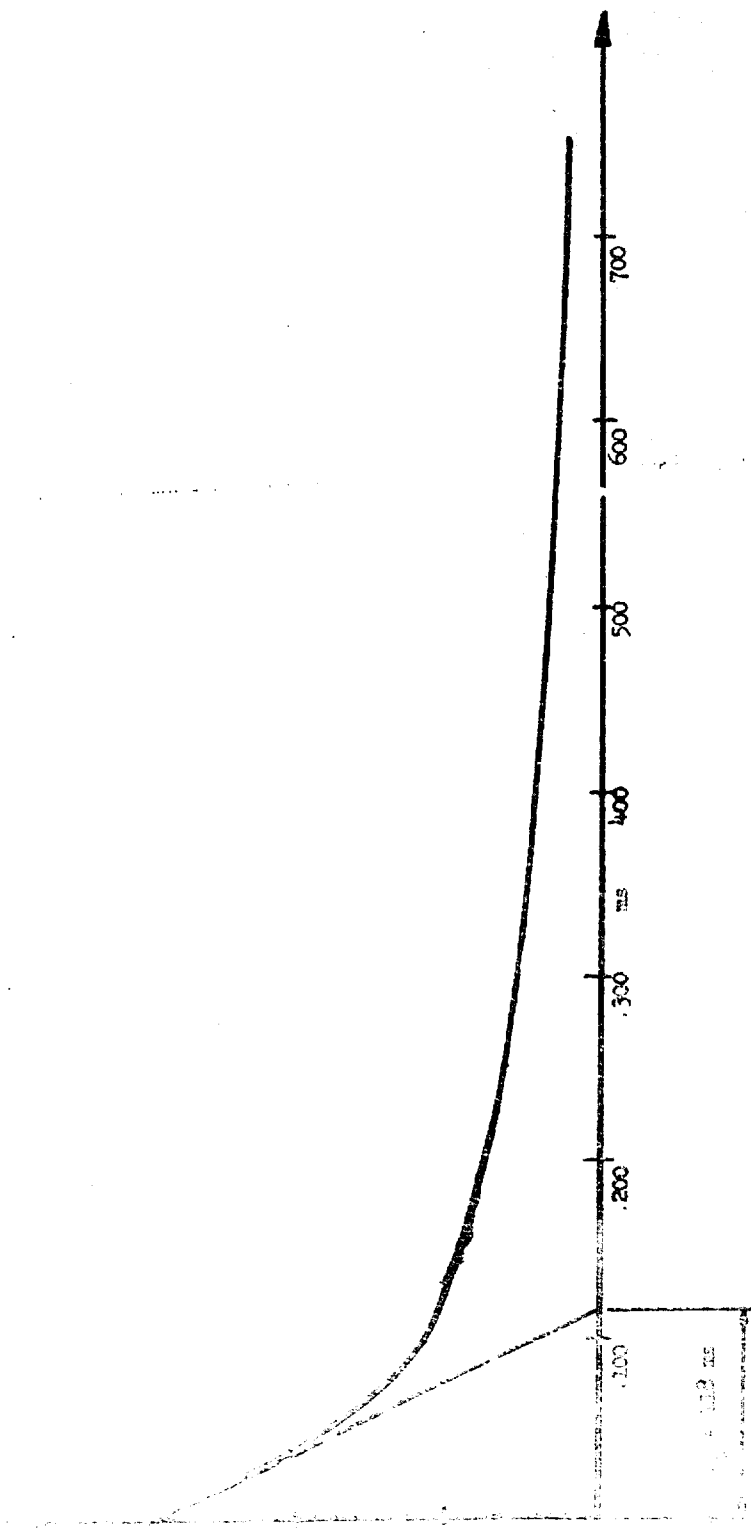


Figure 4.14 OVERPRESSURE WAVE

Best Available Copy

At 300 psi and 1 MT		At 300 psi and 10 MT
P = 90 psi	$t_{30} = 75$	$t_{30} = 161$
P = 60 psi	$t_{20} = 137$	$t_{20} = 295$
P = 30 psi	$t_{10} = 360$	$t_{10} = 776$

Step 2

Construct the c/c_1 curve corresponding to the stress-strain curve.
(Figure 4.13b)

Step 3

Estimate the propagation velocity. From Figure 4.13b the range of c/c_1 between 100 and 300 psi is about 0.85 to 0.65. Accordingly estimate c to be

$$c = 0.75 \times 2700 = 2000 \text{ ft/sec.}$$

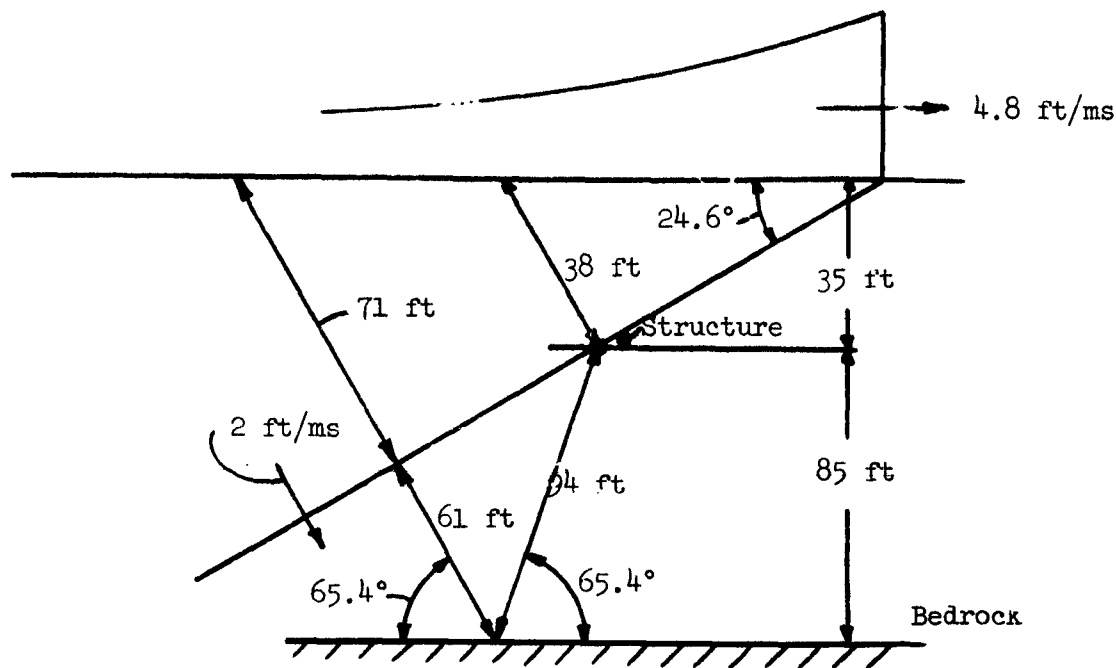
Step 4

Estimate the wave attenuation. At 300 psi the air shock velocity is 4.8 ft/msec. Therefore the first estimate of the Mach angle of the wave is

$$\phi = \sin^{-1} \frac{c}{U} = \sin^{-1} \frac{2}{4.8} = 24.6^\circ$$

and $\sec \phi = 1.1$.

The wave path length from surface to structure is about 38 ft. and from surface to bedrock to structure is about 226 ft. (see sketch).



The subtangent duration of the wave is (Figure 4.14) 118 msec. Therefore the subtangent length L_s is about

$$L_s = c t_s = 2 \times 118 = 236 \text{ ft.}$$

The wave path lengths in terms of the subtangent length are

for the direct wave $n = 38/236 = 0.16$

for the reflected wave $n = 226/236 = 0.95$

and $\delta n/\pi$ is ($\delta = 0.2$)

for the direct wave $\frac{\delta n}{\pi} = 0.01$

for the reflected wave $\frac{\delta n}{\pi} = 0.06$

From Figure 4.10 the attenuation factors are

for the direct wave 95%

for the reflected wave 71%

Peak attenuated pressures are then

for the direct wave 285 psi

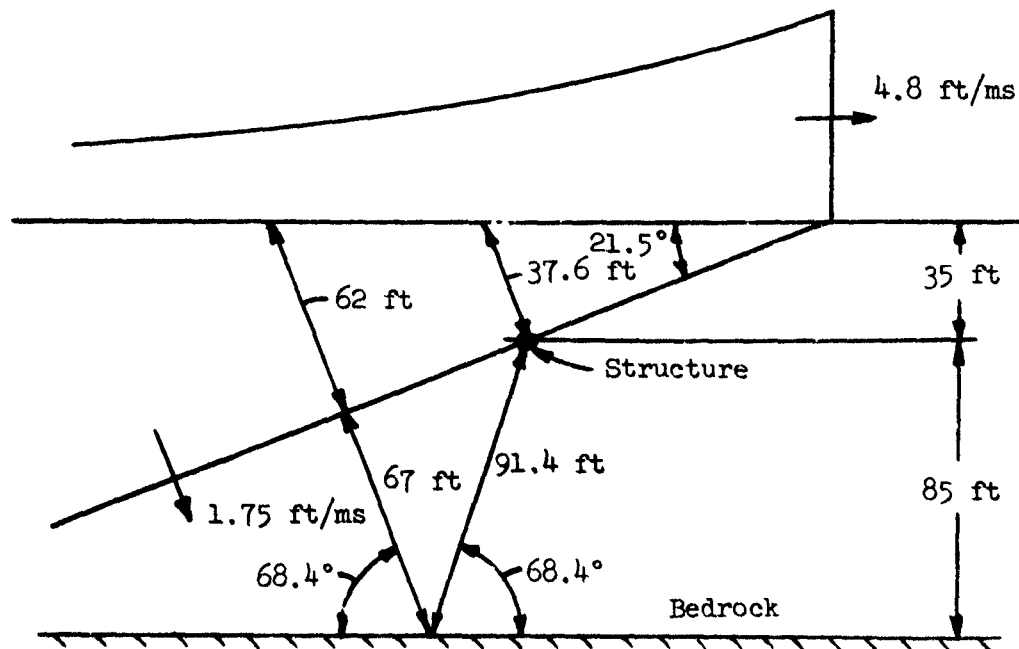
for the reflected wave 212 psi

Step 5 - Correct Wave Velocity

Entering these pressures into Figures 4.13 a and b we see that a better average for c/c_1 is 0.65. Then

$$c = 0.65 \times 2700 \text{ ft/sec} = 1750 \text{ ft/sec}$$

Recomputing L_s , n_1 , attenuation and peak attenuated pressure (see sketch) we obtain



	L_s	n	$\frac{\delta n}{\pi}$	Attenuation Factor	Attenuated Pressure
Direct wave	206'	0.18	0.011	95%	284
Reflected wave	206'	1.07	0.07	69%	207

These values check the corrected wave propagation velocity, 1750 ft/sec.

Step 6 - Estimate Rise Times

The rise times are computed from

$$\text{for the direct wave } t_r = \frac{38}{c} - \frac{38}{c_1} = 7.6 \text{ ms}$$

$$\text{for the reflected wave } t_r = \frac{210}{c} - \frac{210}{c_1} = 42 \text{ ms}$$

Step 7 - Estimate Arrival Time of Reflected Wave

The distance traveled by the reflected wave from the time that the structure is engulfed by the direct wave until the reflected wave reaches the structure is about 158 ft. The toe of the wave, moving at seismic velocity will travel this distance in

$$\frac{158}{2.7} = 59 \text{ msec.}$$

Step 8

Sketch waveforms (see Figure 4.15).

Step 9

Determine maximum impulse in soil below structure.

$$\text{Time of impulse} = \frac{158}{1.75} = 90 \text{ ms}$$

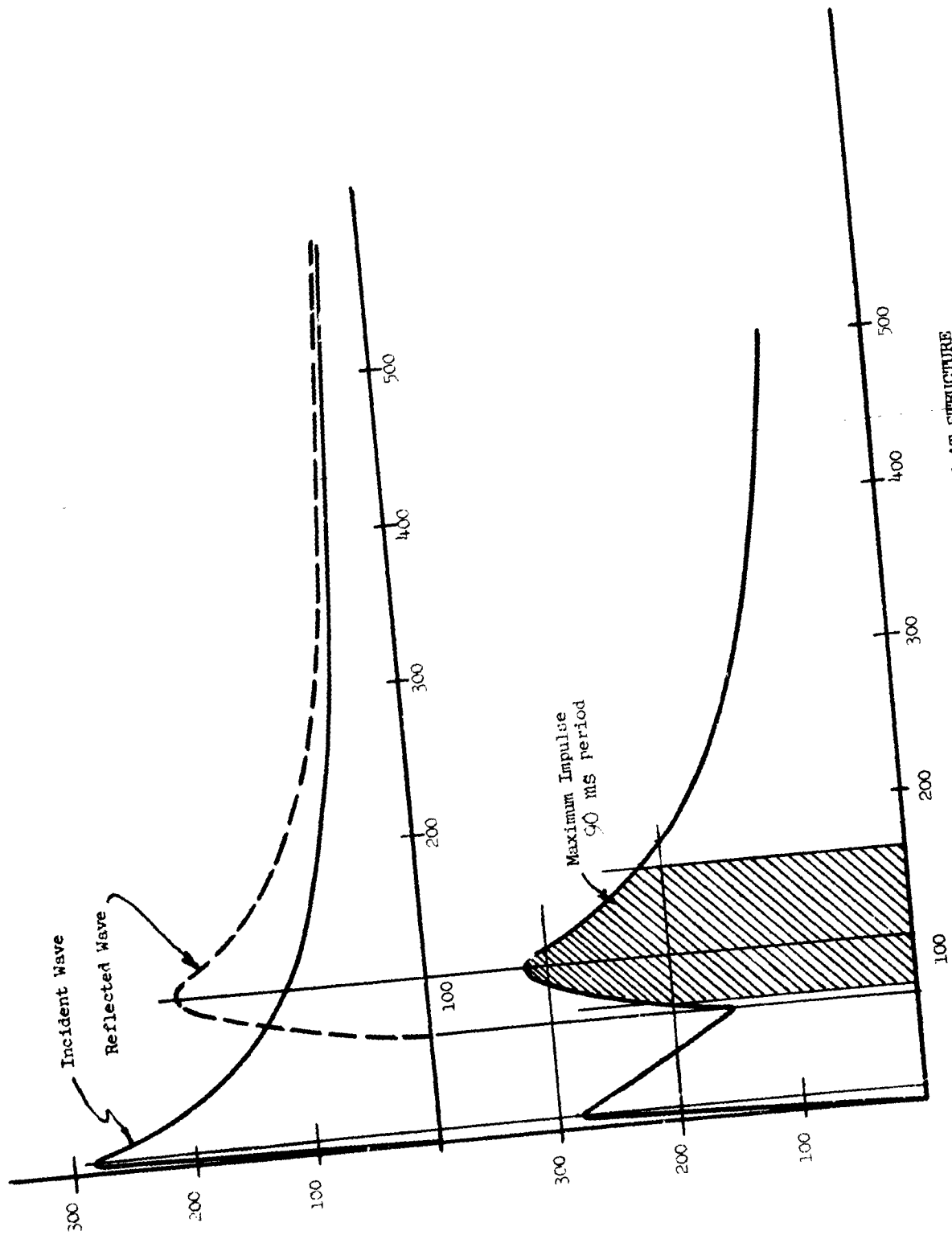


Figure 4.15 SUM OF PRESSURES AT STRUCTURE

The maximum impulse will be the maximum contained within any 90 msec period. This is determined from Figure 4.15 on the pressure sum curve. The maximum impulse is shaded. Within the limits of accuracy imposed by our propagation velocity, peak displacement is given by

$$y = \frac{I}{\rho c}$$

where

- y = peak displacement
- I = impulse (shaded area Figure 4.15)
- ρ = soil density
- c = average wave propagation velocity.

Case II Stress Strain Curve Concave Problem

A structure is to be placed 35 feet below surface; bedrock is 120 feet below surface. The design overpressure is 1000 psi and the design bomb size is 10 MT. The average soil density is 115 lbs/ft³. An estimate of the stress-strain curve below 1000 psi is shown in Figure 4.16

Develop the soil displacement and pressure time curves at the structure level.

The basic one dimensional wave equation is independent of material stress strain characteristics. If compressive stresses are considered positive, the wave equation is

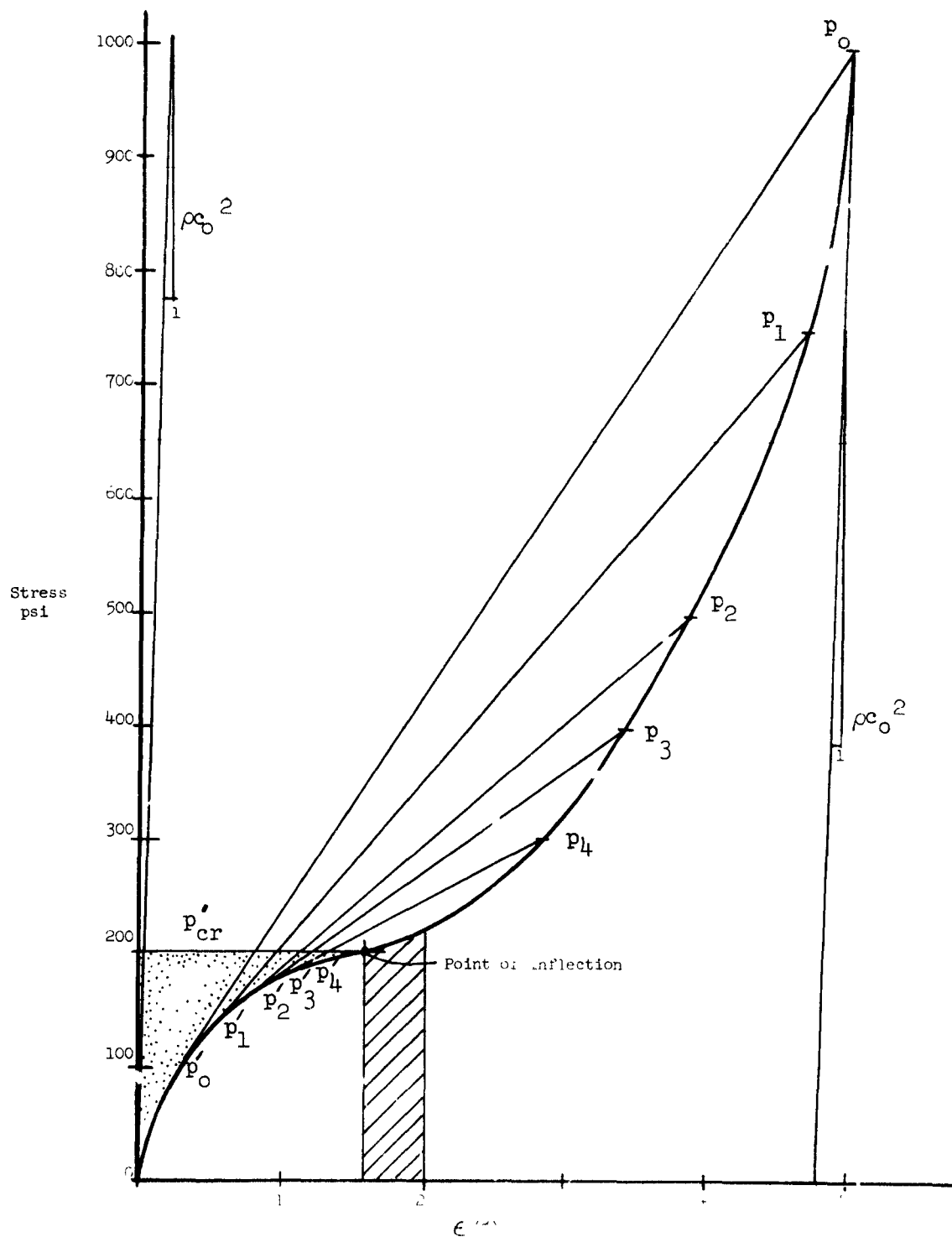


FIGURE 4. ESTIMATED STRESS-STRAIN CURVE

$$\left(\frac{\partial^2 z}{\partial t^2}\right)_x = -\frac{1}{\rho} \left(\frac{\partial p}{\partial x}\right)_{t^*} \quad (4.7)$$

The method suggested involves a series of steps leading to a plot of $-\left(\frac{\partial p}{\partial x}\right)_{t^*}$ for a particular depth, h , as a function of time between t_o^* and t_s^* , the times at which the wave front and shock front respectively reach the point of interest at depth h . Integration of this plot yields particle velocity, $\left(\frac{\partial z}{\partial t}\right)_x$, during the time interval $t_o^* \leq t^* \leq t_s^*$. A special calculation is required to find the increase in momentum due to the shock, and the influence of the unloading portion of the wave can be evaluated using linear elastic theory, since a constant propagation velocity is assumed in the unloading region.

Step 1 - Construct the overpressure-time curve (See Figure 4.17)

From Figure 4.1

At 1000 psi and 1 MT

P = 500 psi	$t_{50} = 8.3$ ms
P = 368	$t_s = 15.7$
P = 300	$t_{30} = 21.8$
P = 200	$t_{20} = 44$
P = 100	$t_{10} = 131$

At 1000 psi and 10 MT

$t_{50} = 17.9$ ms
$t_s = 33.9$
$t_{30} = 47$
$t_{20} = 95$
$t_{10} = 283$

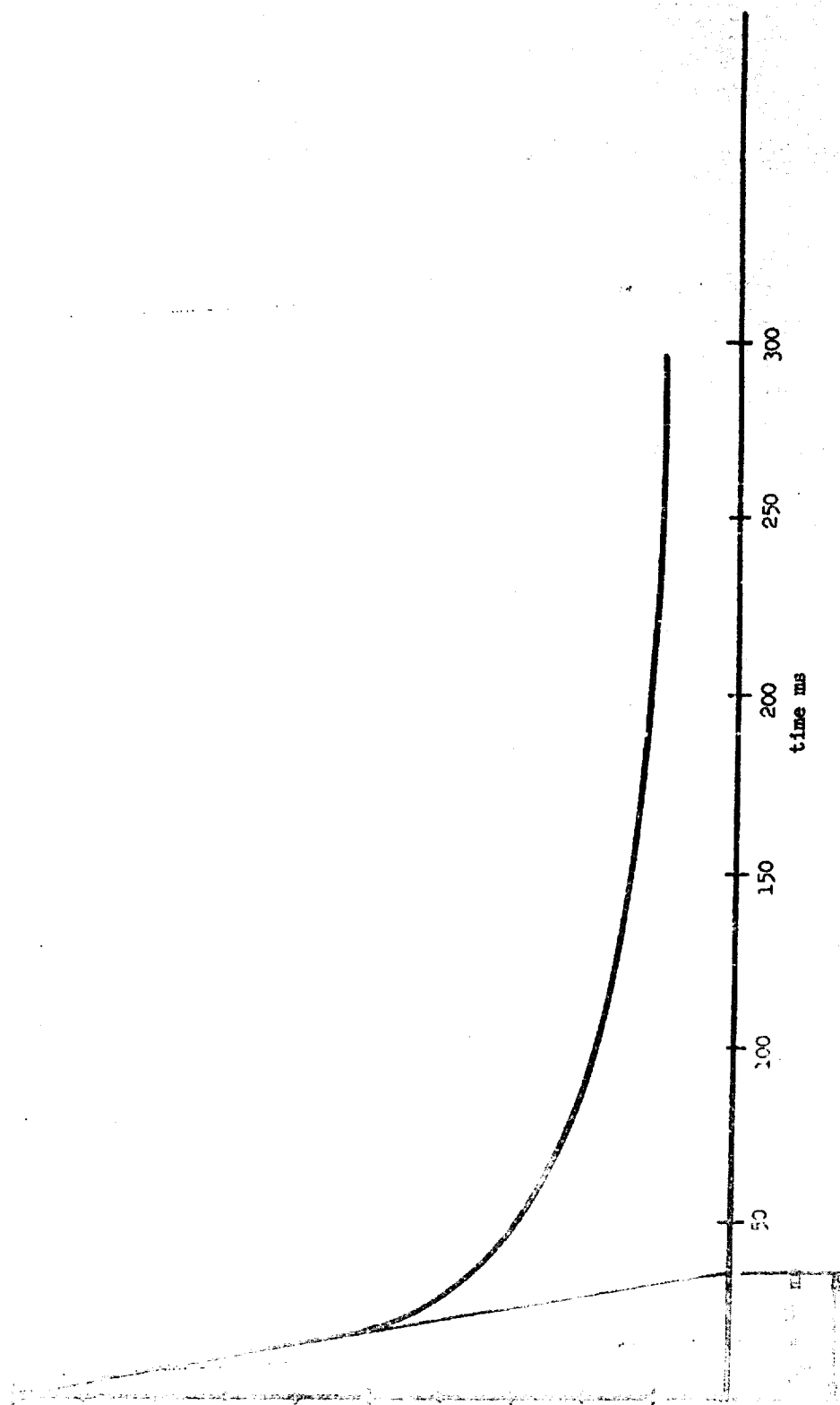


Figure 4.17 OVERPRESSURE-TIME

Step 2

On the soil stress-strain diagram, locate the peak air overpressure and the critical stress (i.e., the stress below which a shock will not propagate, where the stress strain curve has a point of inflection). Also locate the upper and lower points of several intermediate shocks. These steps have been carried out in Figure 4.16.

The following results are obtained from data on this figure.

$$\rho = \frac{115}{386 \times 1728} = 1.72 \times 10^{-4} \frac{\text{lbs sec}^2}{\text{in}^4}$$

$$c_o^2 = \frac{10^4}{1.72} \times \frac{1000}{.002} = 29 \times 10^8 \frac{\text{in}^2}{\text{sec}^2}$$

$$c_o = 4500 \text{ ft/sec}$$

Shock Peak	Precursor Peak	ΔP	$\Delta \epsilon$	Shock Velocity, U_s
1000 psi	105 psi	895 psi	.047	870 ft/sec
750	135	615	.042	762
500	155	345	.032	650
400	175	225	.025	595
300	180	120	.018	515
200	200	000	.000	370

Step 3

Plot the secant shock velocity as a function of the upper shock stress level. This is shown in Figure 4.18.

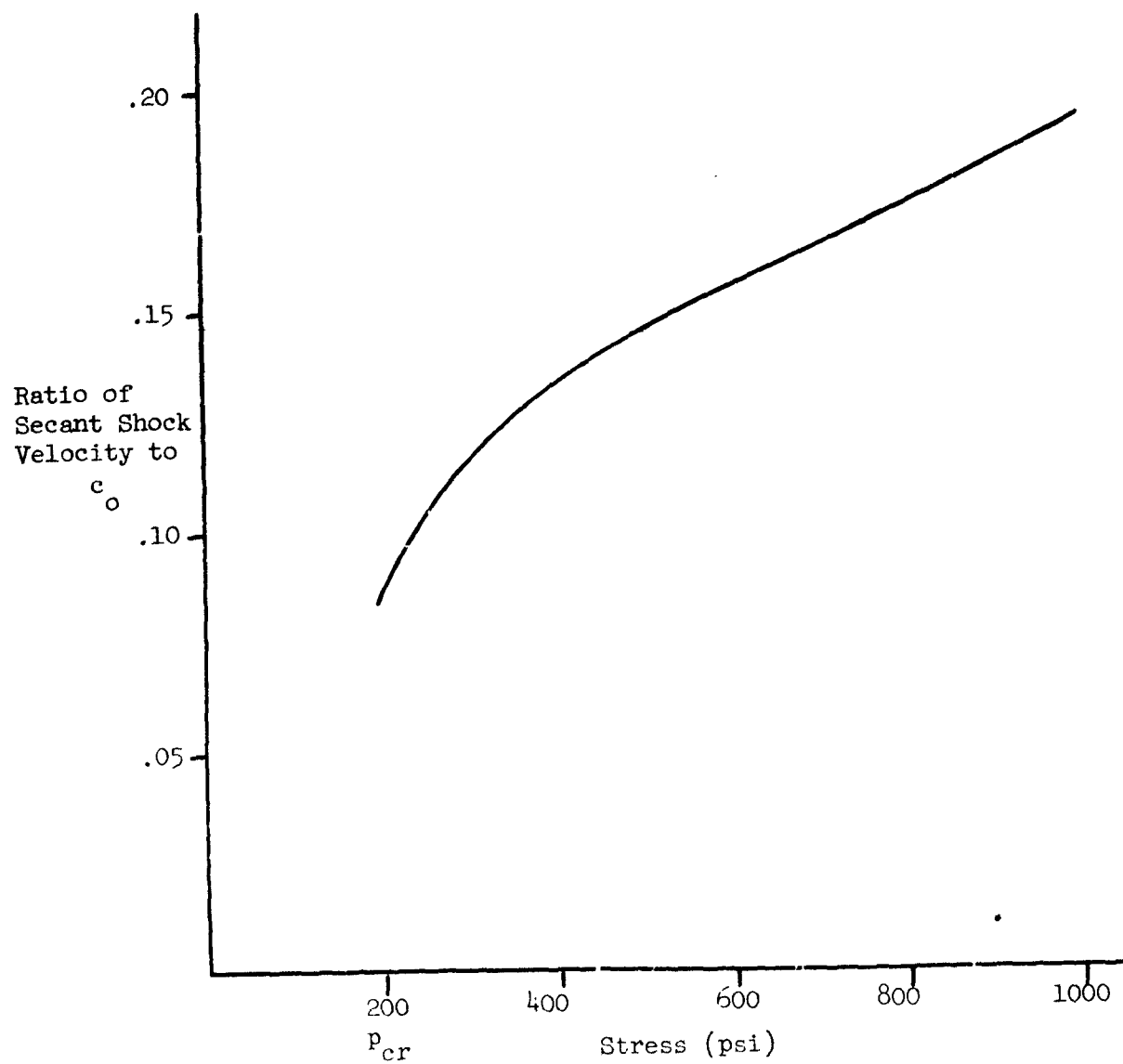


Figure 4.18 RATIO OF SECANT SHOCK VELOCITY TO c_0 VERSUS STRESS

Step 4

Plot the air blast overpressure on a function of $c_0 t$. The plot of pressure versus $c_0 t$ is the waveform that would exist in the soil if the entire wave propagated at velocity c_0 . This is shown in Figure 4.19.

Step 5

Determine the time t^* required for the shock front to penetrate a distance x . Approximate the shock front velocity during a time interval Δt^* with the average of the secant velocities at the initial and final shock pressures for the interval Δt^* . During the time interval Δt^* the toe of the wave moves a distance $c_0 \Delta t^*$ and the shock front moves a distance $U_{ij} \Delta t^*$ where U_{ij} is the average secant velocity between times t_i^* and t_j^* where

$$\Delta t^* = t_j^* - t_i^*$$

Thus during the interval Δt^* the shock front moves backward with respect to the toe of the wave a distance

$$(c_0 t_i - c_0 t_j) = \Delta(c_0 t) = (c_0 - U_{ij}) \Delta t^*$$

distance being represented as $c_0 t$ as used in Step 4.

Solving for Δt^*

$$\Delta t^* = \frac{t_i - t_j}{1 - \frac{U_{ij}}{c_0}}$$

For any point of closely spaced time instants t_i and t_j the corresponding peak pressures can be read from the graph of overpressure versus time. The ratio U_{ij}/c_0 may be read from the graph of Step 3. Also the corresponding

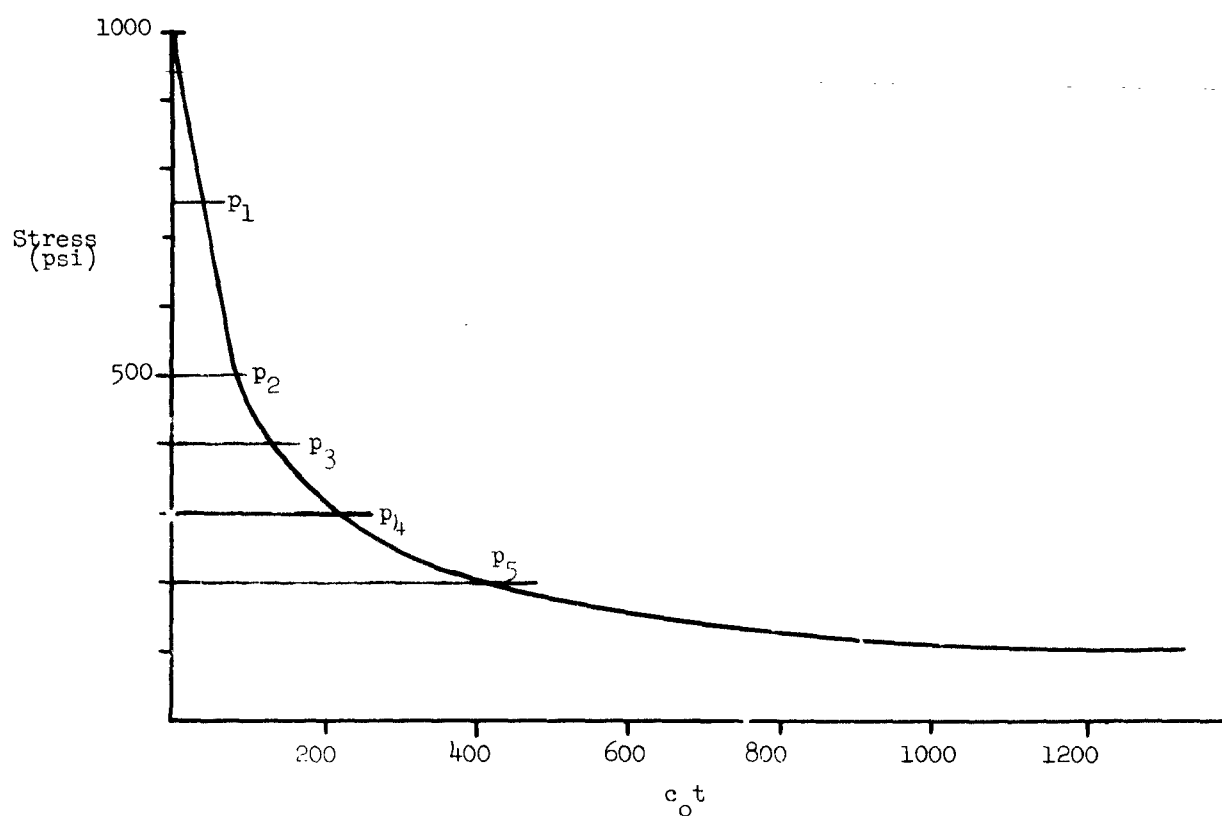


Figure 4.19 OVERPRESSURE VERSUS $c_o t$

lower shock pressure can be read from the graph of Step 2. Thus a graph of upper and lower shock stress values plotted against time t^* can be constructed. The data is shown in the following table; the plot is shown in Figure 4.20.

Peak Pressure (psi)	t (ms)	Δt (ms)	Average Shock Velocity, U_{ij} (ft/sec)	$\frac{1}{1 - \frac{U_{ij}}{c_0}}$	Δt^* (ms)	t^* (ms)	Δx (ft)	x (ft)
750	9	9	816	1.22	11.0	11.0	9.0	9.0
500	18	9	706	1.19	10.7	21.7	7.6	16.6
400	28	10	623	1.16	11.6	33.3	7.2	23.8
300	47	19	555	1.14	21.7	55.0	12.0	35.8
200	95	48	443	1.11	53.5	108.5	23.6	59.4

During the interval Δt^* the shock front progresses a distance

$$\Delta x_{ij} = c_{ij} \Delta t^*_{ij}$$

Therefore a graph of the upper and lower shock stress values can be plotted against the distance the shock has penetrated. This is done in Figure 4.21.

Step 6

Draw the waveforms corresponding to the time $t_0^* = h/c_0$ (the time the wave front first reaches the structure) and $x = h$, and several other intermediate waveforms. This is shown in Figure 4.22

Step 7

Find the slope of the instantaneous stress waveform at the depth h , for each time, t^* , and plot this slope against t^* .

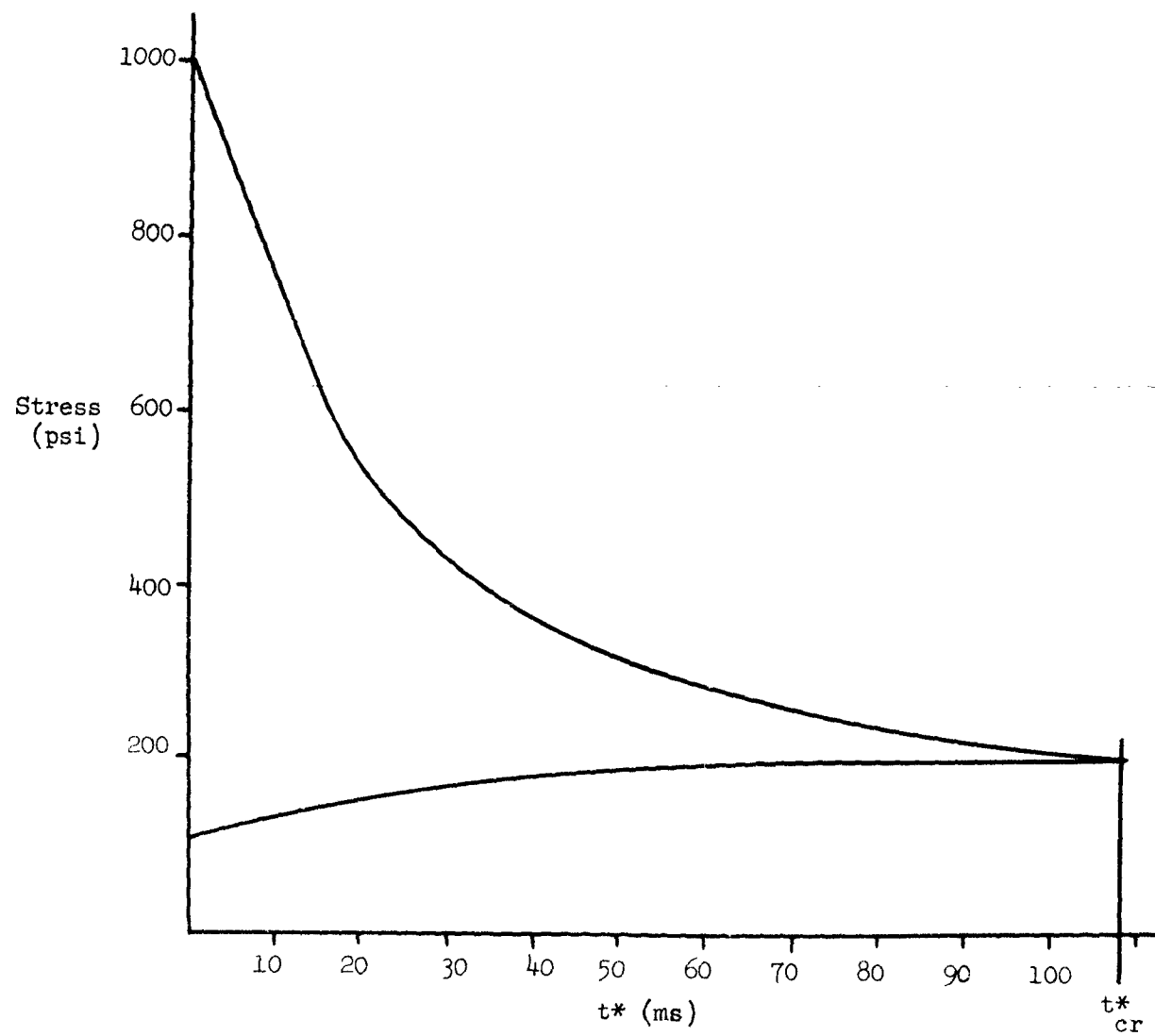


Figure 4.20 STRESS VERSUS t^*

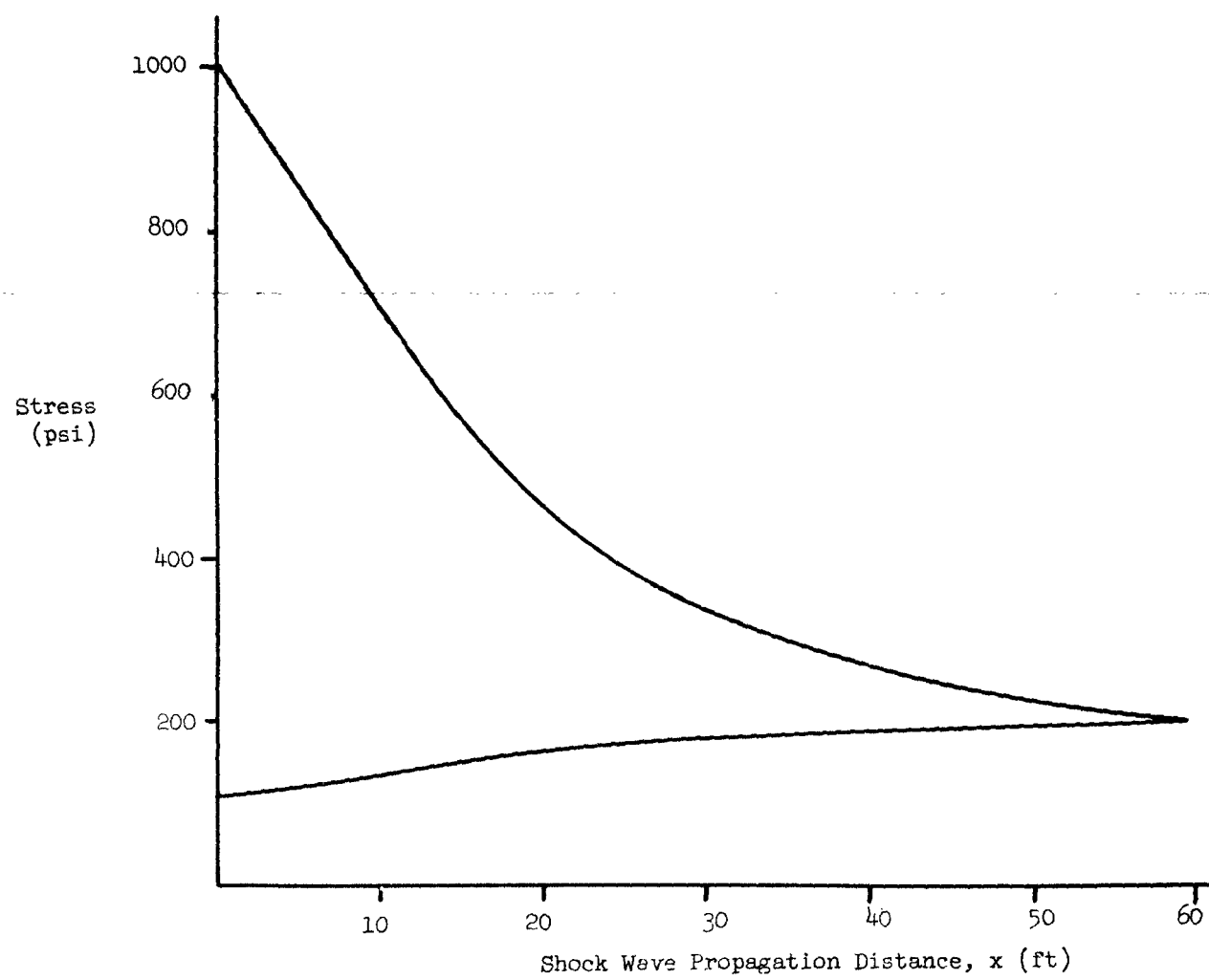


Figure 4.21 STRESS VERSUS SHOCK WAVE PROPAGATION DISTANCE

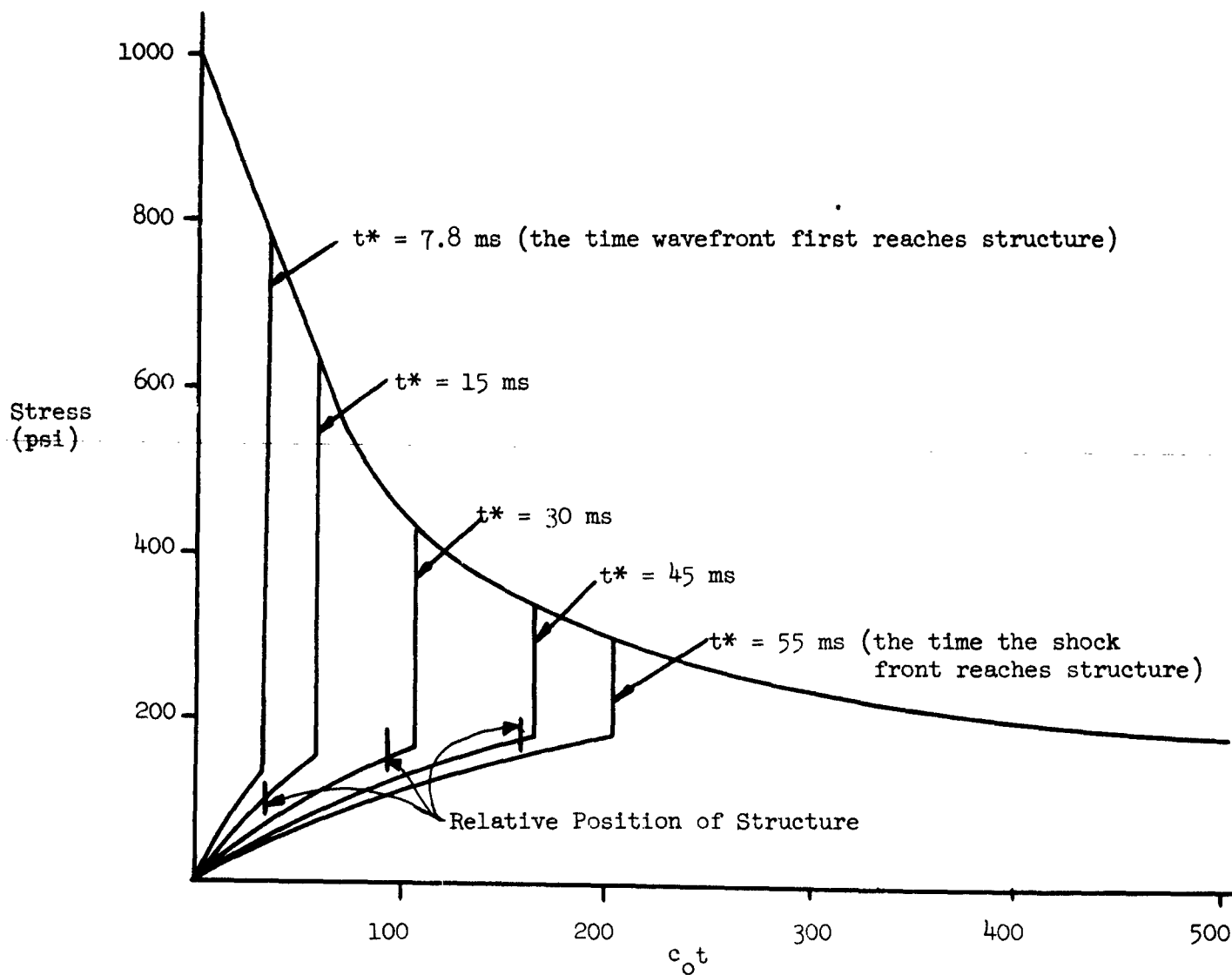


Figure 4.22 WAVEFORMS AT DIFFERENT VALUES OF t^*

The particle velocity, $\frac{1}{\rho} \left(\frac{\partial z}{\partial t^*} \right)_x$, is the shaded area between t_0^* and t^* , for $t_0^* \leq t^* \leq t_s^*$. This is shown in Figure 4.23.

Step 8

The velocity after the shock can be calculated from the expression

$$\dot{z}_j = \sqrt{\frac{1}{E_s \rho} (p_j - p_j')^2 + (\dot{z}_j')^2} \quad (4.8)$$

where

\dot{z}_j' = velocity immediately before the shock

\dot{z}_j = velocity immediately after the shock

ρ = mass density (assumed constant)

p_j' = stress immediately before the shock

p_j = stress immediately after the shock

$E_s = \frac{p_j - p_j'}{\epsilon_j - \epsilon_j'}$

ϵ_j' = strain immediately before the shock

ϵ_j = strain immediately after the shock

Step 9

During the unloading portion, beginning immediately after the shock, elastic theory can be used, so

$$-\frac{1}{\rho} \left(\frac{\partial p}{\partial x} \right)_t = \frac{1}{\rho c_0} \left(\frac{\partial p}{\partial t} \right)_x = \left(\frac{\partial^2 z}{\partial t^{*2}} \right)_x$$

$$\therefore \dot{z}_u = \dot{z}_j - \frac{p_j - p_u}{\rho c_0}$$

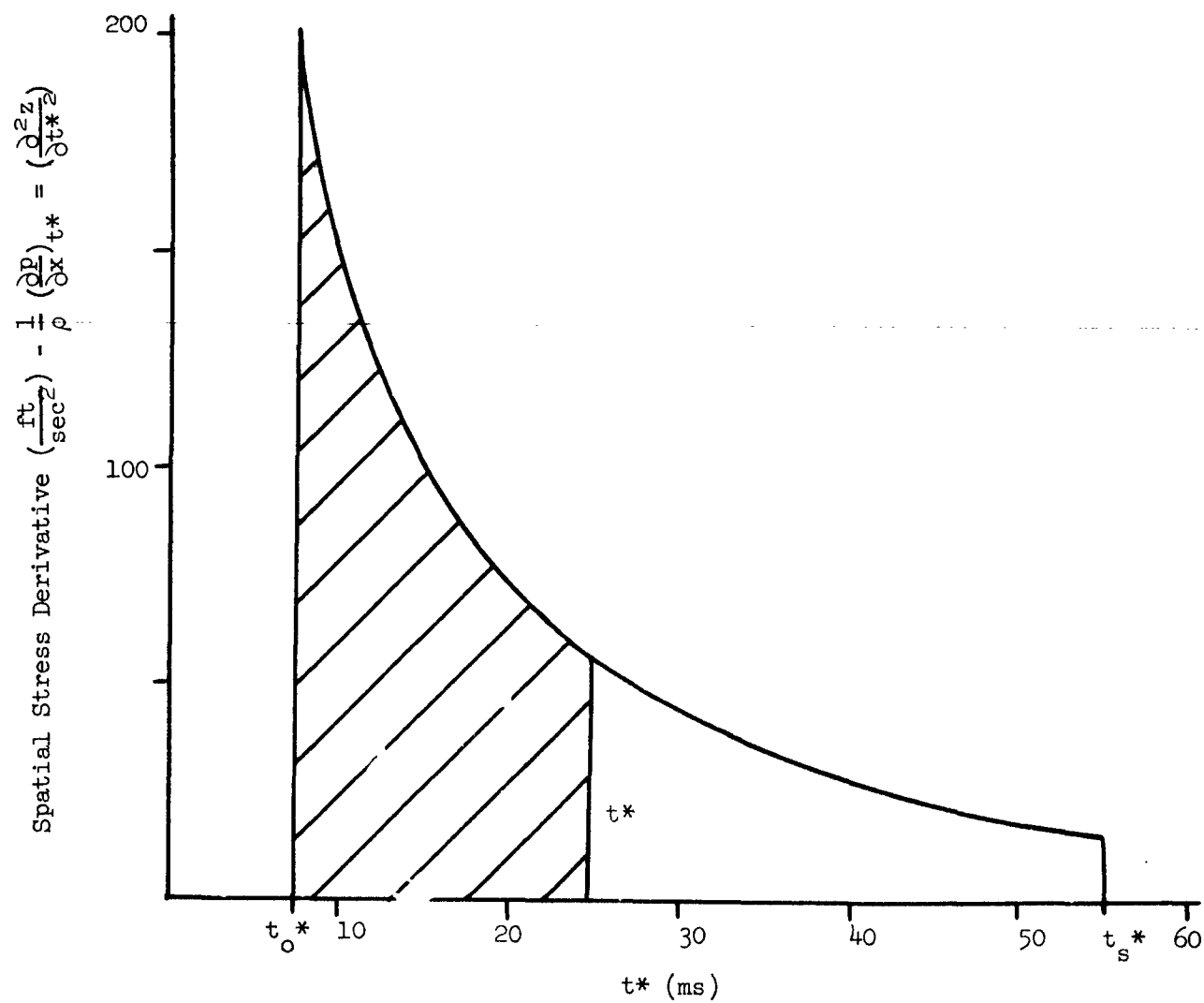


Figure 4.23: $\frac{1}{\rho} \left(\frac{dp}{dx}\right)$ VERSUS t^*

where

- \dot{z}_u = velocity during the unloading phase
- \dot{z}_j = velocity immediately after the shock
- p_j = stress immediately after the shock
- p_u = stress during unloading
- ρ = density (assumed constant)
- c_o = velocity of propagation, computed from the initial tangent modulus and assumed constant, thereby implying linear elasticity

4.1.5 Vertical and Horizontal Free Field Inputs

Strictly speaking the vertical velocity would be obtained by multiplying the velocity curves developed for Cases I and II of Section 4.1.4 by the cosine of the Mach angle. The Mach angles are small however and this refinement therefore is smaller than the errors already included in the curves.

The horizontal motion components are more difficult to estimate. It has been pointed out already that test records diverge grossly from the predictions of elastic theory; the shear wave does not terminate horizontal velocity as predicted by elastic theory.

If suspension systems are used we have found that the horizontal systems should be of low frequency. For this case the only significant input is the total horizontal displacement.

If shock isolation is not used, dependence being placed on equipment ruggedness and the inherent "isolation" provided by soil structure interaction only the initial portion of the horizontal velocity curve is required. If ruggedized

equipment can resist the onset of the ground shock wave it can subsequently resist the onset of the reflected wave.

The initial horizontal velocity can be obtained by multiplying the predicted vertical velocity by the sines of the appropriate Mach angles. Since the Mach angles are small at the higher pressures the resulting velocities will be small. At some pressure, not yet known, the directly transmitted shock will dominate the horizontal component of air induced motion.

The total horizontal displacement is equal to the area under the horizontal velocity curve. However, it must be remembered that the horizontal component of reflected wave velocity adds to the direct component. In a purely elastic medium with perfect reflection at bedrock and no significant wave decay the horizontal displacement, x_h , would be given by

$$x_h = \frac{2I}{\rho c} \sin \phi$$

where

I is the impulse of the aeroshock wave,

ϕ is the Mach angle of the ground shock compression wave.

It does not seem intuitively reasonable though to consider that after vertical motion of the structure reaches its maximum (at arrival of the reflected wave) horizontal motion continues for any length of time. For this motion to continue, the column of soil between structure and bedrock would have to continue to shear, a process that rapidly dissipates energy in real soils.

Therefore we take as a reasonable approximation of peak horizontal displacement

$$z_{h \max} = \sin \phi \ z_{v \max}$$

where $z_{h \text{ max}}$ and $z_{v \text{ max}}$ are the maximum components of horizontal and vertical motions respectively. This formula is equivalent to

$$z_{h \text{ max}} = \frac{\bar{c}}{U} z_{v \text{ max}}$$

where

U is the aeroshock velocity

and \bar{c} is an average wave velocity.

A value of \bar{c} can be computed from

$$\bar{c} = \frac{p}{\rho \dot{z}_{av}}$$

This approximation yields a horizontal to vertical displacement ratio on the order of 1/3 for Nevada Test Site soil and overpressures in the 100 to 300 psi region.

4.2 Approximate Estimates of Input

If preliminary estimates of rattle space requirements must be carried out without the benefit of site information it is suggested that the following approach be used.

1. Estimate bedrock depth from topographic maps. If the site is unknown guess bedrock to be 150 feet below surface.
2. If the general class of soil (clay, sand) is known estimate compression wave velocity (see Section 8). If the soil is unknown guess a wave propagation velocity of 1000 ft/sec.
3. Estimate times required for wave to travel from surface to structure and surface to bedrock to structure.

4. Estimate wave decay according to percylic damping theory. A conservative value of the damping coefficient, δ , can be taken as 0.2. (It will be higher for most real soils.)
5. Estimate the maximum impulse, I , that can be encompassed between structure and bedrock. This will occur at about the time the reflected wave reaches the structure.
6. Estimate maximum vertical displacement, $z_v \text{ max}$, from the formula

$$z_v \text{ max} = \frac{I}{\rho c}$$

7. Estimate maximum horizontal displacement $z_h \text{ max}$, from the formula

$$z_h \text{ max} = \frac{I}{\rho U}$$

where U is the aeroshock front velocity.

Silos are sometimes founded on bedrock. If the silo shell does not contain girth expansion joints the silo vertical motion will be equal to bedrock vertical motion. The latter can be estimated conservatively as follows:

1. Estimate bedrock seismic velocity, c_s . If bedrock is unknown guess it to be 10,000 ft per second.
2. Estimate bedrock density. If bedrock is unknown guess the density to be 150 lbs per cubic foot.
3. Estimate the impulse of the overpressure wave, I .
4. Compute vertical displacement

$$z_v \text{ max} = \frac{1}{2} \frac{I}{\rho c_s}$$

The factor $\frac{1}{2}$ is included to account roughly for geometric dispersion of the wave. Its actual value generally will be more nearly $1/3$ or $1/4$.

SECTION 5

SOIL-STRUCTURE INTERACTION

A simplified analysis of soil-structure interaction is given in Appendix A. Even the simplified analysis, however, is quite complex to apply. In this section the main results of the analysis and estimation procedures accounting for the principal influences of the interaction will be given.

The most important prediction of the interaction study is that the significant modes of most structures in real soils will be damped near critical; the lower modes will be over critically damped. This then implies that the structure will follow the soil motion quite closely except within an interval equal approximately to the first half or three quarters period of undamped vibration of the structure.

A second consequence of the interaction study is that the rise time for the forcing functions of the lower modes (translational rigid body mode and first bending mode) is on the order of $3/4$ to 1 times the transit time of the ground shock wave over the structure. Further, it can be deduced by inspection of Equations (A-19) and (A-24) (Appendix A) that the initial rates of rise of the forcing functions for the higher order modes are no greater and generally less than the rate of rise of the first bending mode and rigid body mode (the initial rates of rise of these are identical). Very shortly after initial impingement of the ground shock wave on the structure the rates of rise of the higher order forcing functions become less than the rates of rise of the rigid body and first bending mode forcing function. Further, the maximum amplitudes of the higher order forcing functions decrease rapidly with increase of modal index. (A

review of Appendix A.4 with attention directed toward the physical meaning of the quantities involved will make this evident without mathematical manipulation.)

The response of the structure modes to their forcing function also decreases rapidly with increase of modal index. Thus we intuitively expect that the significant motion of the structure interior will depend only upon the rigid body modes and the first few distortion modes.

It becomes a practical impossibility to draw general conclusions from purely mathematical deductions because of the complexity of the problem. Accordingly, a computer program was set up and the relative responses of the various modes for a silo-like structure were determined for a range of parameter variations. (The computer program and detailed results obtained are included in the first interim report on this project. They are not repeated in this report.)

The results of this investigation indicate that only two modes need be considered for developable structures:

1. The rigid body mode.
2. The first deformational mode.

An elementary manipulation of the formulas for the soil resistance factor K and the modal damping factor δ_1 shows that for reinforced concrete shells the damping factor for the rigid body mode, δ_r , lies between the limits

$$0.6\sqrt{\frac{R}{h}} < \delta_r < 0.75\sqrt{\frac{R}{h}} \quad (5.1)$$

R/h is the radius to thickness ratio of the shell. (For steel shells the limits of the coefficient are 0.33 to 0.42.)

Thus even for a truly massive concrete shell having an R/h ratio of only 4 the rigid body mode is overcritically damped.

If a structure is so stiff that the first deformational mode is less than critically damped the deformation of the mode is insignificant when compared with the rigid body motion and may safely be neglected.

5.1 Summary of Interaction Theory

The theory developed in Appendix A will be summarized. Since this summary will be concerned only with the rigid body mode and first deformational mode the subscripts r and d respectively will be used to denote them. A subscript "i" will be used to denote a mode in general.

The amplitude, T_i , of the response of the ith mode is given by the equation

$$\ddot{T}_i + 2\delta_i \Omega_i \dot{T}_i + \Omega_i^2 T_i = \tau_i \quad (5.2)$$

where

τ_i is the forcing function for the ith mode, to be defined subsequently

Ω_i is the circular frequency of the ith mode

and δ_i is the damping factor for the ith mode.

For the rigid body mode the circular frequency Ω_r is given by

$$\Omega_r^2 = \frac{K_r}{m} \quad (5.3)$$

and

$$K_r = \frac{\rho c^2}{(1+\nu) \lambda_r} \quad (5.4)$$

where

- m = unit mass of the shell
- c = soil compression wave velocity
- ρ = soil unit mass
- ν = Poisson's Ratio of soil
- λ_r = a characteristic length of the shell.

The K factor is difficult to estimate. Though the simplified equations introduce a constant to account for the soil displacement resistance it is in fact, even for a linear, elastic medium, a variable depending upon the medium characteristics, structure geometry, and manner of loading the structure. For a spherical shell, which can be investigated analytically, the K obtained for uniform radial expansion of the sphere is twice that obtained for a rigid body translation of the sphere.

The average K factor computed for the first deformational mode lies between these limiting cases.

It is suggested that in actual computation two K factors be used, even though the derivation of the basic equations is based on a single constant value.

Equation (5.4) is based on the theory of elasticity so it can, at best, be only approximate for real, nonlinear soils. The characteristic length λ_r is given approximately by the equation

$$\lambda_r = \frac{3V}{A} \quad (5.5)$$

where

- V = structure volume
- A = structure surface area.

Equation (5.5) is accurate within the approximations of the theory of elasticity for spherical shells and any other closed shells so proportioned that a small, rigid lateral displacement of the shell induces a uniform stress in the direction of displacement at the soil-shell interface.

If experience computing static foundation displacements can be considered indicative of the accuracy of Equations (5.3), (5.4), and (5.5) then they must be considered to have an overall uncertainty factor of ± 50 percent or so. However, we simply have not enough experimental evidence available yet to justify development of more precise formulas.

The K_d factor for the first deformational mode can be taken 50 percent higher than K_r .

$$K_d = 1.5 K_r \quad (5.6)$$

For the bending mode

$$\Omega_d^2 = \omega_d^2 + \frac{K_d}{m} \quad (5.7)$$

where

$$\omega_d = \text{circular frequency of first bending mode in vacuum}$$

(See Section 8)

The damping factor δ_i is defined for both modes

$$\delta_i = \frac{1}{2} \frac{c}{m\Omega_i} \quad (5.8)$$

The forcing function, τ_1 , is given by

$$\tau_1 = \frac{1}{N_1} \int_A \bar{p}_1 \cdot \bar{\phi}_1 \, dA, \quad (\text{A.24})$$

the norm, N_1 , is given by

$$N_1 = m \int_A \bar{\phi}_1 \cdot \bar{\phi}_1 \, dA, \quad (\text{A.25})$$

and the input vector, \bar{p}_1 , by

$$\bar{p}_1 = \bar{n} \cdot \bar{p} + K\bar{z} + \rho c \dot{\bar{z}}. \quad (\text{A.19})$$

In these formulas

- A = structure area
- $\bar{\phi}_1$ = vector mode
- \bar{n} = normal unit vector
- \bar{p} = free field pressure tensor
- \bar{z} = free field particle displacement.

Evidently, any system of solution that retains even the major influences of these equations is bound to be complex. It is possible though to deduce the principal influences of the interaction from critical examination of the equations and to frame a much simpler method of solution that is accurate enough for most shock isolation computations.

5.2 Simplification of Interaction Procedure

We begin by considering the input vector \bar{p}_1 .

Appendix Section A.4 is devoted to computation of \bar{p}_1 . Following the method presented there we envision the structure to be enclosed by an imaginary rectangular

parallelepiped having two faces parallel to the "plane" of the advancing ground shock wave. Then the vector \bar{p}_1 can be represented as six scalar forces perpendicular to the faces of the parallelepiped.

For the rigid body motion the forces on the four surfaces that are not parallel to the plane of the shock wave contribute nothing to the forcing function. On the two remaining surfaces the scalar pressures p_1 can be simplified to:

For the windward surface

$$p_1 = p + \rho c \dot{z} + K_r z \quad (5.9)$$

and on the leeward surface

$$p_1 = p - \rho c \dot{z} - K_r z \quad (5.10)$$

where p is the free field wave pressure and \dot{z} is the free field velocity. The free field displacement z can be obtained by integration of the \dot{z} curve.

At any instant $\rho c \dot{z}$ is equal to p . However, in order to carry out the interaction computations an average value of ρc must be chosen. Since the shapes of the p and \dot{z} curves may differ markedly the distinction between the terms has been retained.

For the deformational mode the scalar pressures on the four parallelepiped surfaces perpendicular to the ground shock wave are

$$p_1 = - \nu p \quad (5.11)$$

where

ν is Poisson's Ratio.

Now let us examine the result of evaluation of the forcing functions τ_r and τ_d . The vector mode ϕ_r consists simply of a unit vector in the direction of the advancing ground shock wave. Therefore its scalar projection on the windward face of the parallelepiped is simply +1 and on the leeward face is -1. Thus if the transit time of the wave moving over the structure were small and the rate of decay of p_1 not too great, after engulfment the forcing function τ_r would be given to a very close approximation by

$$\tau_r \approx \frac{2A}{N_r} (\rho c \dot{z} + K_r z) \quad (5.12)$$

For the rigid body mode

$$\frac{A}{N_r} = \frac{1}{2m} \quad (5.13)$$

so

$$\tau_r \approx \frac{1}{m} (\rho c \dot{z} + K_r z) \quad (5.14)$$

We note also that since τ_i is an integral over the surface of the structure, peaks and steps will not appear in τ_i . The abrupt onset of pressure cannot be applied simultaneously to the entire surface of the structure or even to a major fraction of the surface. The effect of the integral is to smooth out irregularities within an interval equal to the transit time.

Since the component of τ_r contributed by p cancels out at any time when the p 's on opposite sides of the structure are equal, the only contributions of p to the forcing function occur when there is a rapid change in the magnitude of p within an interval equal to the transit time. If such rapid changes exist they are averaged over the transit time interval and make small contributions to τ_r .

At this point it is of interest to compare the transit time with the period of vibration of the rigid body mode. For a horizontal cylinder the transit time t_t is given by

$$t_t = \frac{2R}{c} \quad (5.15)$$

The period of vibration, t_r , of the rigid body mode is

$$t_r = 2\pi \sqrt{\frac{m}{k_r}} \quad (5.16)$$

For a cylinder, this is equivalent to

$$t_r = \frac{2\pi R}{c} \left(\frac{h}{R}\right)^{1/2} \left[\frac{3}{2} (1+\nu) \frac{\gamma_c}{\gamma_s}\right]^{1/2} \quad (5.17)$$

Thus the ratio t_r/t_t is

$$\frac{t_r}{t_t} = \pi \left(\frac{h}{R}\right)^{1/2} \left[\frac{3}{2} (1+\nu) \frac{\gamma_c}{\gamma_s}\right]^{1/2} \quad (5.18)$$

where

- h = shell thickness
- R = shell radius
- γ_c = shell density
- γ_s = soil density
- ν = Poisson's Ratio of soil.

For a concrete shell and a Poisson's Ratio of 0.3

$$\frac{t_r}{t_t} = 5 \left(\frac{h}{R}\right)^{1/2} \quad (5.19)$$

Thus for a cylindrical shell having a radius to thickness ratio less than 25 the transient time is less than a period of vibration in the rigid body mode. This mode is overcritically damped. Therefore variations in the τ_r curve will not strongly influence the resulting response curve. Accordingly, the influence

of p on the rigid body mode can be neglected and only the z and \dot{z} components considered.

In accordance with the approximation already adopted (Equation (5.6)) Equation (5.7) can be rewritten

$$\Omega_d^2 = \omega_d^2 + 1.5 \Omega_r^2 \quad (5.20)$$

Substituting the expression for ω_d^2 (Section 8) and Ω_r^2

$$\Omega_d^2 = \frac{3}{5} \left(\frac{h}{R}\right)^2 \left(\frac{c_c}{R}\right)^2 + \frac{1}{(1+v)} \left(\frac{\gamma_s}{\gamma_c}\right) \left(\frac{R}{h}\right) \left(\frac{c_c}{R}\right)^2 \quad (5.21)$$

where

γ_s = soil density

γ_c = shell density

c_c = sonic velocity of shell material

and other symbols are as previously defined. Then the ratio t_d/t_r becomes

$$\frac{t_d}{t_r} = \frac{\pi \left(\frac{h}{R}\right)^{1/2}}{\left[\frac{1}{(1+v)} \left(\frac{\gamma_s}{\gamma_c}\right) + \frac{3}{5} \left(\frac{c_c}{R}\right)^2 \left(\frac{h}{R}\right)^3 \right]^{1/2}} \quad (5.22)$$

Taking for a concrete shell

$c_c = 11,000$ ft/sec

$\gamma_c = 150$ lbs/ft³

and for soil

$c = 1500$ ft/sec

$\gamma_s = 115$ lbs/ft³

$v = 0.3$

$$\frac{t_d}{t_r} = \frac{4.1 \left(\frac{h}{R}\right)^{1/2}}{\left[1 + 5450 \left(\frac{h}{R}\right)^3\right]^{1/2}} \quad (5.23)$$

The damping factor can, after some manipulation, be expressed

$$\delta_d = \frac{1}{2\pi} \left(\frac{R}{h}\right) \left(\frac{\gamma_s}{\gamma_c}\right) \left(\frac{t_d}{t_r}\right) \quad (5.24)$$

These have the values

R/h	=	4	7	10	20
t_d/t_r	=	0.22	0.38	0.51	0.71
δ_d	=	0.118	0.355	0.68	1.88

Examination of the table shows that for some possible values of (R/h) the damping of the first vibrational mode is considerably less than critical. However, we note also that for these cases the period of vibration is only a fraction of the transit time and therefore the response will closely follow the input.

The vector mode $\bar{\phi}_d$ is symmetrical. Therefore, the velocity and displacement terms cancel out except when these have a rapid change of value within the interval of the transit time. Even these rapid changes will not markedly influence the resulting response curves.

Taking v to be 0.3 the forcing function τ_d becomes after engulfment

$$\tau_d \approx \frac{0.27}{m} p \quad (5.25)$$

During the initial half of the engulfment time all three components will contribute to both forcing functions. Therefore, if the initial rise proves to be significant it is suggested that the amplitudes of τ_r and τ_d be computed at

$1/2 t_t$ reflecting the three components. Smooth curves starting at zero, passing through the computed points at $1/2 t_t$ and smoothly merging with the values at t_t then can be sketched.

It is noted that if Equation (5.2) is divided through by Ω_1^2 , then the term τ_1/Ω_1^2 has the dimensions of length and at some distance from the origin will represent the terminal displacement that the damped response asymptotically approaches. In this form the relative importance of the rigid body and deformational modes can be easily judged.

Then, subsequent to engulfment, the equation for the rigid body mode forcing functions becomes

$$\frac{\tau_r}{\Omega_r^2} = \frac{3(1+\nu) v}{\bar{c} A} \dot{z} + z \quad (5.26)$$

where

- v = structure volume
- A = structure surface area
- ν = Poisson's ratio
- \bar{c} = average compression wave velocity
- \dot{z} = free field particle velocity.

Now the expression

$$3(1+\nu) \frac{v}{A}$$

is of the same order of magnitude as the structure "radius" regardless of structure complexity. Thus the first term of Equation (5.26) is approximately equal to

$$\frac{R\dot{z}}{c}$$

From a typical example it can be shown that the maximum contribution of the velocity term to the displacement is on the order of 1 inch for a 30 ft diameter cylinder and 1500 ft per second soil. The maximum displacement is about 18 inches for the same structure; thus the velocity term contributes a displacement increment only 5 percent as great as the soil displacement term, z .

The deformational motion is more difficult to investigate because the modal geometry $\bar{\phi}_d$ varies between structures. For a horizontal cylinder the equation becomes

$$\frac{\tau_d}{\Omega_d^2} = \frac{0.27 g \bar{p} R}{\gamma_c \bar{c}^2 \left[\frac{3}{5} \left(\frac{h}{R} \right)^3 \left(\frac{c}{\bar{c}} \right)^2 + \left(\frac{1}{1+\nu} \right) \left(\frac{\gamma_s}{\gamma_c} \right) \right]} \quad (5.27)$$

For a reinforced concrete shell of $R/h = 7.5$ and $\bar{c} = 1500$ ft/sec, the term in brackets becomes about 0.66. Therefore

$$\frac{\tau_d}{\Omega_d^2} = \frac{p(\text{psi})}{1000} \quad [\text{in}] \quad (5.28)$$

for a 30 ft diameter shell.

This is a small displacement in comparison with the rigid body displacement. Another fact emerges, however, that is of practical importance. The displacement indicated by Equation (5.27) is almost exactly the displacement suffered by the structure surrounded by the soil and statically loaded.

In Section 5.3 a simplified design method based on these observations is given.

5.3 Simplified Design Method

It is again pointed out that this design procedure is necessary only if isolators are to be omitted or if the more desirable and economical low frequency systems are not used. A method for determining when isolators can be omitted is given in Section 7.

The interior structure motion consists of two components:

1. A rigid body motion T_r
2. A deformational motion T_d

The rigid body motion is the solution of Equation (5.29)

$$\frac{\ddot{T}_r}{\Omega_r^2} + \frac{2\delta_r}{\Omega_r} \dot{T}_r + T_r = z \quad (5.29)$$

where

$$\Omega_r^2 = \frac{\rho \bar{c}^2 A}{3(1+\nu)mV}$$

$$\delta_r = \frac{\rho \bar{c}}{2m\Omega_r}$$

$$\frac{2\delta_r}{\Omega_r} = \frac{(1+\nu)3V}{\bar{c} A}$$

and

- | | | |
|-----------|---|------------------------------------|
| z | = | free field displacement |
| m | = | structure mass per unit area |
| V | = | structure volume |
| A | = | structure surface area |
| ρ | = | soil unit mass |
| \bar{c} | = | average compression wave velocity. |

If t_t is the transit time of the ground shock wave over the structure and

$$t_r = \frac{2\pi}{\Omega_r} \quad (5.30)$$

the response T_r will be practically identical with z after a time period t^*

where

$$t^* = t_r + t_t \quad (5.31)$$

If necessary T_r can be determined within the interval

$$0 < t < t^*$$

by solution of Equation (5.29)

The deformational motion can be approximated by Equation (5.32)

$$\frac{\ddot{T}_d}{\Omega_r^2} + (1+\nu) \frac{3V}{cA} \dot{T}_d + T_d = \hat{z} \quad (5.32)$$

where

$$\Omega_d^2 = \omega_d^2 + 1.5 \Omega_r^2 \quad (5.33)$$

ω_d = circular frequency of structure vibration in vacuum

\hat{z} = static deformation of structure in soil under the imposed pressure.

For computing \hat{z} the actual soil pressure at the structure depth should be averaged out within an interval equal to the transit time t_t .

The net interior structure motion, T , is then

$$T = T_r + T_d \quad (5.34)$$

One of many methods for solving Equations (5.29) and (5.32) is given in Appendix B.

In this section the pressures and velocities used have been the net values acting in the direction of soil particle motion. These are the appropriate inputs for "floating" structures completely surrounded by soil.

If a structure founded on bedrock is used, e.g., some silos already built, only the horizontal component of motion need be considered. The equations of this section are valid for the horizontal component if horizontal pressures and velocities are used as inputs and if substantial vertical motion is prevented by the bedrock.

SECTION 6

NONLINEAR SYSTEMS

Nonlinearities of shock isolation system must be considered from two standpoints.

1. All real systems contain nonlinear elements even though for practical design purposes we may simplify the analysis by "linearizing" the systems. In most instances the errors so introduced are of no practical importance and, therefore, the procedure is perfectly acceptable. However, occasionally, the nonlinearities introduce qualitative changes in the behavior of the real system which are of sufficient importance that they must be considered in the design.
2. For various reasons it may be desirable to deliberately design nonlinear isolation systems in order to gain specific advantages.

The theory of nonlinear vibrations is extremely complex and still in its infancy. Further, by far the largest portion of the work already carried out understandably has been directed towards solution of steady-state problems since these comprise the largest proportion of nonlinear problems of practical importance. Because the principle of superposition cannot be used for the solution of nonlinear mechanical problems the variety of existing steady-state solutions are of very limited value to designers interested in the transient response of nonlinear systems. No analog of the Duhamel integral exists for nonlinear vibration problems.

At the present state of our knowledge no general, well developed theory of transient nonlinear vibration exists. The mass of theory and data available is directed toward solution of certain specific problems or of problems that can be characterized by certain specific nonlinear differential equations. Further, even at best, application to particular problems of the methods that have been developed is generally quite tedious and time-consuming and, if carried out analytically, almost invariably requires the use of a high speed computer.

It was believed that no purpose would be served by burdening this report with a compendium of solutions and techniques for analyzing specific nonlinear problems. Determination of the effects of nonlinearities on nearly linear systems is appropriate to the refined final design of shock isolation systems which is not within the scope of this report. However, preliminary design of nonlinear systems that might be used in lieu of the more conventional linear types is within the scope of this report. Therefore, on the project some effort was expended to develop criteria that would point out the advantages or disadvantages of nonlinear systems under particular circumstances and to develop methods to expeditiously determine rattle space requirements, acceleration limits, etc. for nonlinear systems. An attempt was made to do this for the general nonlinear system as opposed to cataloging specific types of nonlinearities. Obviously, the results presented are far from complete even for cases to which they most strictly apply. Again we emphasize that the purpose of this section is to afford the designer fairly rapid methods that he can use to expeditiously establish limits for the important parameters of rattle space requirements and

peak accelerations to which the isolated body will be subjected. Even more important, perhaps, is presentation of means by which he can determine whether a nonlinear system has any clear cut advantages or disadvantages over a more conventional linear system.

Nonlinear systems can be characterized in a number of ways. In this section we will find it convenient to regard the isolator as an energy storing device. Two general classes are considered:

1. Conservative systems in which all the energy delivered to the isolator by mechanical motion and stored within the isolator as potential energy ultimately is released by the isolator as mechanical motion. A conservative system is the nonlinear analogue of undamped linear isolators.
2. Nonconservative systems within which a portion of the energy delivered to the isolator by mechanical motion is dissipated as heat or otherwise and is not subsequently released as mechanical motion, the analogue of damped linear isolators.

6.1 Conservative Nonlinear Systems

Consider a single degree of freedom nonlinear isolator. It can be symbolized by the scheme shown in Figure 6.1. The problem is to determine the displacement $x(t)$ and the force $F(t)$ in terms of the known input $z(t)$ and the isolator characteristics. A variable $y(t)$, corresponding to the rattle space, is defined

$$y(t) = x(t) - z(t) \quad (6.1)$$

Note that $y(t)$ is defined positive for a decrease in the space between the mass and the isolator support.

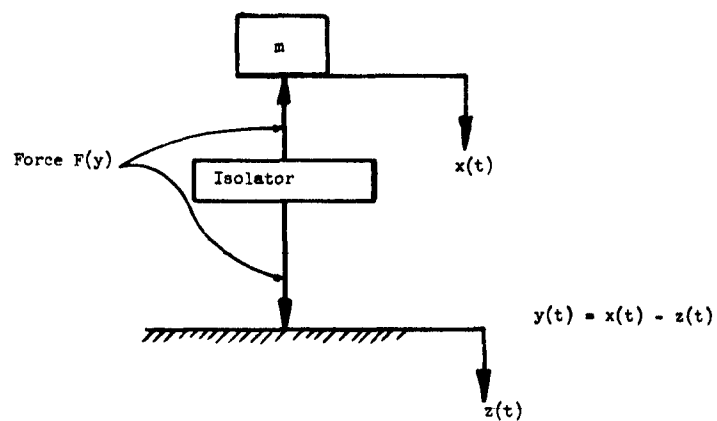


Figure 6.1 SCHEMATIC OF CONSERVATIVE NONLINEAR SYSTEM

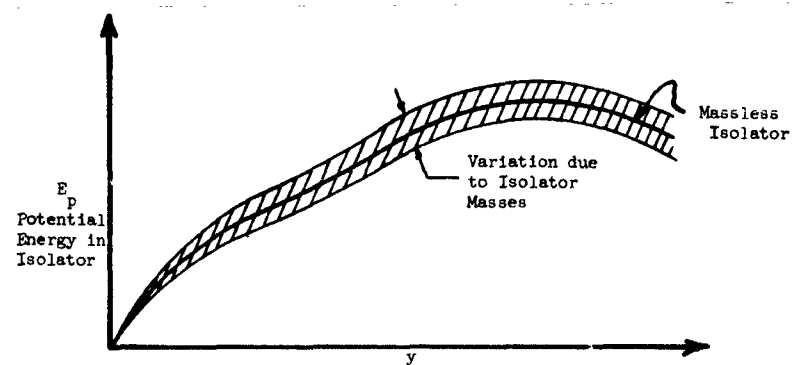


Figure 6.2 ENERGY-STROKE DIAGRAM OF ISOLATOR

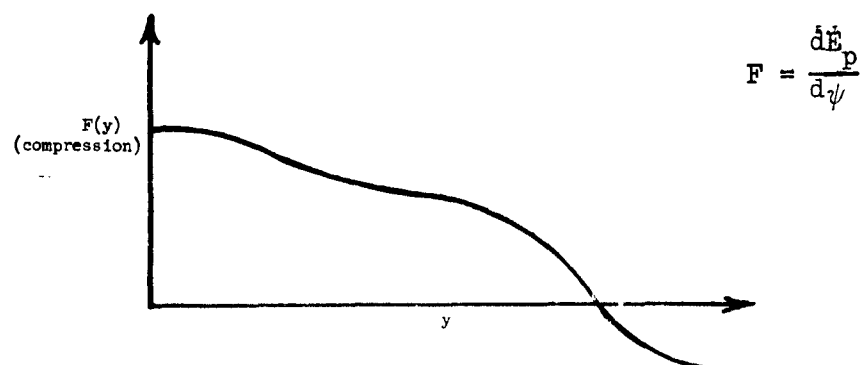


Figure 6.3 FORCE-STROKE DIAGRAM OF ISOLATOR

Now, regardless of the mechanical complexity of the isolator, if it is conservative, its mechanical characteristics can be represented by a curve similar to Figure 6.2 if the mass of the isolator is taken to be zero. If the masses of the isolator elements are considered the curve of Figure 6.2 broadens somewhat, the amount of broadening being proportional to the ratio of the kinetic energy of the masses to the potential energy stored. This condition is roughly analogous to a spring-mass system having a spring so heavy its mass must be included in the analysis. Even for the linear system this greatly complicates analysis. Therefore, in this section the mass of the isolator will be presumed small enough to neglect.

For the massless isolator the force developed is equal to the derivative of potential energy, i.e.,

$$F = \frac{dE_p}{dy} \quad (6.2)$$

Assume now that the isolator has been placed on its support. Its compression y and potential energy E_p are zero. Then as the supported mass is gradually lowered on the isolator it compresses an amount y , stores potential energy E_p , and develops a force F .

At equilibrium the force F must be equal to the weight mg .

Figure 6.4 illustrates two differing energy-displacement curves and their resulting equilibrium positions. A practical value of nonlinear systems is immediately evident. The equilibrium energy of system 2 is much smaller than that of system 1 for the mass chosen. Now as a first approximation the cost of an isolation system is roughly proportional to the equilibrium energy. Therefore

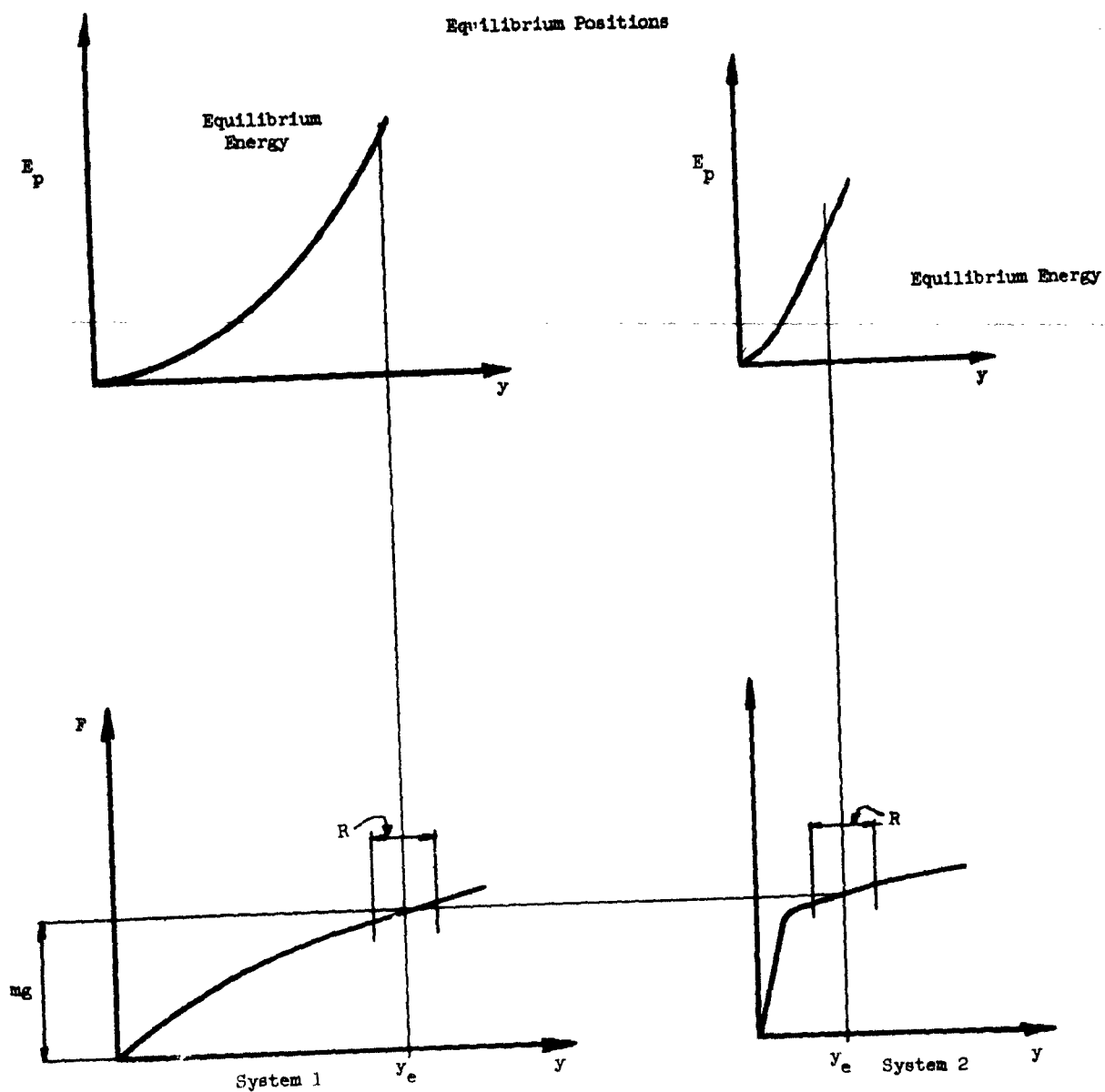


Figure 6.4 COMPARISON OF EQUILIBRIUM ENERGY OF TWO NONLINEAR SYSTEMS

if system 2 were of the same order of mechanical complexity as system 1, it would be considerably cheaper than system 1.

We also note that if the two systems were designed so that

$$\frac{dF}{dy} = \frac{d^2 E_p}{dy^2} \quad (6.3)$$

were nearly equal and constant within the stroke range R centered on the equilibrium position the systems would be nearly linear within R and of the same frequency. A bi-linear system such as system 2 could be designed for a protective structure by making R equal to twice the relative displacement taken from a shock spectrum at frequency

$$f = \frac{1}{2\pi} \sqrt{\frac{1}{m} \left. \frac{dF}{dy} \right|_{y_e}} \quad (6.4)$$

A close approximation of the rattle space requirements can be quickly made using the E_p versus y and F versus y graphs.

The time required for the vertical component of structure motion to reach its maximum is about equal to the time required for the ground pressure wave to travel from the structure to bedrock and reflect back to the structure. Now, generally, the structure will be within 100 feet of bedrock and the ground pressure wave propagates at 500 to 1000 ft/sec. minimum. Thus the time to maximum downward displacement of the structure is on the order of 250 msec. or less. The magnitude of the structure displacement is given with fair accuracy by

$$z_{\max} = \frac{I(t^*)}{\rho c} \quad (6.5)$$

$$t^* = \frac{2D}{c} \quad (6.6)$$

where

$I(t^*)$ - impulse of blast wave (ground wave) between
time zero and time t^*

D = Depth of bedrock below structure

\bar{c} = Soil compression wave propagation velocity

ρ = soil mass density

As soon as the floor of the structure begins to descend the isolator begins to expand and deliver some of its stored energy to the floor and soil below. In expanding the force, F , exerted against the mass decreases somewhat so the mass begins to descend, thereby gaining kinetic energy due to its velocity and losing potential energy as measured in a motionless coordinate system. However, the potential energy of the mass with respect to the floor increases because the floor descends faster than the mass and therefore the mass rises with respect to the floor.

Since isolator systems generally are of long period (a second or so) and maximum vertical displacement of the floor occurs generally in less than $1/4$ second, as a first approximation we can assume that the mass remains motionless during floor descent to maximum. Then, if necessary we can correct for initial mass motion.

If the mass remains motionless during floor descent a distance Δz the isolator opens an amount $-\Delta y$ and the potential energy of the mass, with respect to the floor, increases an amount $mg\Delta y$.

Figure 6.5 shows normalized E_p versus y and F versus y curves for a hypothetical system. The curves have been normalized by dividing both E_p and F by the weight of the isolated mass. The rest position is indicated by point A on both curves. Now, if the floor instantaneously dropped a distance Δz the isolator would expand a distance $-\Delta y$ and the energy stored in the isolator would decrease from point A to point B on the E/mg curve. However since the potential energy of the mass with respect to the floor increased an amount $mg\Delta y$ the total energy in the mass-isolator system, measured with respect to the floor would be equivalent to that at point C.

Now, since we have postulated a conservative system, the total energy of the system would remain constant if the floor suffered no further motion. However, point C is not a position of equilibrium because the force represented by point M is less than the weight of the isolated mass. The mass therefore begins to descend losing potential energy and gaining kinetic energy. Also the compression of the isolator increases so the isolator gains energy. During the motion the potential energy of the mass would be represented by line CH, the potential plus kinetic energy of the mass by curve CJH and the potential energy of the isolator by the curve BAD.

At the point of maximum displacement the mass would be motionless and the kinetic energy zero. Therefore the loss in potential energy of the mass would be just equal to the potential energy of the isolator. Thus point D, at maximum displacement can be established by projecting line CD at 45° , point D being the intersection of the line with the isolator energy curve.

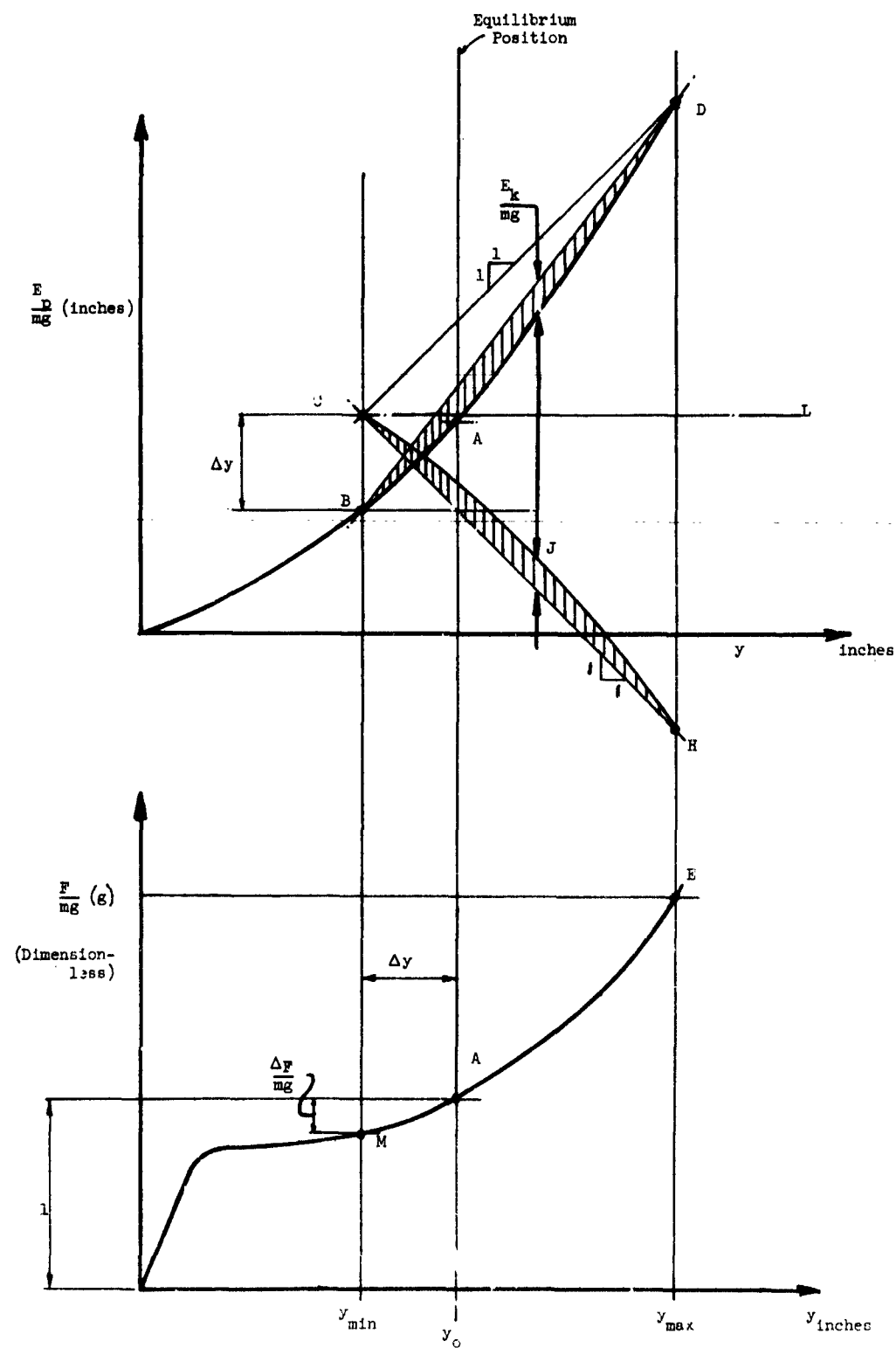


Figure 6.5 RATTLE SPACE REQUIRED BY NONLINEAR SYSTEM

If point B and point D are connected with a straight line the ordinate between line BD and curve BAD is the kinetic energy of the mass at the corresponding displacement, y.

The period of vibration of the system, T, can be obtained by integrating the reciprocal of velocity.

Thus

$$T = \sqrt{\frac{2}{g}} \int_B^D \frac{dy}{\left[\frac{E_k}{mg} \right]^{1/2}} \quad (6.7)$$

For a real system the floor does not descend instantaneously; a time we have denoted t^* is required. During time t^* the mass descends slightly and gains kinetic energy E_k^* .

If we approximate the descent of the floor as a linear function of time during the time t^* and, further approximate the arc MA on the force versus y curve by a straight line the loss of potential energy, ΔE_m , is given by

$$\Delta E_m = \frac{1}{4} \Delta F t^{*2} g \quad (6.8)$$

$$\frac{\Delta E_m}{mg} = \frac{1}{4} \left(\frac{\Delta F}{mg} \right) (t^{*2} g) \quad (6.9)$$

and the gain in kinetic energy by

$$\Delta E_k = \frac{1}{8} \frac{(\Delta F)^2 t^{*2}}{m} \quad (6.10)$$

$$\frac{\Delta E_k}{mg} = \frac{1}{8} \left(\frac{\Delta F}{mg} \right)^2 (t^{*2} g) \quad (6.11)$$

We note that both of these corrections will be quite small for real conditions similar to those illustrated in Figure 6.5.

Figure 6.6 reproduces the energy curve of Figure 6.5 and illustrates a method for correction for t^* .

Subsequent to time t^* the floor of the structure will rise. However, since the rise is due to the decay of the ground pressure wave the rate of rise is slow, a second to several seconds depending on bomb size. This rise will modify somewhat the response of the system but the slow rise alternately adds and subtracts energy from the oscillating system so the net change over a period of time is small. In any event, for a forcing function of small duration with respect to the system period, neglect of the rise is on the conservative side, i.e., y_{\max} is greater for no rise.

An alternate method of plotting the energy curves may be preferable for actual design purposes. In Figure 6.7 curve (A) is the normalized isolator strain energy curve, analogous to curve BAD of Figure 6.5. The static equilibrium position of the mass is at the point where the slope of curve (A) is unity. Curve (B) is the normalized mass potential energy curve and curve (C) is the total potential energy curve, the sum of curves (A) and (B).

Since the system is conservative the sum of potential and kinetic energies must remain constant, and can be represented by the horizontal line (D). The difference between (C) and (D) is the kinetic energy of the mass. Points (1) and (2) for which the kinetic energy is zero are points of extreme relative displacement between mass and foundation.

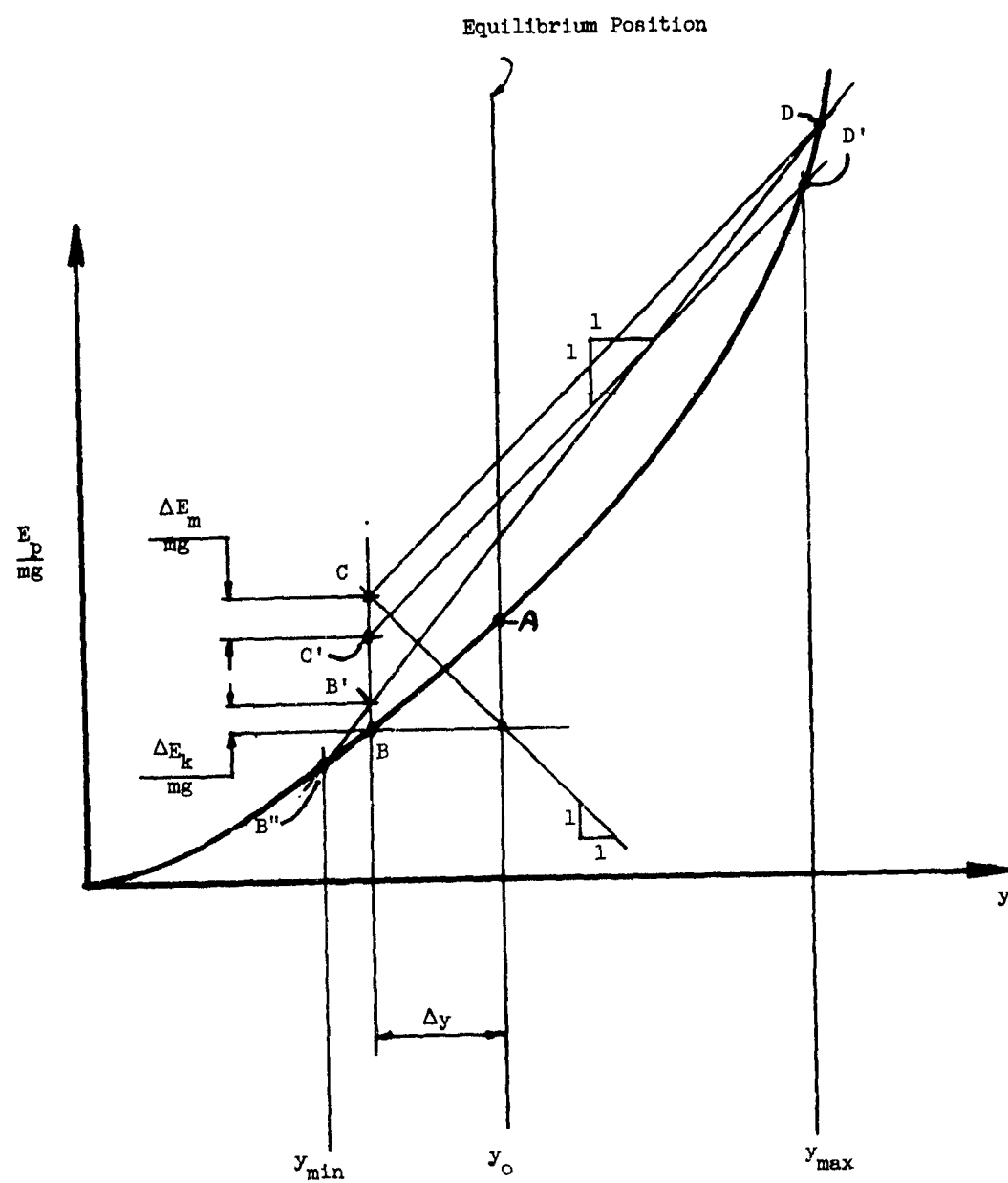


Figure 6.6 RATTLE SPACE REQUIRED BY NONLINEAR SYSTEM; RISE TIME CORRECTION

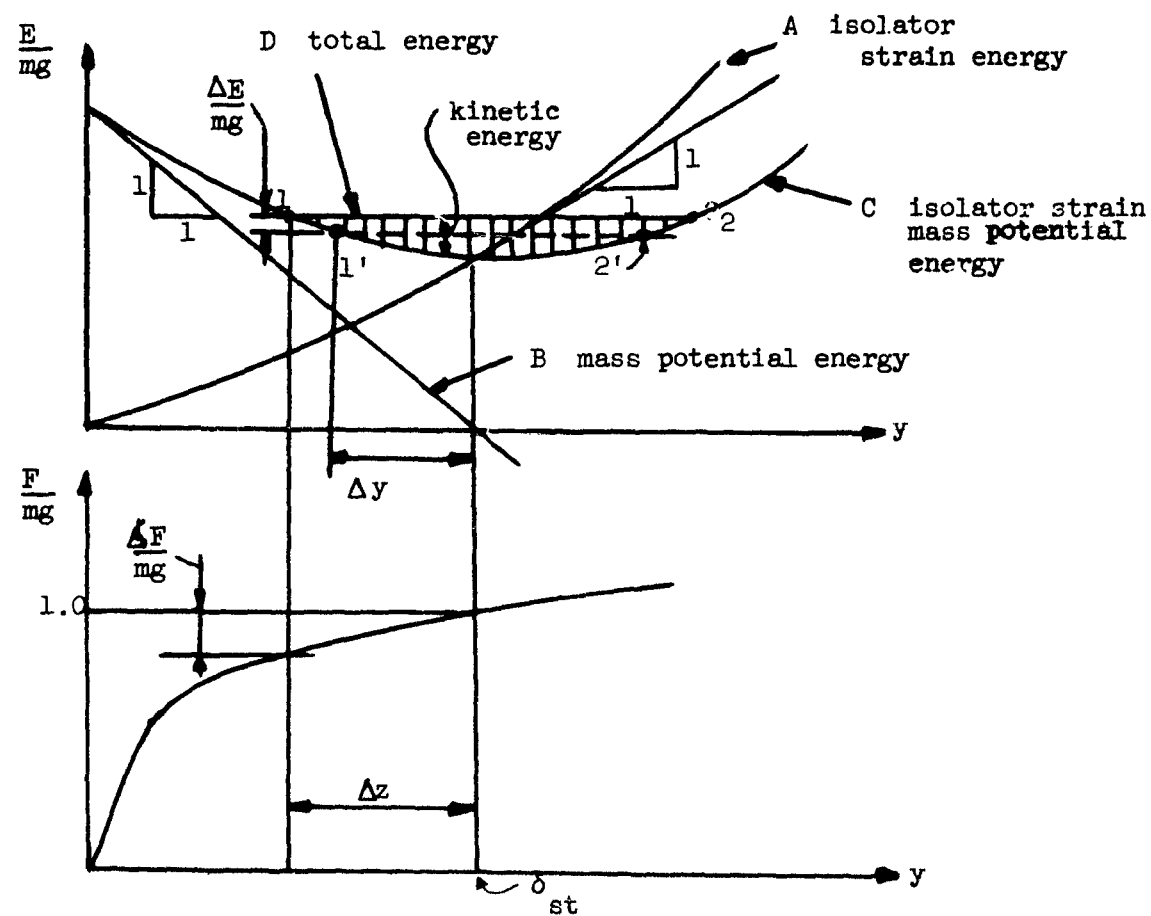


Figure 6.7 ISOLATOR ENERGY CURVES

The rise time correction can be made by computing $\frac{\Delta E_m}{mg}$ and $\frac{\Delta E_k}{mg}$ from Equations 6.9 and 6.11. Then the normalized increment of total energy is

$$\frac{\Delta E}{mg} = \frac{\Delta E_m}{mg} - \frac{\Delta E_k}{mg}$$

This can be plotted as shown on Figure 6.7. Then the range of mass motion with respect to the floor is between the limits of points 1' and 2' on the graph.

Should it be necessary to determine the response of a nonlinear system to a forcing function having a duration of a quarter period or more one has little recourse other than to carry out a step-by-step numerical solution. For a complex system this is best done with the aid of a digital computer.

6.2 Nonconservative Nonlinear Systems

If the general conservative nonlinear system shown schematically in Figure 6.1 is modified to include energy dissipative elements it can, with perfect generality, be represented by Figure 6.8. In Figure 6.8, I_c represents an energy storage device having the properties of a conservative isolator. Block I_d represents an energy dissipative device. No energy communicated to I_d is returned to the system. Thus the force F_d always resists the motion y regardless of whether y and its derivatives are positive or negative.

It may not be apparent that any nonconservative single degree of freedom system, regardless of its complexity, can be represented by a scheme as simple as Figure 6.8. Energy is a scalar variable. In classical mechanics all energy components of a system are linearly related. Therefore all conservative energy components can be lumped, if we so choose, and all dissipative components can also be lumped.

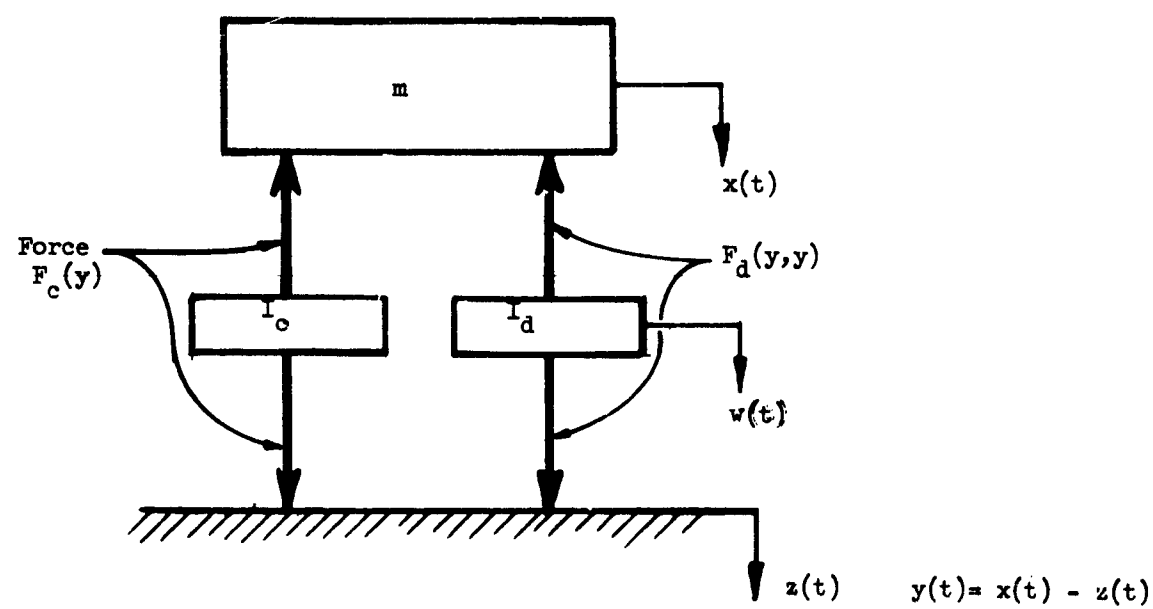


Figure 6.8 SCHEMATIC OF NONCONSERVATIVE NONLINEAR SYSTEM

It is pointed out, however, that the forces F_c and F_d probably would not exist separately in individual physical members.

We denote the energy stored in isolator I_c by E_{pc} . The curve of E_{pc} versus y can be deduced from the physical characteristics of any real system. It simply is the energy within the isolator at position y with all time derivatives of y zero. The F_c versus y curve is then simply dE_{pc}/dy .

No energy curve analogous to Figure 6.2 exists for the dissipative element; energy dissipated depends on the history of y and its derivatives as well as their instantaneous values. However, the F_d curve does exist but is much more complicated than Figure 6.3. F_d , in many real system is a function of at least y and \dot{y} . It may depend also on \ddot{w} , the absolute acceleration of the isolator. For instance, the friction against an unlubricated shaft turning in a reamed hole would depend to a degree upon the acceleration force exerted by the shaft against the hole. Each element of a complex system would have a separate time dependent position coordinate so that if we attempted to lump them into some generalized coordinate, w , as shown on Figure 6.8, w would be a function of x , z , and all of their derivatives.

If the mass of the isolator can be considered small enough to neglect in comparison with the supported mass, m , then the force F_d is a function of y and \dot{y} only. The dissipative force can be quite accurately approximated by a function of \dot{y} only for many real systems.

Because the energy dissipated during any particular time interval is a function of the previous history of motion the technique of Section 6.1 cannot

be extended to cover the dissipative case. This is because the simplicity of the technique is due ultimately to the fact that only the terminal points of motion are used. If the technique is extended to account for the effects of intermediate velocities and displacements it loses its simplicity.

If it were necessary to consider damping for an impulse excited nonlinear system the simplest approach would be to use the phase plane method which is well presented in the literature*. Actually, for a system of a fair degree of complexity probably the best procedure would be to program the problem for a digital computer.

Unless the nonlinear system is quite heavily damped acceptable design estimates of rattle space and acceleration can be obtained by neglect of the damping altogether and the method of Section 6.1 used. These conditions generally will be true for the low frequency systems used in shock isolation of sensitive elements of hard systems.

Since ground shock isolators are invariably subjected to an initial high velocity \dot{z} shortly after onset of the ground shock wave (within several milliseconds) velocity sensitive dampers should not be used; they would communicate a high pulse of acceleration to the isolated equipment. Coulomb dampers, however, are insensitive to velocity and further have the desirable property that the force applied to the isolated equipment can be made nearly constant.

A Coulomb damped nonlinear system proportioned so that the ratio of energy dissipated to circulating energy for the first, or largest amplitude cycle of

*See, for instance, "Introduction to Nonlinear Mechanics", N. Minorsky, J. W. Edwards, Ann Arbor.

vibration, is 10 percent, will apply a force to the isolated element at least 10 percent of the peak conservative element force F_c but less than 20 percent of the peak force F_c . Even for a linear conservative element i_c (spring) the peak force ratio generally is less than 15 percent.

Such a system would ring through no more than ten periods following the decay of the ground shock wave.

6.3 General Consideration of Nonlinear Isolation Systems: Their Advantages and Disadvantages

An important advantage of some nonlinear systems was pointed out in Section 6.1; for a given supported weight the equilibrium energy of a "bi-linear" type system can be much smaller than an equivalent linear system having approximately the same frequency of perturbations about the equilibrium point. Stated another way, a truly bi-linear system needs far less energy capacity at a given frequency and excursion range than does a linear system of the same frequency.

A second advantage of Coulomb damped systems discussed in Section 6.2 is that reasonable damping of the ringing of the system following ground shock excitation can be obtained without the consequent high accelerations that would be communicated to the isolated equipment by velocity sensitive dampers. Further, Coulomb (constant dry friction) dampers (e.g., brake drums) are probably simpler and more reliable than any other.

The characteristics of nuclear blast induced ground motion are such that below a certain vibration frequency the excursion of the isolated mass (rattle space) remains constant. (This is represented by the left, displacement, branch

of the shock spectrum.) However, as the frequency of the system is reduced, the acceleration of the isolated mass is reduced and, perhaps of more importance, the kinetic energy delivered to the mass is reduced proportionately. Therefore its tendency to oscillate after the ground shock wave has passed is reduced. In Section 6.4 some practical systems that can be built to support sizeable masses at frequencies two or even three orders of magnitude lower than the 1 cps range of most present hard isolation systems are briefly discussed.

The disadvantages of nonlinear systems, with one notable exception, are three.

1. The mechanical complexity of nonlinear systems generally is considerably greater than that of linear systems.

2. The mathematical problems in designs of nonlinear systems are quite formidable as soon as the single degree of freedom elements are departed from. Even for the elementary single degree of freedom systems the computations may require a digital computer for any other than impulse loading.

3. The coupling between elements of a complex nonlinear system can be very strong, introducing detrimental motions to the isolated element as well as grossly complicating the analysis.

The exception mentioned is the Coulomb damped mass-spring system. Its mechanical complexity is generally less than that of any other damped system and its response to an arbitrary input can be determined by simple graphical or numerical techniques (Reference 8).

6.4 Negative Spring Isolators

If the slope of the energy curve of Figure 6.2 became negative then the force of Figure 6.3 would become negative and within the negative region the isolator would have a variable negative spring constant.

A toggle provides a simple physical example of such a device. Figure 6.9 schematically shows the force-displacement curve for a toggle. It has a substantial negative spring region centered on the snap through position. Further, by proper design a nearly linear region of about $1/3 h$ (see Figure 6.9) can be obtained.

Negative spring devices are not limited to toggles. Any energy storage device having a negative energy versus displacement curve following an initially positive curve has a negative spring characteristic. Mechanical devices can consist of cams sliding against loading rollers, (Figure 6.10) the rollers being loaded by any appropriate means. Note also that by preloading the cam followers the lower portion of the cam can be truncated.

A negative spring connected in parallel with a positive spring having nearly the same spring constant (slightly higher for stability) yields a spring system of substantial energy capacity but practically zero spring constant at the operating range (Figure 6.11).

Reference 5 describes a negative spring system actually installed that isolated a ten ton suspended mass to 10^{-6} g.

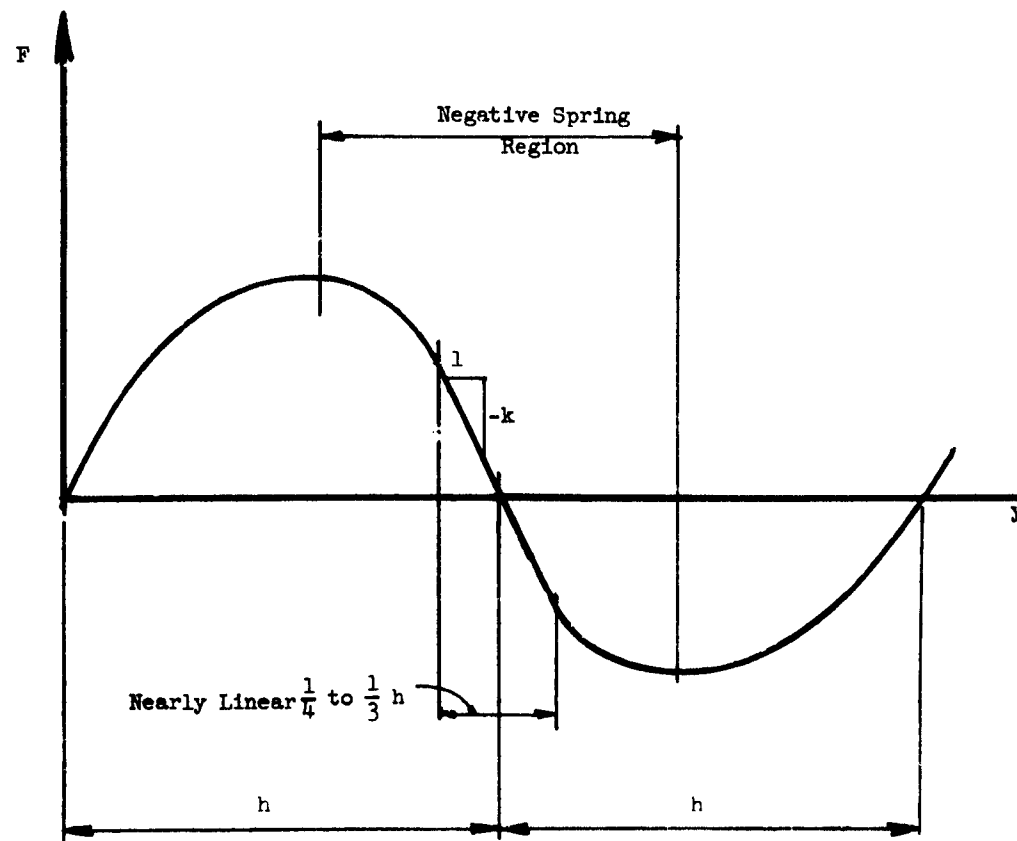
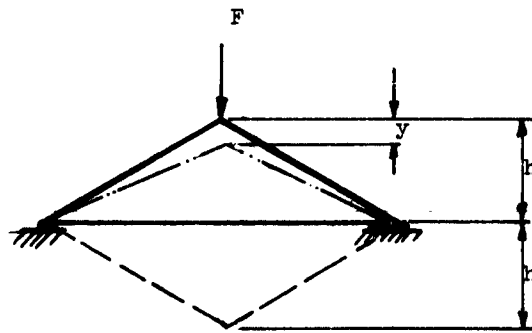


Figure 6.9 TOGGLE NEGATIVE SPRING CHARACTERISTICS

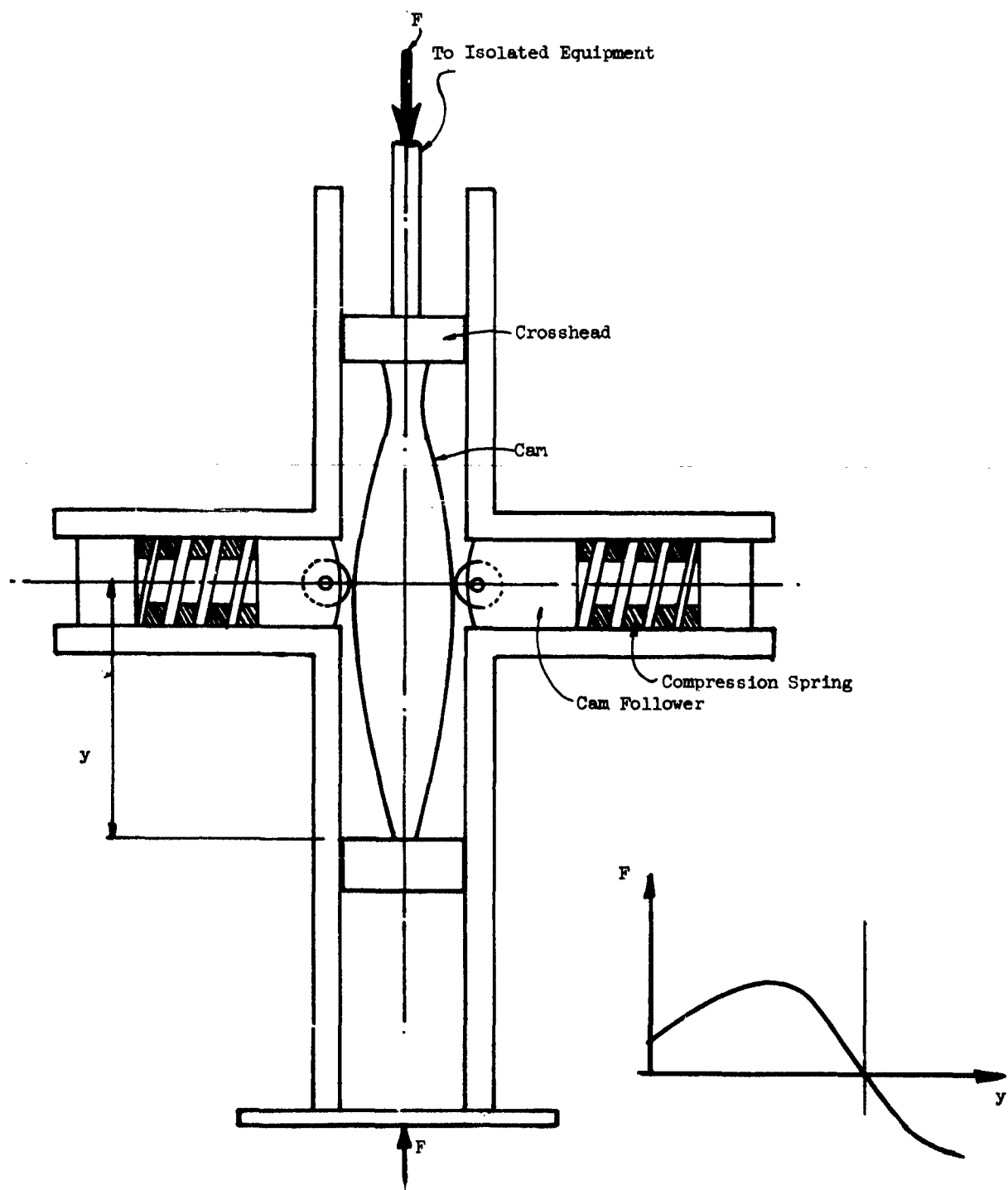


Figure 6.10 SCHEMATIC OF CAM OPERATED NEGATIVE SPRING

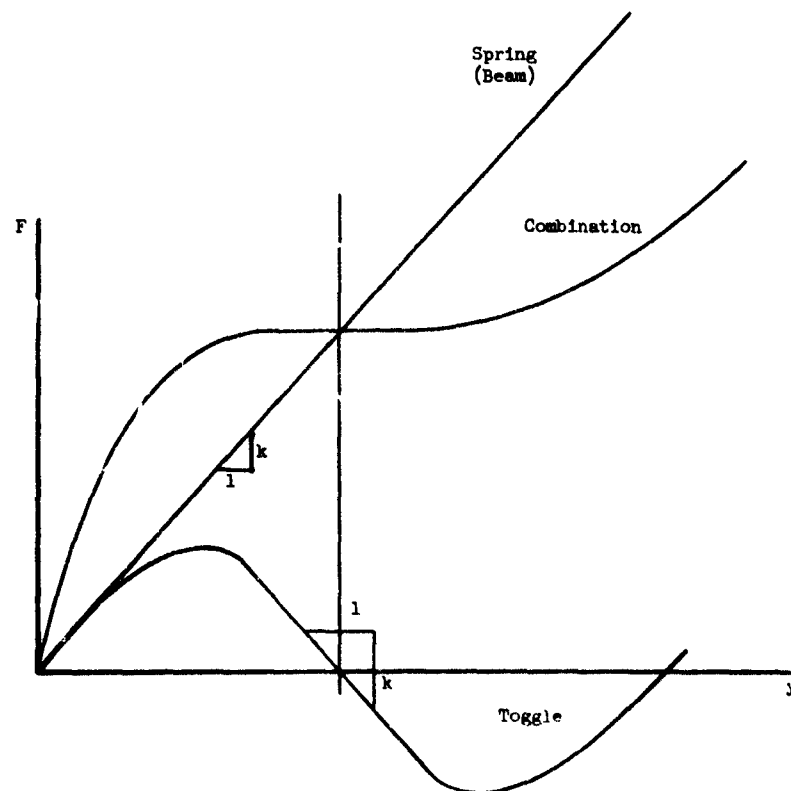
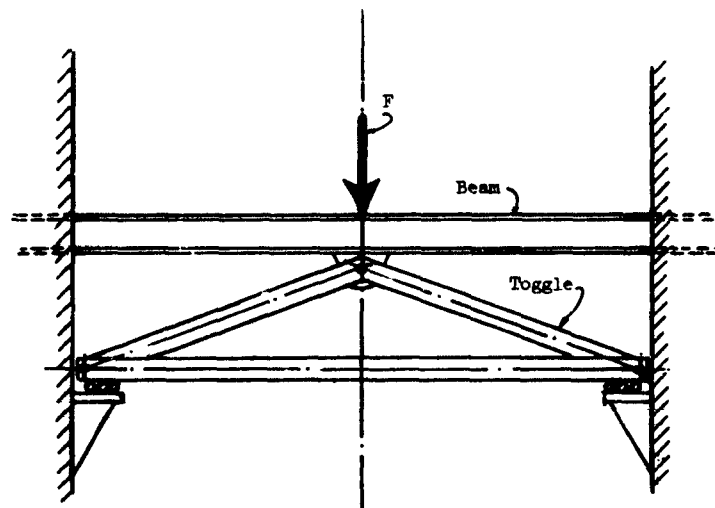


Figure 6.11 NEGATIVE SPRING ISOLATION SYSTEM

The principal adverse criticism of a negative spring system is that it is bulky. However it is believed that with sufficient design effort the bulk could be greatly reduced. If this conjecture proves to be true they would then provide particularly desirable elements for hard installation shock isolation. The only input parameters required are stroke and suspended weight. (Even for the toggle system the suspended weight can be varied within limits for any particular isolator and still maintain the frequency at near zero). In operation the isolated mass moves only minutely; therefore no significant kinetic energy is gained by the mass and there is no coupling between isolation elements nor ringing subsequent to ground shock excitation. The isolated mass remains at 1 g vertical throughout the attack.

SECTION 7

ISOLATOR ELIMINATION

The possibility that isolators can be eliminated from the system when ruggedized equipment is used should be checked.

Any criterion for isolator elimination must be approximate; variations in equipment characteristics are too great to allow development of an accurate general method. It is believed that the method presented here for development of a criterion for any particular installation, though quite conservative still will serve to indicate that isolators can be omitted in many specific instances.

Before proceeding with development of the criterion an aspect of the shock isolation problem that has not been touched in other parts of this report will be considered.

It is a matter of experience that certain peculiar effects take place in a true shock environment which theory is hard put to explain. For instance it has been observed that if a large charge of explosive is detonated under water and close to a ship, though the ship structure and machinery may suffer no observable damage, certain brittle elements are destroyed. The ship may be left undamaged but in darkness because the filaments of incandescent lamps are broken.

In an attempt to "explain" these phenomena, Weiner (Reference 10) postulated that such damage is caused by very sharp rises of stress, rises occurring in one or two microseconds. Though, to our knowledge, Weiner's predictions and conclusions have not been tested, his hypothesis, if accepted, does account for many shock peculiarities.

Further, Weiner shows that conventional shock tests would not disclose such equipment weaknesses because the rise times of the tests are too long. In addition, Weiner points out that many materials used in construction have concave stress-strain curves and that sharp pulses would be generated.

His report also points out that if the sharp rise postulated is the reason for failure of small, more delicate elements of equipment then such damage can be prevented by a simple technique: mount the equipment on brackets so constructed that no stress can be communicated from input to equipment by any path that does not include a flexural element. Weiner showed that the postulated damaging pulses, though propagated considerable distances as tension or compression waves, are attenuated to the vanishing point when propagated as bending through a distance of one or two beam thicknesses.

Now the required "beams" could be simply wall brackets made of bent plates and having elements in three mutually perpendicular planes. Most bent plate brackets would qualify.

In the following development it is assumed that sharp spikes of stress developed inside the structure and mounting equipment are avoided by use of simple mounts, or brackets, so constructed that there are no direct compression or tension paths between equipment and input; somewhere along the line all reactions are resisted by bending moments. It imposes no great hardship on the designer to specify that the natural frequency of any bending element in the bracket be no higher than 500 cps.

In brief, the criterion for elimination of isolators is expressed as an equivalent drop to a hard surface. As is repeatedly inadvertently demonstrated in electronics laboratories, even sensitive test equipment can withstand a drop of a few inches to a hard floor. On a simple bracket or flexible mount much equipment can stand a drop of two or more feet.

The question is "How high a drop corresponds to the interior motion of a hard shelter?"

This question can be answered with fair accuracy by the five following steps:

1. Estimate the free field motion as accurately as possible in accordance with the methods of Section 4.
2. Estimate the resulting interior structure motion in accordance with the methods of Section 5.3. Carry out at least a rough solution of Equations (5.29) and (5.32) to obtain the early history of interior motion.
3. Using the Newmark-Hansen Report (Volume III of this report) sketch the peak relative response spectrum for a combination of simple pulses that approximate the early history of interior structure motion obtained in Step 2.
4. Determine the peak pseudo velocity from the spectrum. Denote it \hat{v}_{\max} .
5. Compute the equivalent drop, x_{eq} , from

$$x_{eq} = \frac{1}{2} \frac{\hat{v}_{\max}^2}{g}$$

where g is the gravity constant.

No exact rules for the maximum drop that can be withstood by various items of equipment can be given. A typical value of maximum interior velocity is 4 ft per second having an equivalent drop height of only 3 inches. Most of the equipment in a hard structure could resist a drop of 3 inches without damage.

It may be desirable to have available a rough, conservative estimate of the equivalent drop. This can be obtained for vertical motion from Figures 7.1 through 7.3. The equivalent drop for the horizontal component can be taken as the product of the vertical drop and the tangent of the Mach angle of the compression wave.

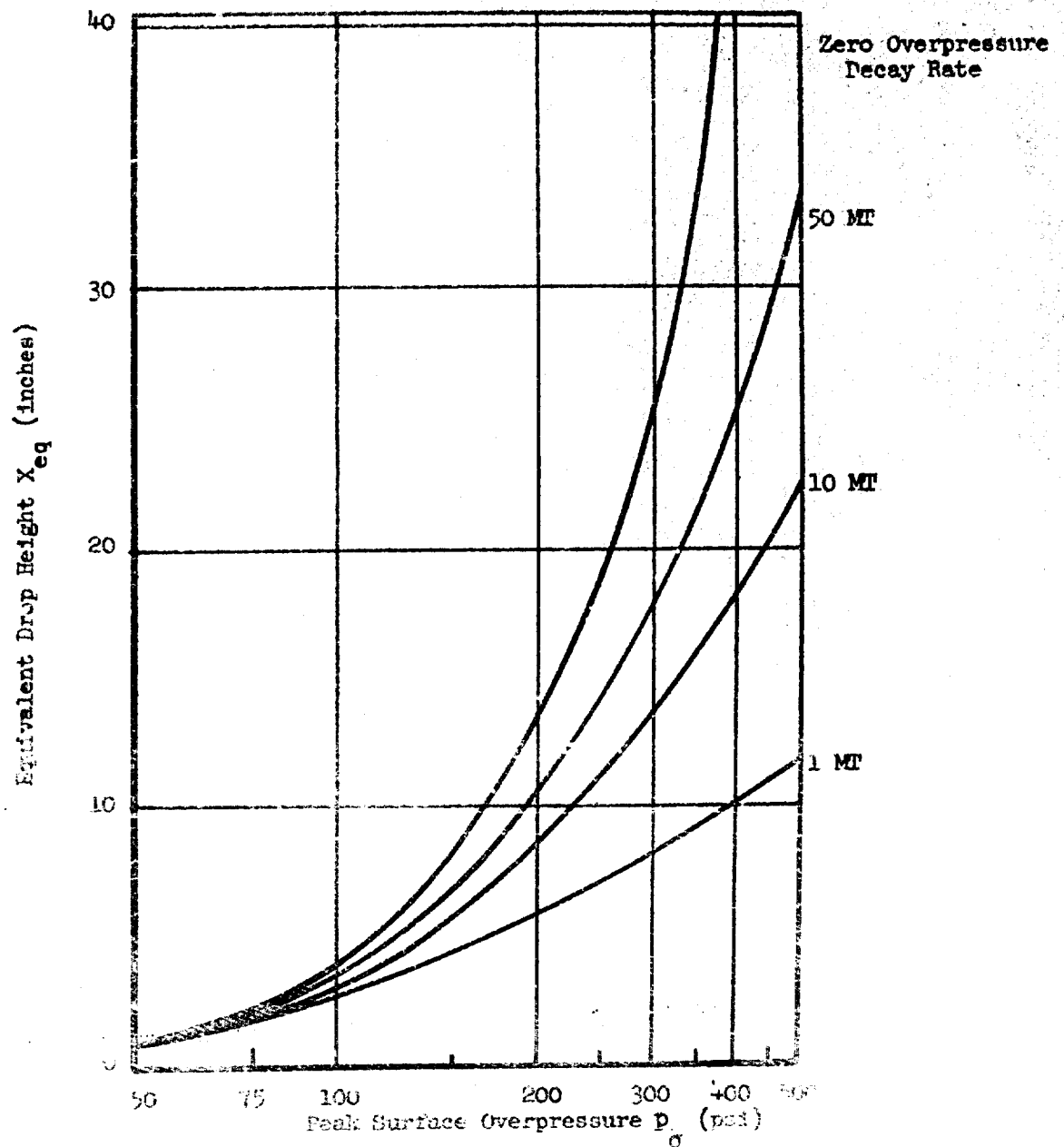


FIGURE 7.1 EQUIVALENT DROP HEIGHT VS. PEAK SURFACE OVERPRESSURE
 FOR YIELDS 1-50 MT
 (BASED ON 1000 PSI/SEC DECAY RATE)

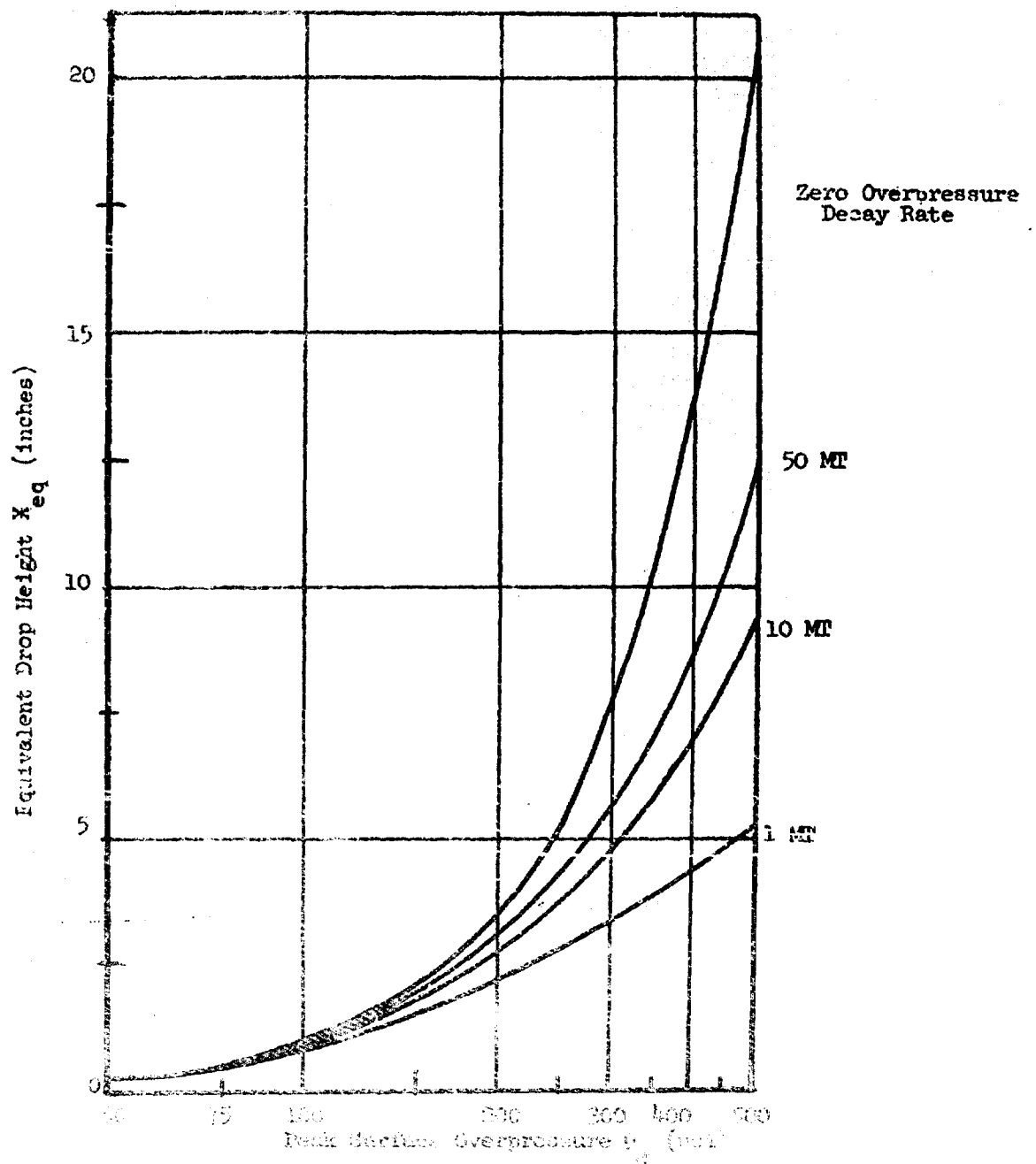


Figure 1. EQUIVALENT DROP HEIGHT VS. PEAK SURFACE OVERPRESSURE
 (Assuming $\gamma = 1.2$)
 (Source: U.S. Army Research Office, Durham, NC)

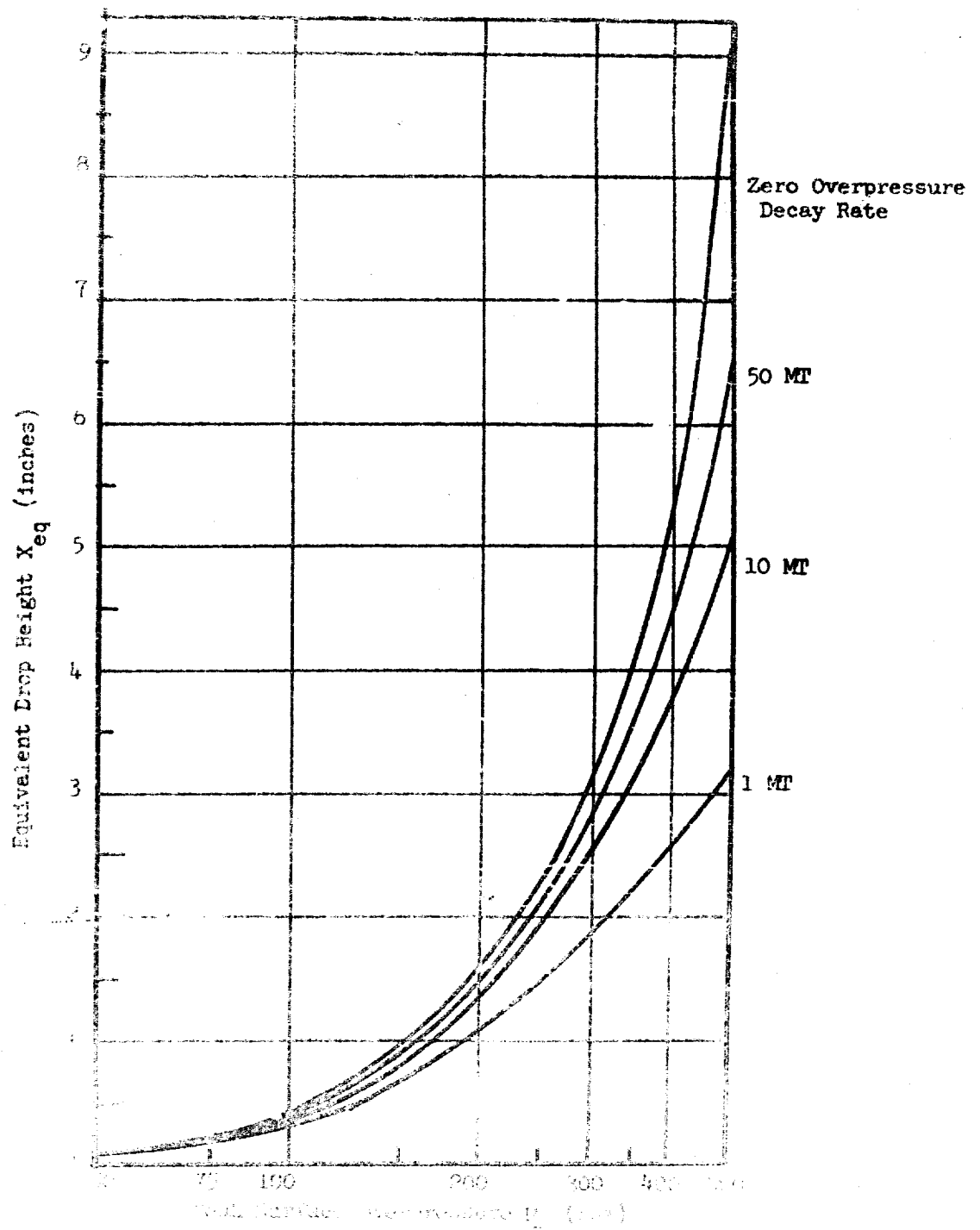


Figure 1. Equivalent Drop Height versus Peak Surface Overpressure P_s (psi) for various explosion yields.

For $W_{eff} = 10^4$ lb (4536 kg) (10 MT) (1000 tons).

SECTION 8

DETERMINATION OF INPUT PARAMETERS

Even though some of the input parameters entering into the ground shock isolation problem can only be estimated it is necessary in order to carry out a design to have firm procedures for making the estimates. In this section formulas and data useful in making these estimates are compiled. An attempt has been made to simplify some of the formulas at the expense of theoretical accuracy. The accuracy remaining however is more than is generally significant in view of the inherent errors in input data.

8.1 Simplified Structure Frequency Formulas

Notation

f	=	frequency of vibration	[cycles/sec]
f_n	=	frequency of vibration of nth mode	[cycles/sec]
n	=	modal index	[dimensionless]
c	=	sonic velocity of shell material	[ft per sec]
h	=	shell thickness	[ft]
R	=	shell radius	[ft]
ℓ	=	distance between circumferential nodal lines	[ft]
θ	=	half central angle of arch	[radians]

All frequencies of vibration are computed for structures vibrating in vacuum.

8.1.1 Domes

For all modes

$$f = \frac{c}{2\pi R} \quad (8.1)$$

8.1.2 Circular Cylinders

For all extensional (breathing) modes

$$f = \frac{c}{2\pi R} \quad (8.1)$$

For deformational (bending) modes having no circumferential nodal lines and free ends

$$f_n = \left[\frac{1}{2\sqrt{3}} \frac{n(n^2-1)}{[n^2+1]^{1/2}} \left(\frac{h}{R}\right) \right] \frac{c}{2\pi R} \quad (8.2)$$

These modes have $2n$ longitudinal nodal lines.

For deformational modes having circumferential nodal lines spaced a distance

$$f_{n\ell} = f_n \left\{ 1 + \left[\frac{\frac{\pi R}{\ell}}{n(n^2-1)} \right]^2 \left[(2n^2-1)(n^2-1) + n^2 \left(\frac{\pi R}{\ell}\right)^2 + 6 \left(\frac{R}{h}\right)^2 \right] \right\} \quad (8.3)$$

f_n is computed by Formula (8.2).

8.1.3 Circular Arches

For deformational modes having no circumferential nodal lines and free ends

$$f_n = \left[\frac{1}{2\sqrt{3}} \frac{\Gamma_n(\Gamma_n^2-1)}{(\Gamma_n^2+1)^{1/2}} \left(\frac{h}{R}\right) \right] \frac{c}{2\pi R} \quad (8.4)$$

where

$$\Gamma_n = \frac{n}{2} \frac{\pi}{\theta} \quad (8.5)$$

These modes have n nodal lines between the spring lines.

For deformational modes having circumferential nodal lines spaced a distance ℓ

$$f_{n\ell} = f_n \left\{ 1 + \left[\frac{\frac{\pi R}{\ell}}{\Gamma_n(\Gamma_n^2-1)} \right]^2 \left[(\Gamma_n^2-1)(\Gamma_n^2-1) + \Gamma_n^2 \left(\frac{\pi R}{\ell}\right)^2 + 6 \left(\frac{R}{h}\right)^2 \right] \right\}^{1/2} \quad (8.6)$$

f_n and Γ_n are computed by formulas (8.4) and (8.5) respectively.

8.1.4 Rectangular Slabs

For bending modes having nodal lines spaced at "a" in one direction and spaced at "b" in the perpendicular direction

$$f = \frac{\pi}{4\sqrt{3}} \text{ ch } \left[\frac{1}{a^2} + \frac{1}{b^2} \right] \quad (8.7)$$

or

$$f = \frac{\pi}{4\sqrt{3}} \text{ ch } \frac{d^2}{A^2} \quad (8.8)$$

where d is the rectangle diagonal and A is its area.

8.2 Normal Mode Geometry

Unless for some reason a detailed analysis of an interaction problem is to be carried out the normal mode geometry will not be required. If such an analysis is to be carried out the modes can be obtained for most structures from the literature.

If the method of Section 5.4 is used modal geometry is not required; the statically computed deflection is used instead.

8.3 Soil Parameters

8.3.1 Bedrock Elevation and Material

These data should be obtained from borings. If not available they can be estimated from topographic maps. If these are not available estimate bedrock to be 150 ft below surface and having a seismic velocity of 10,000 ft per second.

8.3.2 Stress-Strain Parameters

If at all possible a confined compression test stress-strain curve should be obtained from soil samples.

If a design must be carried out to be applicable to a number of unspecified sites assume an "elastic" soil weighing 100 lbs/ft³ having a compression wave velocity of 1000 ft per second, and a percylic damping factor of 0.25. (The latter number is quite conservative; a more realistic value would be 0.35.)

If a minimal description of soil conditions at a site is unavailable, elastic theory and the following approximate values can be used.

Soil Type	Approximate Density	Approximate Compression Wave Velocity
Top soil, light dry or moist loamy silt	100 lbs/ft ³	650 ft/sec
Clayey top soil, semi- consolidated sandy clay, nubble or gravel, loose rock talus, wet loam	100 lbs/ft ³	1200 ft/sec
Cemented sand, sand and clay	100-110 lbs/ft ³	2000 ft/sec
Saturated consolidated clay	120 lbs/ft ³	3000 ft/sec

8.3.3 Percyclic Damping Factors for Real Soils

The following values have been extracted from the geophysical literature.

Material	Percyclic Damping Factor
Fine sand and silt	0.21
Course sand	0.35 (0.25-0.50)
Clay	0.25
Shale	0.043
Limestone	0.047
Sandstone	0.060
Granite	0.030

APPENDIX A

DEVELOPMENT OF MOTION-TIME METHOD FOR DISTRIBUTED SYSTEMS

A.1 Statement of the Problem; Method of Approach

Assume a position in the free-field and the time history of free-field pressure at the selected position. The time history is presumed to include all effects that influence the pressure waves arriving at the selected position, such as, the incident compression wave, the incident shear wave, the directly transmitted wave, and any reflected or defracted components of any of the foregoing waves. In this section a method will be developed for determination of the motion-time history of the interior of a structure placed at the selected position in the free-field. The word "method" in the previous sentence is underlined to emphasize that a general procedure is developed, not a series of formulas to be applied in specific instances. The method presented admits of gross approximation or of application to problems deserving of a high degree of accuracy for which an electronic digital computer would be necessary to carry out the computations. Thus, if only the free-field compression wave can be estimated with any degree of accuracy a solution can be obtained within this degree of accuracy. On the other hand, if site conditions are sufficiently well known so that all of the pressure components stated above are known within tolerable accuracy then this information can be reflected in the computed interior structure motion, if desired.

A difficulty with all engineering methods, and a difficulty that becomes more pronounced with increasing generality of the methods, is that they must be understood for their successful application. It is not enough merely to determine which numbers should be substituted into a series of formulas in order to compute a resulting number desired. For this reason in the following subsection the mathematical expressions used will be developed in considerable detail and the emphasis will be placed upon the physical meaning of the mathematical expressions used. This is considered to be very important because in actual application most of the precise mathematical expressions will be approximated by their physical counterparts. The ease and facility, therefore, with which a given degree of accuracy can be achieved in the results will hinge, to a great extent, on the thorough understanding of the processes used by the designing engineer and good intuitive estimates of the accuracy of approximations used.

The general methods of mathematical applied mechanics are so well understood that their application has become almost standardized in technique amounting, in a sense, to something of a cult. Without meaning to disparage the considerable mass of excellent solutions that have been obtained by this approach it is pointed out that sometimes the formal mathematics tends to obscure the physics of the problem being investigated. The development of the next subsection, in particular, does not approach the problem in the classical manner. Considerable physical insight is gained by this departure from custom.

A.2 The Differential Equation

Consider a linear, elastic, statically loaded shell structure*. Its

* Since shells are the structures of interest this development is carried out in terms of shell characteristics. Appropriate modifications render it applicable to any linear, elastic structure.

equation can be represented

$$D L(\bar{u}) = \bar{p} \quad (A.1)$$

where

D is a scalar constant

\bar{u} is the absolute vector displacement of a point on the shell

\bar{p} is the vector pressure at a point on the shell

$L(\bar{u})$ is a linear vector operation, a function of \bar{u} and its spacial coordinates. Equation (A.1) can be taken as the definition of $L(\bar{u})$.

It should be appreciated that the pressure vector \bar{p} of equation (A.1) includes the forces that we normally term reactive. In other words, if the pressure \bar{p} was summed over the entire structure the resultant would be zero, and the moments of the pressure \bar{p} summed over the entire structure must be zero. The following elementary examples are included to fix the meaning of the linear vector operator and the circumstances under which the vectorial nature of \bar{u} and \bar{p} become significant.

For a flat plate laterally loaded the analog of Equation (A.1) is

$$D \nabla^2 \nabla^2(\bar{u}) = \bar{p}$$

where

∇^2 = Laplacian operator

$$D = \frac{1}{12} \frac{Eh^3}{(1 - \nu^2)}$$

E = modulus of elasticity
 h = plate thickness
 ν = Poisson's ratio

It should be observed, however, that since the displacement and pressure vectors are in the same direction over the entire surface of the plate, the vector character of displacement and pressure do not contribute anything significant to this particular problem and therefore they might as well be written as scalars (as they usually appear in the literature). If the flat plate were of nonuniform thickness then the equation would be

$$\frac{1}{12} \frac{E}{(1-\nu^2)} \nabla^2 h^3 \nabla^2 (\bar{u}) = \bar{p}$$

For an inextensible circular arch of central angle 2θ and radius R the analogue of Equation (A.1) is

$$\frac{EI}{R^4} \left\{ \frac{\frac{d^2}{d\theta^2} \left(\frac{d^2}{d\theta^2} + 1 \right)^2}{\left(\frac{d^2}{d\theta^2} - 1 \right)} \right\} \bar{u} = \bar{p}$$

where

EI is the stiffness of the arch

\bar{p} is the vector pressure per unit length of rib.

Now, for the arch

$$\bar{u} = u_r \bar{n} + u_\theta \bar{t}$$

where \bar{n} and \bar{t} are unit vectors in the radial and tangential directions respectively.

Also, for the inextensible theory

$$u_r = \frac{d}{d\theta} u_\theta$$

Since each component of the vector displacement must satisfy the differential equation

$$\frac{EI}{R^4} L(u_\theta) = p_\theta$$

$$\frac{EI}{R^4} L\left(\frac{du_\theta}{d\theta}\right) = p_r$$

where

$$\bar{p} = p_r \bar{n} + p_\theta \bar{l}$$

we see that, although the vector $L(\bar{u})$ must be colinear with the vector \bar{p} , in general the vector \bar{u} is not colinear with \bar{p} . Physically the situation will arise for any structure that, under the influence of a concentrated load, moves laterally with respect to the load.

Equation (A.1) is not sufficient in itself to determine an actual deflection even though the loads are given. It only expresses the relation between the deflection at one point to that at another. In order to get absolute values for the displacements we must prescribe a set of boundary conditions to the problem, i.e., a set of points where the displacements, moments, shears, or slopes are zero. The complete set of equations for a particular problem then consists of Equation (A.1) plus the appropriate boundary conditions.

It is well to emphasize at this point that for any particular problem an equation analogous to (A.1) always exists but it may be too complex mathematically

to use or even to write. An example of an essentially simple physical system that does not have a tractable equation analogous to (A.1) is a steel building frame; however, the general conclusions that can be drawn by operating with Equation (A.1) are applicable to the steel building frame.

The equations of free vibration of the above system in vacuum are then (damping neglected)

$$D L (\bar{u}) + m \ddot{\bar{u}} = 0 \quad (A.2)$$

$$B_n (\bar{u}) = 0 \quad (n=1, 2, \dots) \quad (A.3)$$

where

m is the unit mass of the shell, a function of the spacial coordinates

$B_n ()$ are the boundary conditions

n is an index denoting the individual boundary conditions.

Equations (A.2) and (A.3) can always be solved in the form

$$\bar{u} = \sum_{i=1}^{i=\infty} A_i \bar{\phi}_i \sin (\omega_i t - \theta_i) \quad (A.4)$$

where

A_i are arbitrary constants

and θ_i are arbitrary phase angles

$\bar{\phi}_i$ are a set of orthogonal vector functions of the spacial variables only, satisfying the boundary conditions and the orthogonality relation

$$\begin{aligned} \int_A \bar{\phi}_i \cdot \bar{\phi}_j m \, dA &= 0 \quad \dots \text{if } i \neq j \\ &= N_i \quad \dots \text{if } i = j. \end{aligned} \quad (A.5)$$

The area integral is taken over the entire surface of the shell.

The N_i are constants, termed the norms, of the orthogonal system. Then the circular frequencies, ω_i , satisfy the relations

$$D L (\bar{\phi}_i) = m \omega_i^2 \bar{\phi}_i. \quad (A.6)$$

The physical meaning of Equations (A.4) through (A.6) is that any steady state vibration \bar{u} can be represented as the sum of an infinite number of rather special displacement configurations, $\bar{\phi}_i$, vibrating sinusoidally at specific frequencies ω_i , each frequency being related to the associated displacement configuration by Equation (A.6). Particular displacement configurations, \bar{u} , are obtained by adjusting the values of the arbitrary constants A_i and θ_i .

Physically it is by no means obvious that this situation should be true. If we regard ω_i^2 in Equation (A.6) as simply an arbitrary number then certainly the equation could be solved for some function $\bar{\phi}_i$. We might make a guess as to the general shape of $\bar{\phi}_i$, substitute it into the linear operator, divide by $m \omega_i^2$ and obtain a better approximation for $\bar{\phi}_i$. If this procedure were carried out an infinite number of times we would expect to find some particular displacement configuration satisfying Equation (A.6) for the particular value of ω_i used. In this manner $\bar{\phi}_i$ could be generated for any arbitrary value of ω_i ; however, it would be found that only those functions $\bar{\phi}_i$ corresponding to certain particular values of ω_i would also satisfy the boundary conditions. We would still have an infinite number of $\bar{\phi}_i$ left satisfying the boundary conditions but this infinity would be smaller than the number that did not. A fairly long mathematical development then shows that any two functions $\bar{\phi}_i$ and $\bar{\phi}_j$ satisfying both Equation

(A.6) and the boundary conditions also satisfy Equation (A.5)*.

Evidently since the geometry of the $\bar{\phi}_i$ are influenced by the boundary conditions this influence is reflected in the associated frequencies of vibration ω_i . Thus if two structures identical, except as to boundary conditions, were to be placed in steady state vibration the vibrations of the two structures might be markedly different. The most familiar example of this situation is the difference in vibrations between a hinged end and a fixed end beam that are otherwise identical.

Since the element of mass, $m \, dA$, is always positive it can be concluded from Equation (A.5) that in general $\bar{\phi}_i$ and $\bar{\phi}_j$ will have positive and negative portions, otherwise their product would not average out to zero over the surface of the structure. In most treatises on orthogonal functions the functions are considered to be scalars rather than vectors and to be functions of one independent variable only rather than two required for a general description of a shell structure, the two dimensional functions for the shell being represented as the product of two one dimensional functions each of one of the coordinates of the shell surface. Such one dimensional functions and two dimensional functions comprising a product of two one dimensional functions have a series of nodal points or nodal lines, i.e., points or lines at which the value of the function is zero. For the two dimensional case the nodal lines divide the function into alternate positive and negative zones somewhat similar to a checkerboard. As the index number, i , increases, the number of nodal lines on such modes increases also.

* See, for instance, Air Force Special Weapons Center Technical Report TR-59-2 "Protective Construction", T.G. Morrison, Part III (U).

The vector functions $\bar{\phi}_i$ in general do not exhibit this characteristic. The scalar value of the vector displacement is always positive or possibly zero and, in general, if the vector is resolved into its components, at a point where one component is zero the other components will not be zero; therefore, the vector modes do not have clearly defined nodal lines. The components of the modes, however, do have nodal lines but the nodal lines of, say, the radial component and the lateral component of the vector modes of a circular cylinder occur at different positions. This observation is quite important when setting up the technique for numerical evaluation in a later section.

If the structure is subjected to a dynamic load \bar{p} then the equations of motion become

$$D L (\bar{u}) + m \ddot{\bar{u}} = \bar{p}$$

$$B_n (\bar{u}) = 0. \quad (A.7)$$

Equations (A.7) have a solution in the form

$$u = \sum_{i=1}^{\infty} T_i(t) \bar{\phi}_i \quad (A.8)$$

where $T_i(t)$ are the solutions of equations of the form

$$\ddot{T}_i + \omega_i^2 T_i = \tau_i(t) \quad (A.9)$$

The functions τ_i are given by

$$\tau_i(t) = \frac{1}{N_i} \int_A \bar{p} \cdot \bar{\phi}_i dA. \quad (A.10)$$

In subsequent sections considerable space will be devoted to methods for computing the value of $\tau_i(t)$. It is worthwhile, therefore, to get some feeling for the physical significance of this expression. Since the dimensions of \bar{p} are pounds per square inch, the dimensions of $\bar{\phi}_i$ are inches, and those of dA are square inches, the integral in Equation (A.10) simply represents the total energy that would be delivered to the $\bar{\phi}_i$ mode by the pressure \bar{P} if the pressure were held constant and the mode allowed to move from a position of zero displacement to its maximum. Thus, the product $N_i \tau_i(t)$ represents a time varying function at any instant equal in value to the energy that could, at that instant, be delivered to the mode by the pressure function \bar{p} .

We will now set up the equation of motion of the same structure immersed in an elastic medium that offers resistance to motion of the imbedded structure. We will denote the absolute motion of a particle on the surface of the structure by \bar{u} , the absolute motion of a free-field particle by \bar{z} , and the relative motion of the structure with respect to the free-field by \bar{w} . Thus,

$$\bar{u} = \bar{z} + \bar{w}.$$

The medium, in general, offers three components of resistance to motion of the structure. These will be discussed in some detail.

The first component we will term the displacement sensitive component. Consider a cylindrical shell immersed in an elastic medium. Now, if the shell is uniformly expanded outward against the elastic medium a pressure will be developed by the medium against the shell at the interface, this pressure being proportional to the amount of outward expansion. In a truly elastic medium if the shell were bonded to the medium a tension would be developed at the interface

if the shell were uniformly compressed inward. The proportionality constant for both the compression and tension cases would be the same. Now suppose that the shell was nonuniformly expanded outwards against the elastic medium. Then the interface pressure developed would vary from point-to-point and would be a function not only of the elastic constants of the surrounding material but also of the geometry of the deformation. In general, we could write

$$k F(\bar{w}) \bar{w} = \bar{p}_d \quad (A.11)$$

where

- \bar{p}_d = interface pressure due to relative displacement of structure with respect to free-field
- $F(\bar{w})$ = a dimensionless function of \bar{w}
- k = a proportionality constant.

For the case of uniform expansion or contraction, previously discussed, the dimensionless function $F(\bar{w})$ would be identically unity.

The relative motion of the structure with respect to the free-field, \bar{w} , can, in general, be resolved into three components, one of these normal to the surface of the structure and two more mutually orthogonal with each other and the normal component but tangential to the surface of the structure. The latter two components could be combined into a single tangential component, the direction of which, in general, would vary from point-to-point around the surface of the structure. We will denote the normal component $\bar{w} \cdot \bar{n}$ and the tangential component, $\bar{w} \cdot \bar{l}$ where \bar{n} is the unit vector normal to the shell, and \bar{l} is the unit vector tangent to the shell and lying in the plane defined by \bar{n} and \bar{w} . Now in a truly elastic medium two components of pressure are developed at the interface due to

the time derivative of these components of motion. The normal component of pressure which we will denote \bar{p}_{vn} is given by

$$\bar{p}_{vn} = c_1 \bar{\rho} \dot{\bar{w}} \cdot \bar{n} \quad (\text{A.12})$$

and the tangential component is given by

$$\bar{p}_{ve} = c_2 \rho \bar{\ell} \dot{\bar{w}} \cdot \bar{\ell} \quad (\text{A.13})$$

where

c_1 is the compressional wave velocity

c_2 is the shear wave velocity

ρ is the unit mass of the medium

Equations (A.12) and (A.13) are independent of the stress strain law and are accurate for any material if the instantaneous wave velocities are used.

Practically, their principal value is for materials having constant wave velocities (elastic, viscoelastic, etc.). It is pointed out that these equations are written only for the interface pressures developed and do not represent the time history of the waves radiated from the structure which ultimately result from the interaction.

If the structure were not present in the free-field but the position occupied by the structure was engulfed by a pressure wave, the mathematical surface defining the structure-medium interface would be subjected to a component of pressure, the free-field pressure. In a solid medium, elastic or otherwise, the free-field pressure can be represented by a second order tensor. We will denote this free-field pressure tensor \bar{p} . On any surface arbitrarily described within this second order tensor field the vector pressure on the surface, which

we will denote by \bar{p} , is given by

$$\bar{p} = \bar{n} \cdot \bar{p} \quad (A.14)$$

where \bar{n} is the vector unit normal to the surface.

Now if an actual structure is immersed in the free-field, the vector pressure at the structure-medium interface is equal to the sum of the four components enumerated above. The pressure component that we ordinarily regard as the reflected wave or the doubling of free-field pressure against a motionless surface is simply the sum of components \bar{p}_{zn} and $\bar{p}_{z\ell}$ due to the relative velocity of structure and free-field particles. For equilibrium this interface pressure must be balanced by two pressure components developed by the structure:

1. A component due to the deformation of the structure, which we have symbolized by $DL(\bar{u})$, and
2. The inertia of the structure, $m\ddot{\bar{u}}$.

Thus the equation of motion of a structure immersed in elastic material is

$$DL(\bar{u}) + m\ddot{\bar{u}} = \bar{n} \cdot \bar{p} - k F(\bar{w})\bar{w} - c_1\rho \bar{n} \dot{\bar{w}} \cdot \bar{n} - c_2\rho \bar{\ell} \dot{\bar{w}} \cdot \bar{\ell} \quad (A.15)$$

The minus signs appear on the right side of Equation (A.15) because for an inwardly directed pressure to be developed at the interface due to structure deformation the deformation \bar{u} would have to be positive inward. Since \bar{u} is the sum of the free-field motion and relative motion \bar{w} , a positive \bar{w} would represent a tendency for the shell surface to separate from the free-field particles yielding a tension stress or negative pressure.

Substituting $\bar{w} = \bar{u} - \bar{z}$ into Equation (A.15) and rearranging we obtain

$$DL(\bar{u}) + k F(\bar{w})\bar{u} + c_1 \rho \bar{n} \dot{\bar{u}} \cdot \bar{n} + c_2 \rho \bar{l} \dot{\bar{u}} \cdot \bar{l} + m \ddot{\bar{u}} \quad (A.16)$$

$$= \bar{n} \cdot \bar{p} + k F(\bar{w}) \bar{z} + c_1 \rho \bar{n} \dot{\bar{z}} \cdot \bar{n} + c_2 \rho \bar{l} \dot{\bar{z}} \cdot \bar{l}$$

With the exception of the term $k F(\bar{w})\bar{z}$ the right side of Equation (A.16) is a function only of the free-field pressure, free-field particle motion, and structure geometry. Therefore, with a suitable approximation for $F(\bar{w})$ the right side of Equation (A.16) is computable from initial data. We, therefore, define \bar{p}_1

$$\bar{p}_1 \equiv \bar{n} \cdot \bar{p} + k F(\bar{w})\bar{z} + c_1 \rho \bar{n} \dot{\bar{z}} \cdot \bar{n} + c_2 \rho \bar{l} \dot{\bar{z}} \cdot \bar{l} \quad (A.17)$$

It is instructive to observe the form taken by Equation (A.16) for certain limiting cases. Consider, first, that the soil motion and structure response are so slow that the process becomes quasi-static, i.e., all time derivatives become zero. Then we see that the interface pressure would be just the sum of free-field pressure and a component due to the distortion of the soil around the structure, induced by the disparity between free-field motion and structure motion.

If the structure were a rigid, immovable, flat surface parallel to the advancing wave front then $DL(\bar{u})$ would vanish, \bar{z} would be equal to \bar{u} , and \bar{v} would be equal to zero. It is not apparent, but for this case the function $F(\bar{w})$ would be zero and also the dot product $\dot{\bar{z}} \cdot \bar{l}$ would be zero. Then since $\dot{\bar{z}}$, the particle velocity, is just equal to $\frac{\bar{p}}{\rho c}$ for a plane wave, the right side of Equation (A.16) would become simply $2\bar{p}$ as it should for this condition, the 2 representing one hundred percent reflection.

Equation (A.16) is extremely difficult to solve. The term $kF(\bar{w})\bar{u}$ renders the equation nonlinear. Also, the two first derivative terms having different constant factors c_1 and c_2 mitigate against the use of a normal mode solution even without the complication of the nonlinear term. At this point, then, there would be two general courses open to us. One, we could insist on a mathematically rigorous solution and carry out the evaluation of Equation (A.16) by means of a large digital computer; two, we could simplify Equation (A.16) and perhaps carry out the evaluation by simpler means. When we consider the degree of uncertainty that must exist for the several parameters entering into Equation (A.16) the latter course seems to be the most reasonable to adopt. A rigorous solution of a problem for which the input data is probably accurate to no better than a factor of ten or twenty percent yields only illusory accuracy in the final results. However, we must be careful in simplifying the equation that the elimination of a complicating factor does not change the qualitative behavior of the system and that the simplifications do not introduce numerical inaccuracies greater than can be tolerated.

It will be found that the nonlinear term has small influence on the net response of the structure. Actually, it contributes only a small increment to the "spring constant" of the structure, by far the larger portion being contributed by the factor $DL(\bar{u})$ for most cases. The single exception occurs for rigid body motion of the structure in which case the linear operator contributes zero. But for this case the function $F(\bar{w})$ is identically unity. We will, therefore, approximate the nonlinear term by the linear term $K\bar{u}$ and develop rational methods for estimation of an average value of K to use for any particular structure.

The velocity terms are a little more difficult to handle. We begin by determining graphically the meaning of the sum of the two velocity terms. We note, first of all, that c_1 is always greater than c_2 , generally, on the order of two or three times as great as c_2 . Figure A.1a shows the graphical construction of the vector representing the sum of the two velocity terms. It is seen that in general this sum will have a numerical magnitude different than that of \dot{z} and that the direction of the resulting vector will differ from \dot{z} . In Figure A.1b the two wave velocities c_1 and c_2 have been replaced by some average wave velocity c such that the length of the resulting vector has the same length as that appearing in Figure A.1a. However, this approximation yields a resultant having the same direction as the vector \dot{z} . Now, in general, for a normal mode, the angle β may vary between zero and 90° for different locations on the mode; however, at the points where the angle β is 90° the length of the vector \dot{z} is a minimum and at the point where β is zero the length of \dot{z} is a maximum. Further, a little trigonometry discloses that the maximum value possible for the angle γ is about $18-1/2^\circ$ for which its cosine is about .95. This occurs for a ratio of $\frac{c_1}{c_2} = 4$. For the more likely value of $\frac{c_1}{c_2} = 2$, the maximum value of γ is less than 16° . Therefore, since the net effect of the \dot{z} terms is to remove energy from the vibrating system we can make a very accurate approximation by substituting $c\rho\dot{z}$ and $c\rho\dot{u}$ for the first derivative terms in Equations (A.16) and (A.17). In a subsequent section the value of the adjusted c is computed so that the energy radiated by the approximate term is equal to the energy radiated by the two accurate terms. It is found that for most conditions c will be equal to more than 90 percent of c_1 .

With these approximations our working equations become

$$DL(\bar{u}) + K\bar{u} + c\rho\dot{\bar{u}} + m\ddot{\bar{u}} = \bar{p}_1 \quad (A.18)$$

$$\bar{p}_1 = \bar{n} \cdot \bar{p} + K\bar{z} + c\rho\dot{\bar{z}} \quad (A.19)$$

A.2.1 Physical Meaning of Terms of Fundamental Equations

The terms in Equations (A.18) and (A.19) have been grouped into components representing the motion of the structure and components representing the motion of the soil. The pressure \bar{p}_1 is a fictitious quantity, it does not represent the pressure at the interface between the structure and soil. The latter would be just the sum of the pressure components necessary to maintain the structure in its deformed condition, $DL(\bar{u})$, and the inertia component, $m\ddot{\bar{u}}$. All of the other terms represent the effects of the free-field pressure and soil structure interaction, however, since \bar{p}_1 is immediately computable once the pressure wave \bar{p} has been established, it forms a convenient forcing function for the equation of motion (A.18).

Actually, the term \bar{p}_1 is not quite as fictitious as it appears. If Equation (A.18) is multiplied through by $\dot{\bar{u}}$, the velocity of the structure, and then integrated with respect to surface area and time, each of the resulting terms has physical significance.

$$\begin{aligned} \int_0^t \int_A DL(\bar{u}) \cdot \dot{\bar{u}} dA dt + K \int_0^t \int_A \bar{u} \cdot \dot{\bar{u}} dA dt \\ + c\rho \int_0^t \int_A \bar{u} \cdot \ddot{\bar{u}} dA dt + m \int_0^t \int_A \ddot{\bar{u}} \cdot \dot{\bar{u}} dA dt = \int_0^t \int_A \bar{p}_1 \cdot \dot{\bar{u}} dA dt \end{aligned} \quad (A.20)$$

Thus, in Equation (A.20) the first integral represents the potential energy stored as strain energy in the entire structure between the times zero and t . (All energies are here computed with respect to the fixed coordinate system.) The second integral represents the recoverable potential energy stored as strain energy in the soil surrounding the structure. The third integral represents the energy dissipated during time zero to t in the form of a wave radiated from the structure. The fourth integral represents the kinetic energy delivered to the structure within the interval zero to t . Therefore, the integral on the right hand side of the equal sign represents the total energy delivered to the soil-structure system during the time intervals zero to t . Thus, the pressure \bar{p}_1 represents the component of pressure around the structure available to deliver energy to the soil-structure system during motion of the structure.

Immediately we see that if \bar{u} and $\dot{\bar{u}}$ have been estimated, Equation (A.20) provides a useful check of the results. This is particularly true for rigid body motion because in this instance \bar{u} and $\dot{\bar{u}}$ are invariant over the surface of the structure and the first integral becomes identically zero. Then any over-estimate of \bar{u} would indicate a larger total energy on the left side of Equation (A.20) than right, clearly a physical impossibility.

A.2.2 Range of Applicability of the Basic Equations

$$\text{Define} \quad \bar{p}_2 = \bar{p}_1 - K\bar{z} \quad (\text{A.21})$$

Substituting (A.21) and

$$\bar{u} = \bar{z} + \bar{w}$$

into Equation (A.20) there results

$$\begin{aligned} \int_0^t \int_A DL(\bar{u}) \cdot \dot{\bar{u}} dA dt + \int_0^t \int_A K \bar{w} \cdot \dot{\bar{u}} dA dt + c\rho \int_0^t \int_A \bar{u} \cdot \dot{\bar{u}} dA dt \\ + m \int_0^t \int_A \ddot{\bar{u}} \cdot \dot{\bar{u}} dA dt = \int_0^t \int_A \bar{p}_2 \cdot \dot{\bar{u}} dA dt \end{aligned} \quad (A.22)$$

We see now that \bar{p}_2 is not influenced by K and that the second integral appears in terms of $\bar{w} \cdot \dot{\bar{u}}$, where \bar{w} is the departure of the structure motion from the free-field motion, \bar{z} .

Equation (A.22) provides a useful means for estimating the degree of approximation introduced into the solution when nonlinear or nonelastic soils are approximated by an elastic soil with suitable adjusted constants. We observe first that the factor $DL(\bar{u})$ is numerically equal to the pressure that must be distributed over the surface of the structure in order to maintain it in its deformed configuration. Also, we note that even if the structure were highly nonlinear there would be some other nonlinear operator, $N(\bar{u})$, for instance, that would replace the linear operator throughout the entire argument to this point. Also, this nonlinear operator would be equivalent to the static pressure necessary to maintain the structure in its deformed condition. Now, whether elastic or inelastic, the pressure so computed is equal to the design pressure for the structure, or more properly the equivalent static design pressure. For most underground structures this equivalent static pressure is on the order of the peak overpressure that the structure is designed to resist.

The factor \bar{Kw} also represents a pressure. Thus, we can compare the relative influence of the first and second integrals of Equation (A.22) by comparing \bar{Kw} with peak design overpressure, inasmuch as all of the other factors in the integrals are identical. If the real soil were highly nonlinear, and a linear approximation substituted, probably the best approximation would be to take a value of K that would yield the same energy content at a specific displacement level as did the real soil. In other words, the triangular area under the stress-strain curve of the approximating elastic soil would be made equal to the area under this stress-strain curve of the nonlinear soil at its expected maximum strain. It is interesting to note that although the second integral in Equation (A.22) represents reversible energy for the elastic case, for the inelastic case it represents both reversible and irreversible (hysteresis) energy stored in the surrounding soil. In the elastic case all of this energy may be delivered to the structure at some point during its vibration but for the inelastic case only a portion could be delivered. Thus, the net effect of substituting an elastic equivalent for a real inelastic soil is slightly conservative because the possible maximum relative displacement and maximum absolute acceleration of the structure are proportional to the square root of the energy available to the structure. To gain an estimate of the relative magnitude of the first two integrals we form the ratio, $R(t)$

$$R(t) = \frac{\int_0^t \int_A \bar{Kw} \cdot \dot{u} \, dA \, dt}{\int_0^t \int_A DL(\bar{u}) \cdot \dot{u} \, dA \, dt}$$

Since we desire order of magnitude values only we define \hat{R}

$$\hat{R} = \frac{K \bar{w}_{av} \cdot \int_0^t \int_A \dot{\bar{u}} dA dt}{DL(\bar{u})_{av} \cdot \int_0^t \int_A \dot{\bar{u}} dA dt}$$

where \bar{w}_{av} and $L(\bar{u})_{av}$ represent average values. Since the integrals are identical we can substitute

$$\hat{R} = \frac{K \bar{w}_{av}}{DL(\bar{u})_{av}} = \frac{K \bar{w}_{av}}{DL(\bar{w})_{av} + DL(\bar{z})_{av}}$$

Each of the three terms in the last equation represent a pressure. The individual terms become more meaningful if we separate the motions represented into components of the structure motion.

The total structure motion \bar{u} can be represented as the sum of four components

$$\bar{u} = \bar{z}_0 + \bar{z}_c + \bar{w}_0 + \bar{w}_c$$

where

\bar{z}_0 = free-field motion at structure centroid, constant for entire structure

\bar{z}_c = $\bar{z} - \bar{z}_0$

\bar{w}_0 = departure of structure centroid from free-field position of structure centroid. This would be zero for a perfect impedance match between structure and soil

\bar{w}_c = $\bar{w} - \bar{w}_0$

Now

$$DL(\bar{w}_0) = DL(\bar{z}_0) = 0$$

because these represent undistorted motion.

Thus

$$\hat{R} = \frac{K\bar{w}_0 + K\bar{w}_c \text{ av}}{DL(\bar{w}_c)_{\text{av}} + DL(\bar{z}_c)_{\text{av}}}$$

Now the pressure component $DL(\bar{w}_c)_{\text{av}}$ is equal to the static pressure required to deform the structure an amount \bar{w}_c from its rest configuration. This is on the order of a small fraction of the peak overpressure that the structure is designed to resist. The pressure component $DL(\bar{z}_c)_{\text{av}}$ however represents the pressure that would be required to uniformly compress the structure the amount that the pressure wave compresses the free-field. This is a very large pressure, particularly for soft soils having a small K.

Now, the departure of the structure centroid from the free-field centroid is very small and becomes zero shortly after engulfment. Thus the term $K\bar{w}_0$ is small in comparison with the others.

Therefore, within the accuracy being attempted we may write

$$\hat{R} \sim \frac{K\bar{w}_c \text{ av}}{DL(\bar{z}_c)_{\text{av}}}$$

Now, \bar{w}_c and \bar{z}_c are of the same order of magnitude, probably within a factor of 1.0 to 2.

$$\therefore \hat{R} \sim \frac{K\bar{z}_c \text{ av}}{DL(\bar{z}_c)_{\text{av}}}$$

Thus, the ratio \hat{R} , is of the same order of magnitude as the ratio of the pressure required to reduce the volume of displaced soil to the pressure required to reduce the structure volume by the same amount.

In general, this is a small number.

For instance, for a circular cylinder the pressure ratio is of the order

$$\frac{p_{\text{soil}}}{p_{\text{cyl}}} \sim \left(\frac{E_s}{E_c}\right) \left(\frac{R}{h}\right)$$

where

E_s = modulus of elasticity of soil

E_c = modulus of elasticity of cylinder

(R/h) = radius to thickness ratio of cylinder.

For a thin concrete silo in fairly stiff soil

$$\frac{p_{\text{soil}}}{p_{\text{cyl}}} = \frac{50000}{4000000} \times 20 = \frac{1}{4}$$

For a typical existing silo

$$\frac{p_{\text{soil}}}{p_{\text{cyl}}} = \frac{20000}{4000000} \times 5 = \frac{1}{40}$$

This lengthy discussion has been included in order that the reader might appreciate that the conclusion that net response is insensitive to K , is quite general, and does not hinge on numerical values chosen for a few specific structures.

Therefore, we can use quite approximate values of K without seriously influencing the accuracy of results obtained. An exception to this statement

is that K should be estimated as accurately as practical when computing the rigid body motion of the structure. However, we are fortunate in that K can be estimated with best accuracy for this mode of motion.

It is not generally appreciated that the formula

$$p = \rho c v$$

is independent of any assumed stress-strain law if the c value used is the instantaneous wave velocity. Of course the wave velocity does in general depend upon the stress and stress-strain laws. However, for both the linear elastic and linear viscoelastic stress-strain laws c is constant. Therefore, if the correct value of c for a particular soil is determined the only errors introduced by the velocity terms are those following from neglect of the inclination of the pressure vector with respect to the velocity vector. This angle (γ of Figure A.1a) is generally quite small. Further, since the value of c in the equation is adjusted to radiate the correct total amount of energy during one cycle (the rate during the cycle will not be quite correct, in general) the influence on structure motion is negligible.

In conclusion, it is believed that Equations (A.18) and (A.19) provide nearly the best accuracy attainable with linear equations. A slight improvement could be made without loss of linearity if the constant K were replaced with a linear operator but this would greatly complicate computation. Any further improvement would introduce the considerable difficulties associated with nonlinear equations.

A.3 Formal Solution of the Fundamental Equations

The fundamental equations are

$$DL(\bar{u}) + K\bar{u} + c\rho \dot{\bar{u}} + m\ddot{\bar{u}} = \bar{p}_1 \quad (A.18)$$

$$\bar{p}_1 = \bar{n} \cdot \bar{p} + K\bar{z} + c\rho \dot{\bar{z}} \quad (A.19)$$

If we have any set of orthogonal functions $\bar{\phi}_i$ satisfying Equation (A.6)

$$DL(\bar{\phi}_i) = m\omega_i^2 \bar{\phi}_i \quad (A.6)$$

and some set of boundary conditions and, further, if the mass per unit area of the structure is constant then the fundamental equations can be solved by the following set of equations

$$\bar{u} = \sum_{i=1}^{\infty} T_i(t) \bar{\phi}_i \quad (A.23)$$

$$\tau_i = \frac{1}{N_i} \int_A \bar{p}_1 \cdot \bar{\phi}_i \, dA \quad (A.24)$$

$$N_i = \int_A m \bar{\phi}_i \cdot \bar{\phi}_i \, dA \quad (A.25)$$

$$\ddot{T}_i + \frac{\rho c}{m} \dot{T}_i + (\omega_i^2 + \frac{K}{m}) T_i = \tau_i \quad (A.26)$$

If the mass per unit area were not constant we see that the velocity term in Equation (A.26) would render the equation meaningless because all of the other terms in the equation are functions of time only.

It should be noted, further, that although we have chosen to carry the soil spring constant K as a separate factor and that although this appears in Equation (A.26) as the ratio $\frac{K}{m}$ there is no necessity that K be taken as an average constant

factor. If we were to define a new linear operator

$$D \hat{L}(\bar{u}) = D L(\bar{u}) + K \bar{u}, \quad (A.27)$$

then a somewhat different set of orthogonal functions $\bar{\phi}_i$ would be generated by the equation analogous to (A.6) and the factor $\frac{K}{m}$ in (A.26) would vanish. Thus, the only intrinsic limitation on the soil resistance factor is that it be given by some linear operator operating on the displacement \bar{u} .

There is an element of arbitrariness in the solution as presented to this point because, as has been stated, the orthogonal functions $\bar{\phi}_i$ employed can be that set of functions generated by any arbitrarily assumed set of boundary conditions. One would suspect, however, that of all of the possible sets that might be used in a given instance some particular set will result in the least amount of computational effort required. This aspect of the theory, though of considerable practical importance to the engineers who must carry out the computations, generally is glossed over in treatises on orthogonal functions. Therefore, it will be developed in detail in the following paragraphs as it applies to solution of equations (A.18) and (A.19).

Our general method of procedure is to divide the total motion \bar{u} into a rigid body component \bar{u}_r plus a deformational component \bar{u}_d . We then expand both \bar{u}_r and \bar{u}_d in terms of the orthogonal functions $\bar{\phi}_i$ and determine boundary conditions for $\bar{\phi}_i$ resulting in the simplest overall solution. Thus,

$$\bar{u} = \bar{u}_r + \bar{u}_d \quad (A.28)$$

$$\bar{u} = \sum_{i=1}^{i=\infty} S_i \bar{\phi}_i + \sum_{i=1}^{i=\infty} T_i \bar{\phi}_i \quad (A.29)$$

Since \bar{u}_r is a rigid body motion

$$DL(\bar{u}_r) = 0 \quad (A.30)$$

Then, substituting (A.24) and (A.29) into (A.18)

$$(\ddot{S}_i + \ddot{T}_i) + \frac{\rho c}{m} (\dot{S}_i + \dot{T}_i) + \frac{K}{m} (S_i + T_i) + \omega_i^2 T_i = \tau_i \quad (A.31)$$

Suppose, however, that it were permissible to set

$$\bar{u}_r = S_r \bar{\phi}_r, \quad (A.32)$$

that is the entire rigid body motion could be represented by the r th mode of the system. We know, for instance, that this is true for a complete cylinder where the first mode represents the rigid body motion. Then for all values of the index i , other than r , Equation (A.31) would become

$$\ddot{T}_i + \frac{\rho c}{m} \dot{T}_i + (\omega_i^2 + \frac{K}{m}) T_i = \tau_i \quad (i \neq r) \quad (A.33)$$

In view of Equation (A.30) the frequency as given by Equation (A.6) would be zero for the r th mode, i.e.,

$$\omega_r^2 = 0 \quad (A.34)$$

Thus for the r th mode equation (A.31) becomes

$$(\ddot{S}_r + \ddot{T}_r) + \frac{\rho c}{m} (\dot{S}_r + \dot{T}_r) + \frac{K}{m} (S_r + T_r) = \tau_r \quad (A.35)$$

where we see that for the r th mode the distinction between S_r and T_r is arbitrary and T_r may be taken equal to zero, in conformity with definitions (A.28) and (A.29) which restricted \bar{u}_d and the associated time functions T_i to deformational motion.

Thus, if a rigid body mode $\bar{\phi}_r$ satisfying Equation (A.32) can be shown to exist then all of the rigid body motion would result from a single solution of Equation (A.26); no summations of the type indicated by Equation (A.29) would be necessary. Inasmuch as the rigid body motion comprises by far the largest percentage of the total motion for small stiff structures, such as solid propellant missile silos, a criterion for establishing the rigid body mode is of considerable practical importance.

If a rigid body mode exists it will satisfy the equation

$$\bar{\phi}_r = \text{Constant Vector} \quad (\text{A.36})$$

then from the orthogonality definition

$$\int_A \bar{\phi}_r \cdot \bar{\phi}_i m \, dA = 0, \quad r \neq i \quad (\text{A.37})$$

$$\bar{\phi}_r \cdot \int_A \bar{\phi}_i m \, dA = 0 \quad (\text{A.38})$$

Denote

$$\bar{\psi}_i = \int_A \bar{\phi}_i m \, dA \quad (\text{A.39})$$

Thus, the vector $\bar{\psi}_i$ is either equal to zero or perpendicular to the vector $\bar{\phi}_r$. Since in general the infinite set of vectors $\bar{\phi}_i$ will not all have the same direction cosines we can conclude

$$\int_A \bar{\phi}_i m \, dA = 0 \quad (\text{A.40})$$

Now consider the structures to be in space, not acted upon by any exterior forces, and in steady state vibration in the $\bar{\phi}_i$ mode about the mass center. The mass center under these conditions is motionless. Then the structure displacement is given by

$$\bar{w} = A_i \bar{\phi}_i \sin \omega_i t \quad (A.41)$$

where

A_i is arbitrary.

The velocity and structure momentum are given by

$$\bar{v} = \omega_i A_i \bar{\phi}_i \cos \omega_i t \quad (A.42)$$

$$\bar{m} = m\bar{v} = m\omega_i A_i \bar{\phi}_i \cos \omega_i t \quad (A.43)$$

where \bar{m} is the momentum of an element of the structure.

Since the centroid of the structure is motionless the total momentum of the structure, \bar{M} , must be zero at all times. Thus,

$$\bar{M} = \int_A \bar{m} dA = 0 \quad (A.44)$$

$$A_i \omega_i \cos \omega_i t \int_A m \bar{\phi}_i dA = 0 \quad (A.45)$$

Therefore

$$\int_A m \bar{\phi}_i dA = 0 \quad (A.46)$$

Equation (A.46) is identical with Equation (A.40); thus the criterion for the existence of a rigid body mode is that the mode should be computed for structure vibration about its centroid without influence from external forces or reactions.

For self-closing shells, such as cylinders or toroids, normal modes are customarily computed for the motionless center-of-mass condition. However, for open shells, such as domes and arches, normal modes generally are computed for a position-fixed boundary, the spring line of the shell, that is not in the plane

of the mass centroid. For domes the normal modes computed for the motionless mass centroid will not differ greatly from those appropriate to the position fixed spring line; however, for cylindrical arches having no tie between the foundations the difference between these two conditions will result in marked divergence between the mode geometries.

Use of the centroidal normal modes imposes one complicating factor on computation of the forcing function. Since the footing bases move with respect to the centroid during vibration of the structure the generalized forcing functions, τ_1 , must include the effect of foundation reactions. \bar{p}_1 as defined by Equation (A.19) does not include this term. Essentially the intensity of the reaction at any given instant of time would be equal to the static reaction necessary to balance the forces distributed over the surface of the structure at that same instance of time. These forces include the three components on the right side of Equation (A.19).

As a practical matter when open structures, domes, arches, toroidal arches, etc., are used, generally they are very large structures, aerodynamic systems shelters, command and communication centers, etc. For the large structures the rigid body motion may be quite small in comparison with the deformation motion. When this is true the functions S_1 will be considerably smaller than the functions T_1 of Equation (A.31). If the functions S_1 are small enough to neglect then Equation (A.31) becomes identical to Equation (A.25) and if position-fixed boundary normal modes were to be used the boundary reaction forces would contribute no energy to the system and, therefore would not have to be included in the computation of the generalized forcing function. Unfortunately, no general rules can

be laid down for determination of the negligibility of S_i with respect T_i ; however, if the rigid body motion were to be computed using the centroidal rigid body mode (which is just a lateral translation of the rigid structure) and the deformational motion computed for position-fixed foundation modes the results obtained would be conservative, i.e., the deformational motion would be somewhat overestimated though the degree of conservatism might be difficult to establish.

An important characteristic of the modal motion can be determined from the free vibration solution of Equations (A.26) (and equivalently Equations (A.33) and (A.35)). If we define Ω_i

$$\Omega_i^2 = \omega_i^2 + \frac{K}{m} \quad (A.47)$$

and δ the damping coefficient expressed as a fraction of critical damping

$$2\delta_i \Omega_i = \frac{\rho c}{m} \quad (A.48)$$

then the free vibration corresponding to Equation (A.26) becomes

$$\ddot{T}_i + 2\delta_i \Omega_i \dot{T}_i + \Omega_i^2 T_i = 0 \quad (A.49)$$

This is the familiar equation of the damped oscillator. Solving for δ_i we obtain

$$\delta_i = \frac{\rho c}{2\Omega_i m} \quad (A.50)$$

If δ_i is greater than one, the mode is over-critically damped. For the over-critically damped modes the response function T_i asymptotically approaches the forcing function τ_i . If the latter contains no spikes or jumps the response function generally remains less than the forcing function. In fact, these

conclusions are substantially correct even for oscillatory motions occurring when δ_1 is less than one but greater than the square root of one-half.

Many methods are known for solution of equations of the general form of Equation (A.26). One method is presented in Appendix B of this report; however, it should be appreciated that a designer has his choice of the various analytic, phase plane, computer, or other methods for solution of the equation.

One problem in the solution of Equation (A.26) is evaluation of the forcing function τ_1 . A detailed general method of approach is presented in the next section.

A.4 Evaluation of Generalized Forcing Functions

In this section a general method for evaluation of the forcing functions τ_1 will be presented. The method is applicable to hand numerical, graphical, and digital computer computation.

In the development that follows it is presumed that the geometry of the normal modes $\bar{\phi}_1$ is known. For most structures likely to be used the modal components are available in the literature.

In general the ground shock wave will not be a plane wave. However, by far the largest portion of the energy delivered to the structure will come from the air-induced ground shock wave. This wave, strictly speaking, is not plane, but the portion of the wave actually impinging against the structure can be taken as plane with negligible error even for structures of a couple of hundred feet span and waves resulting from very small bombs. It should be noted that the air-induced wave, in general, will have at least six components, two direct and four reflected from bedrock. The six components of the wave are:

1. The incident compression wave
2. The incident shear wave
3. The compression wave resulting from reflection of the compression wave.
4. The shear wave resulting from reflection of the compression wave
5. The compression wave resulting from reflection of the shear wave
6. The shear wave resulting from reflection of the shear wave.

These six components are shown in Figure A.2. It should be noted that for a substantially level bedrock layer that the unit vectors perpendicular to the advancing wave fronts all lie in the same vertical plane, but that the inclination of the unit vectors with respect to horizontal varies among the components.

In a nonhomogeneous soil consisting essentially of differing horizontal strata with fairly well defined interfaces the number of components of the ground shock wave, each still substantially plane, arriving at the structure could be considerably increased. In addition to these, at the position of the structure, there generally will be a large number of randomly oriented, low intensity waves resulting from diffraction of the air-induced ground shock wave around boulders and other local discontinuities and a component of the directly transmitted shock originating at the crater and propagating outward through the soil to the structure. Since this latter component must travel through a much longer soil path than does the air-induced shock to reach the structure the number of random defractions that have occurred is considerably greater for the directly transmitted component of shock than for the air-induced. In the 100 to 1000 psi range the directly transmitted component generally appears essentially as hash consisting

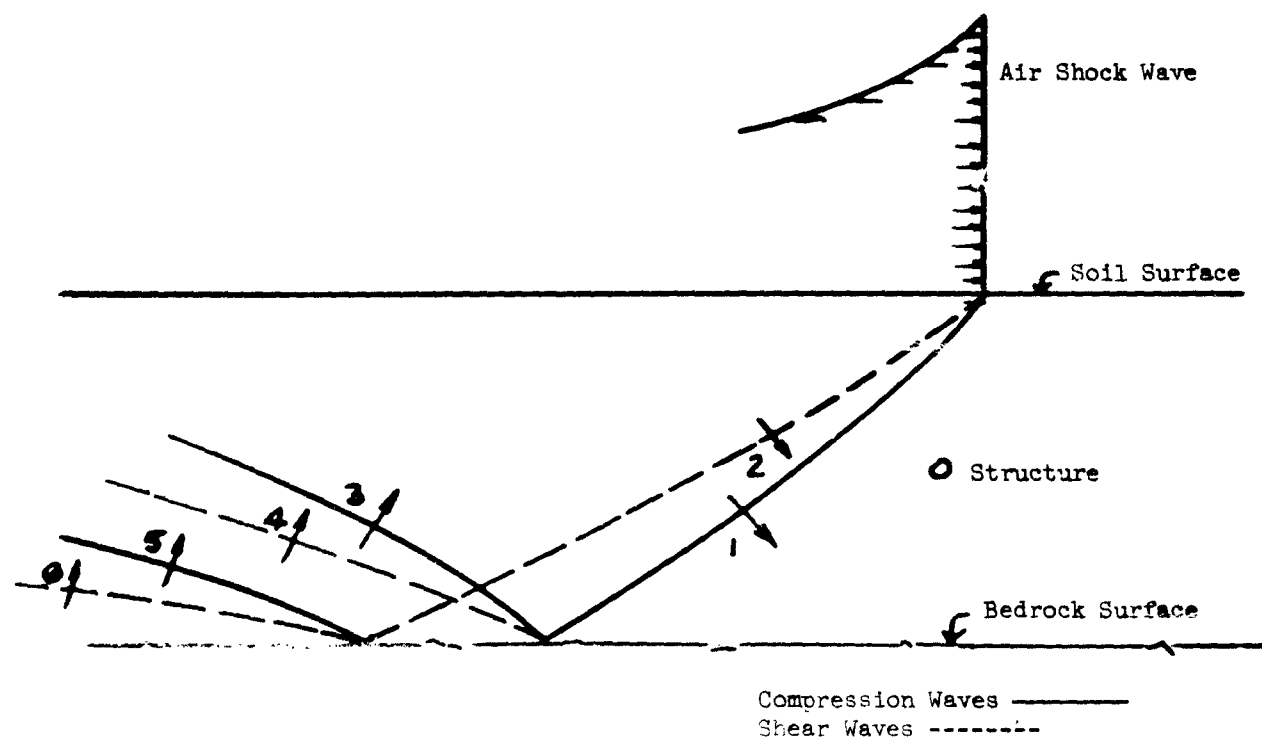


Figure A.2 GROUND WAVES INDUCED BY BLAST WAVE AND BEDROCK

of spikes of acceleration of fairly high intensity but short duration, a fraction of a millisecond to a few milliseconds.

It is not our purpose in this report to present detailed methods for determining the free-field ground motion at the structure position. This information is contained in a number of lengthy reports devoted exclusively to that topic. Indeed, this is one of the major areas of research still being investigated. However, in Section 4 of this report we do present some general rules for estimating the order of magnitude of importance of the various components of shock that might reach the structure.

Whatever methods or data are used to establish the free-field motion-time history at the structure position these data will include pressure in three directions, particle velocity, and particle displacement, all given as functions of time. Generally, accelerations associated with each wave component also are available.

The equation for the generalized forcing function, τ_i , is

$$\tau_i = \frac{1}{N_i} \int_A \bar{p}_1 \cdot \bar{\phi}_1 dA \quad (A.24)$$

where

$$\bar{p}_1 = \bar{n} \cdot \bar{p} + k\bar{z} + \rho c \dot{\bar{z}} \quad (A.19)$$

It would be possible of course to expand these expressions by the methods of vector analysis and obtain formulas for their evaluation in terms of the scalar magnitudes of the various vectors and the angles between these. However, a much simpler system of evaluation can be developed from a consideration of the physical meanings of the terms and introduction of an artificial device, an imaginary

rectangular parallelepiped circumscribed about the structure. Though this artificiality does introduce one avenue of possible confusion (which is discussed subsequently) it materially simplifies the computations required to evaluate the τ_i integrals, particularly the component due to the free field pressure tensor, \bar{p} .

Now, we note that in integral (A.24) the product of the pressure vector \bar{p}_1 and the differential area, dA , is a differential force. The dot product of this force with the displacement, $\bar{\phi}_1$, then is the differential energy delivered to the structure by the force $\bar{p}_1 dA$ moving through a distance, $\bar{\phi}_1$. Thus the integral in Equation (A.24) is the total energy that could be delivered to the structure by the force field \bar{p}_1 if the latter remained constant while the structure deformed into the displacement configuration, $\bar{\phi}_1$.

Consider any shell structure. About the structure describe an imaginary rectangular parallelepiped. It is not essential that the parallelepiped have any particular orientation; however, computations will be simplest if four faces of the parallelepiped are vertical, two of these parallel to the direction of the advancing ground shock waves. Figure A.3 illustrates such a parallelepiped circumscribed about a vertical cylinder. Three coordinate directions ξ , η , and ζ and three unit vectors $\bar{\xi}$, $\bar{\eta}$, and $\bar{\zeta}$ are defined in the figure. In Section AA of Figure A.3 a differential element of area, dA , has been emphasized. A pressure vector \bar{p}_1 and a displacement vector $\bar{\phi}$ act on the area dA . For clarity these are shown in the $\bar{\xi}$, $\bar{\eta}$ plane though this is not essential.

Now if both the force vector, \bar{p}_1 , and the displacement vector, $\bar{\phi}$, are resolved into their components in the ξ , η , and ζ directions the results are as shown in the figure (only the ξ and η components are shown). Thus the

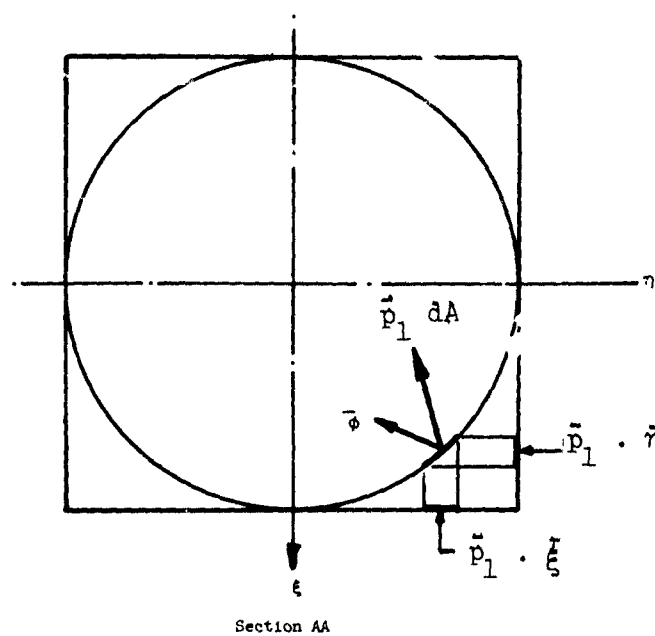
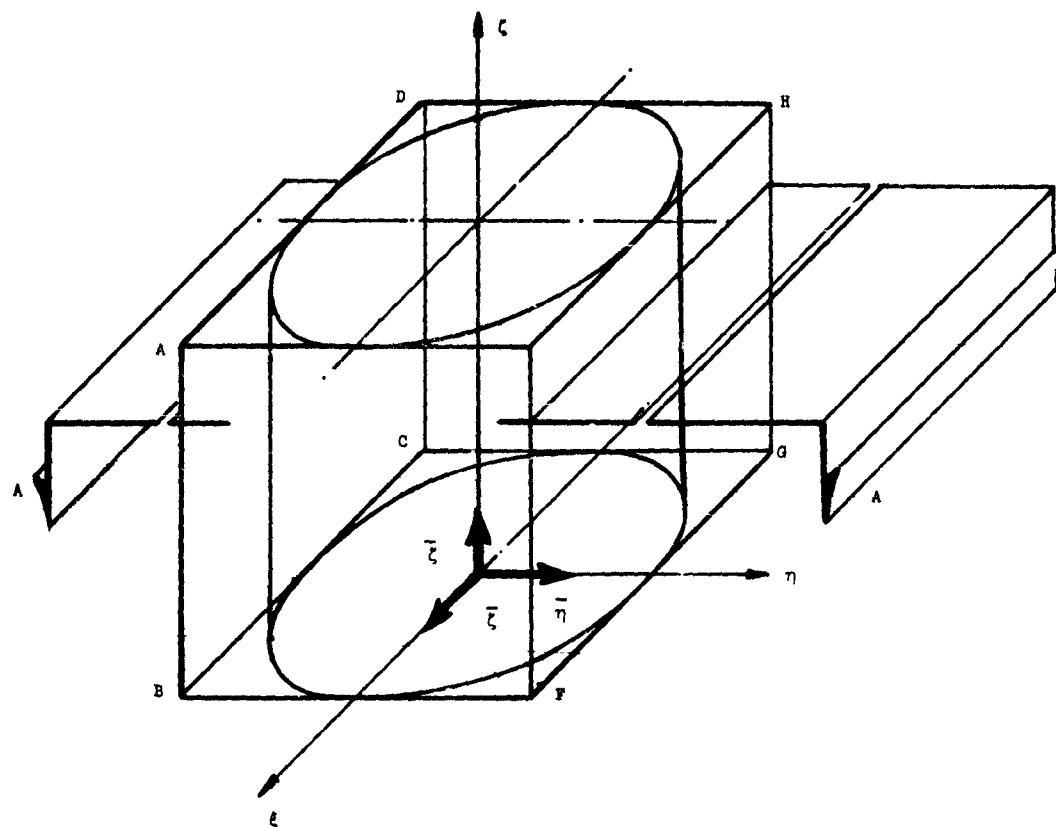


Figure A.3 RESOLUTION OF VECTOR NORMAL MODE MOTIONS

energy delivered to the element dA is equal to the sums of the energies delivered by the components of the pressure vector perpendicular to the faces of the parallelepiped acting through the projections of the displacement volume on the same faces.

The vectors $k\bar{z}$ and $\rho c\dot{\bar{z}}$ present no problems in resolution into their components on the faces of the parallelepiped.

The tensor \bar{p} presents a somewhat different problem. Though the vector $\bar{n} \cdot \bar{p}$ is very simple to represent symbolically its actual numerical computation can become quite tedious. It turns out that this computation need not be carried out. Figure A.4 shows a wave front and also a differential element of soil behind the wave front. The components of pressure acting on the differential element of soil are shown. Generally the components shown as p_b and p_c of Figure A.4 are equal but this is not necessarily true. The Mohr's cycle for the pressure in the η, ξ plane also is given on Figure A.4, and the component of pressure \bar{p} appearing on the vertical face of the parallelepiped ABCD is shown as \bar{p} . The horizontal component of this in the η direction is shown as $\bar{p} \cdot \bar{\eta}$. A factor λ is defined on the Figure where λp_a is equal to $\bar{p} \cdot \bar{\eta}$. Now since behind the wave front, p_a , p_b , and p_c bear a constant relationship to each other the factor λ is a constant applicable to planes ABCD and EFGH. It should be noted that the pressure $\bar{p} \cdot \bar{\eta}$ appearing on plane in ABCD, is the same in numerical magnitude as that appearing on the plane EFGH, other conditions being equal. Thus the pressure at any point on plane ABCD or EFGH is just the wave pressure p_a multiplied by a constant factor λ_η which is easily determinable in any specific instance. Further, if the ground pressure wave decays as a function of time the pressure on a vertical plane

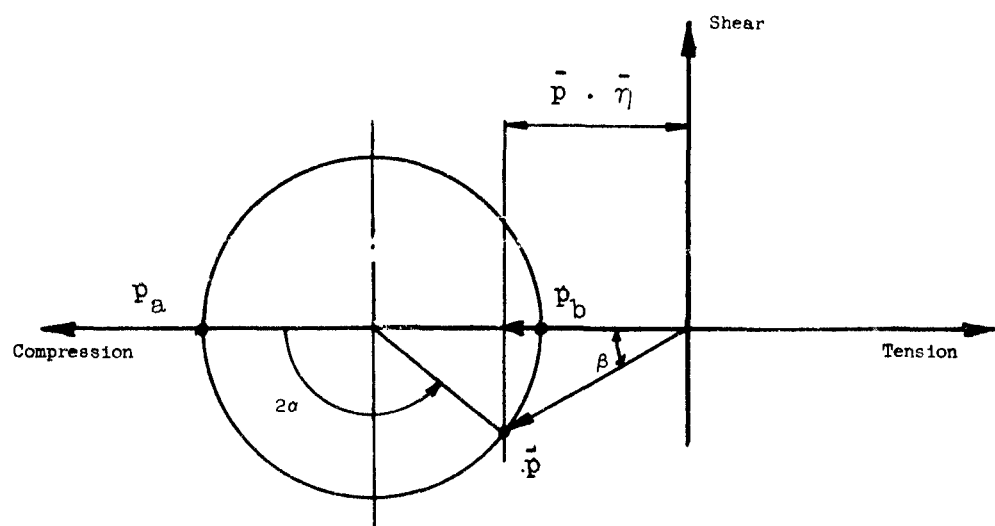
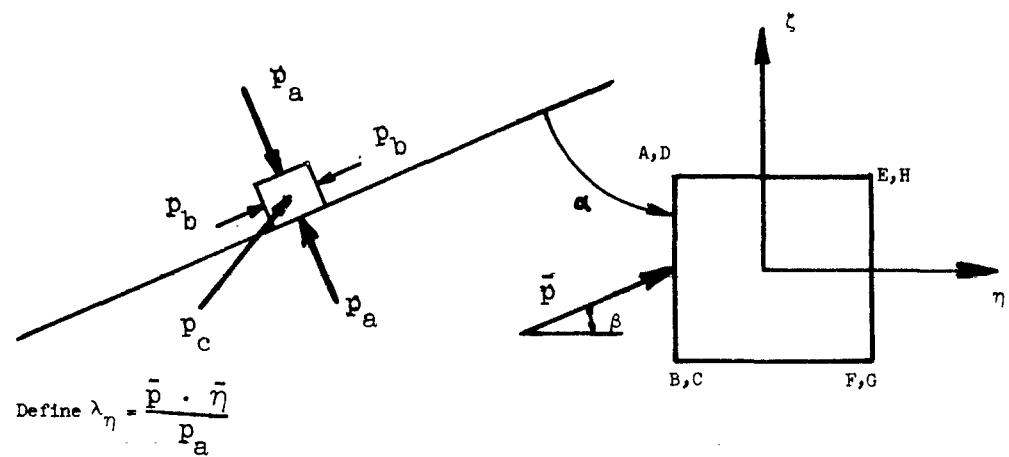


Figure A.4 PRESSURES INDUCED BY PLANE COMPRESSION WAVE

perpendicular to the η axis at any given instant is equal to the pressure p_a existing at that instant multiplied by λ_η . The λ_η factor is neither position nor time dependent for any given plane wave. Factors λ_ξ and λ_ζ can similarly be defined for the other four faces of the parallelepiped.

Figure A.5 shows a similar construction for a shear wave. It should be noted that the shear wave has no component on planes ABFE and DCGH. λ factors for these waves can be defined similarly to those for the compression waves.

The time factor involved in the wave motion has not yet been considered. Figure A.6 shows a section of the cylinder of Figure A.3 taken parallel to the η , ζ axes. A compression wave is shown during the period of engulfment. Now, it should be carefully observed that although the computations are carried out by applying pressure components to the surfaces of the parallelepiped the variation of pressure component versus time on each element of the modal displacement component on the parallelepiped is identical with the pressure versus time at the element of structure surface projected on the faces of the parallelepiped, e.g., pressure on element da_3 at time \hat{t} is equal to the component of pressure on element dA_3 at time \hat{t} projected perpendicular to plane ABCD.

Thus for the instant depicted in Figure A.6 if the pressure versus time curve is represented $p(t)$, where time is taken as zero at the wave front, and if we denote the component of pressure at element da_1 by \hat{p}_1 we have

$$\begin{aligned}\hat{p}_1 &= \text{Projection } p(0) \\ \hat{p}_2 &= \text{Projection } p(0)\end{aligned}\tag{A.51}$$

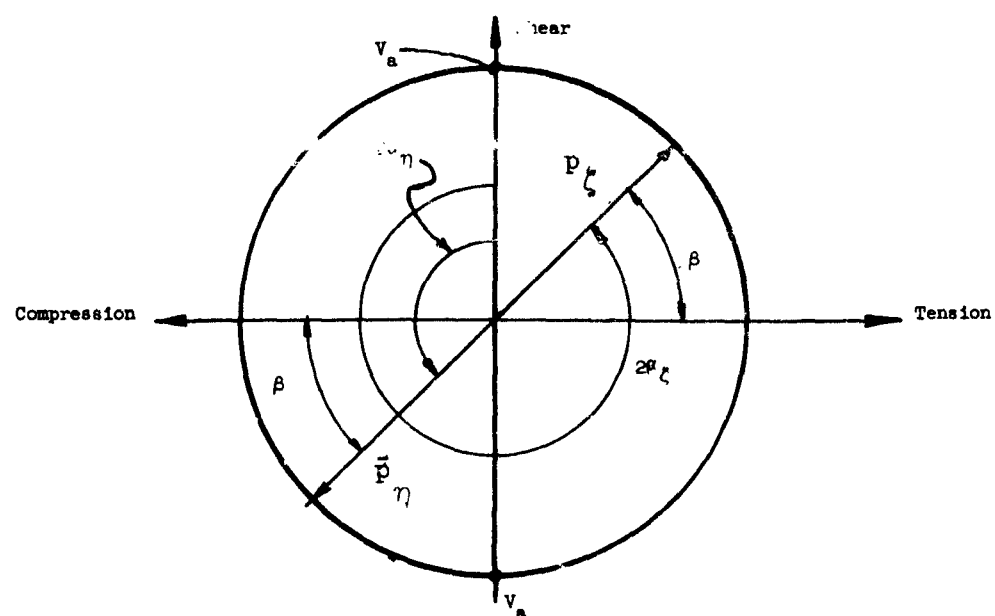
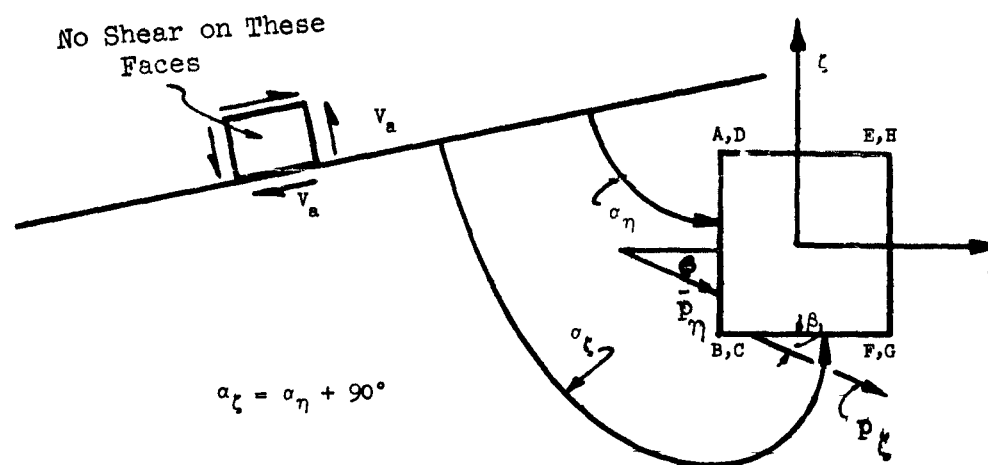


Figure A.5 PRESSURES INDUCED BY PLANE SHEAR WAVE

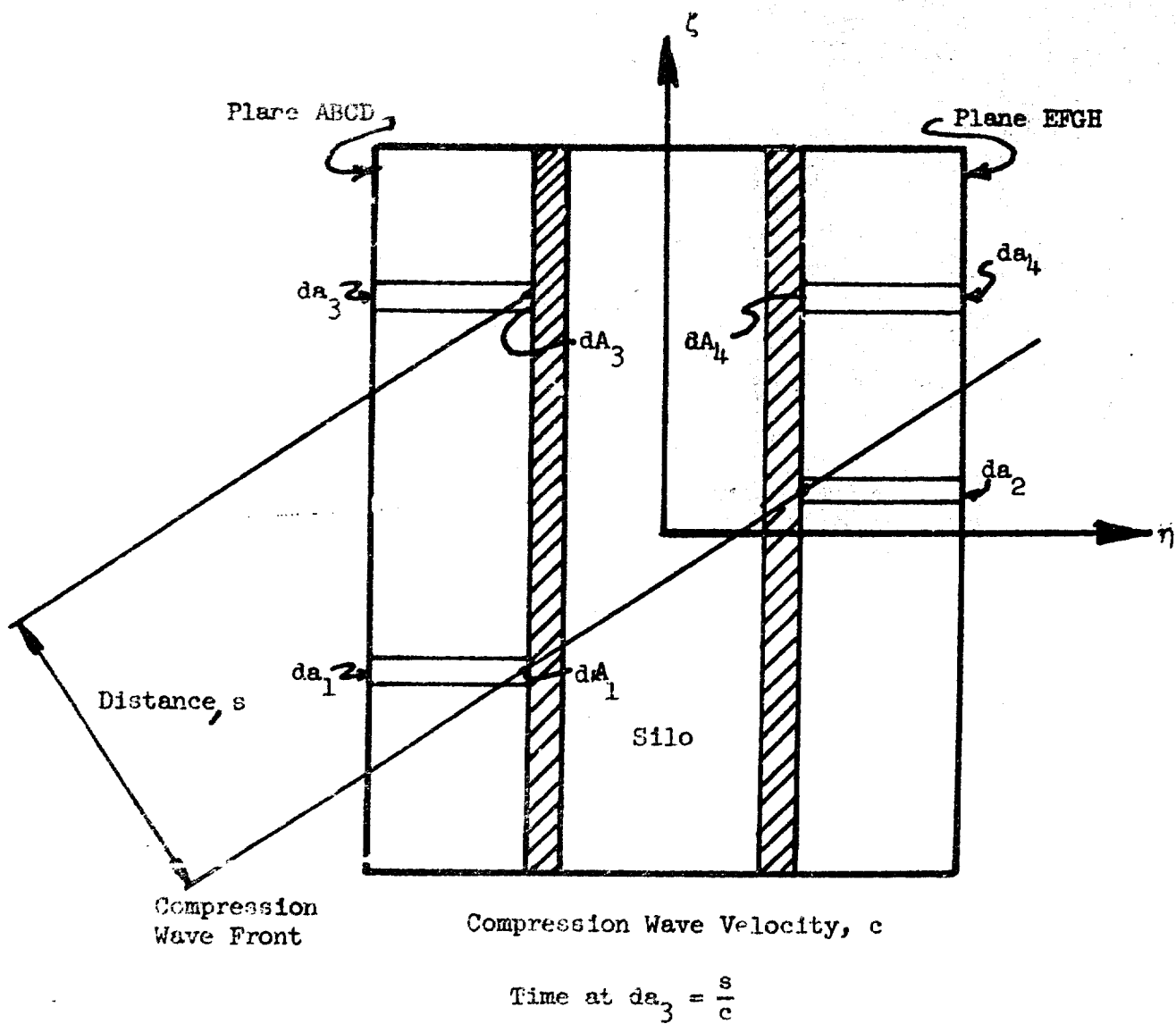


Figure A.6

Best Available Copy

and

$$\hat{p}_3 = \text{Projection } p\left(\frac{s}{c}\right). \quad (\text{A.52})$$

The distance, s , is measured perpendicular to the plane of the wave front.

In summary, the integral (A.24) can be evaluated as follows:

1. For the i th mode $\bar{\phi}_i$ compute the norm N_i .
2. Circumscribe an imaginary parallelepiped about the structure.
3. Impose the displacement of a normal mode upon the structure and translate components of this deformation onto the six faces of the parallelepiped. These, then, will appear as relief maps.
4. Divide the faces of the parallelepiped into a grid of small elements (acceptable accuracy generally can be obtained with a coarse grid of four or five elements in each direction).
5. Determine the time lag for each element.
6. Determine the product of pressure components and volume for each element and each of three components of pressure.
7. Sum the values for all elements at specific time instants and divide by the norm N_i .
8. Plot the results as a function of time. This is the function τ_i .

The actual computation outlined in the previous eight steps becomes a matter of bookkeeping and for different waves and structure characteristics differing techniques will be most expeditious. Several general characteristics that can be used to simplify the overall procedure will be enumerated.

1. For plane waves the factor $\rho c \dot{z}$ is equal in numerical magnitude to p_a of the pressure tensor; however, whereas the latter is compression on both the windward and leeward faces of the structure, i.e., plane ABCD and plane EFGH, the $\rho c \dot{z}$ term is compression on the windward face and tension on the leeward face. The direction of \dot{z} does not change as it passes the structure. Also it should be noted that the factor $\rho c \dot{z}$ contributes no component of pressure to planes ABFE and DCGH if they have been oriented as suggested.
2. The factor $K\bar{z}$ produces a compression stress on planes ABCD and AEHD. It produces a tension stress on planes EFGH and BFGC; it produces no stress on planes ABFE and DCGH.
3. If the structure is subjected to more than a single wave generally the simplest procedure is to compute the effects of each wave separately and then sum the results in the last step.
4. If more than a single mode is to be investigated all factors for the various modes, except the displacement factors $(\bar{\phi}_i \cdot \bar{\eta} da, \text{ for instance})$ are identical for the several modes.
5. For rigid body motion the "relief map" on planes ABCD, EFGH, AEHD, and DFGC represent just displacements of the planes along their normals. The planes ABFE and DCGH, contribute zero to the rigid body motion.
6. Each component of the rigid body motion is orthogonal to all of the other modes of the system and, therefore, may be handled separately.

The reader may well question whether the detailed calculations outlined above are justified in view of the inherent inaccuracy of input data. Generally they

will not be justifiable. However, the general characteristics of the modes and essential geometric relations presented can be used in specific instances to delineate which of the input wave components are significant, which can be neglected (generally all three shear components and the shear reflection induced compression components), and to establish the cardinal characteristics of the forcing functions τ_i such as rise time, peak value, and decay rate. Further, rough estimates of the peak amplitudes and rise times of the higher order modes can be determined generally with the end result that the higher order modes can be neglected.

A.5 Coupled Modes

In reality the modes of the system that we have approximated by Equations (A.18) and (A.19) are coupled, the coupling being introduced by the two first time derivative terms of Equation (A.16).

In this section we will develop the theory of coupled modes for this general system. The results indicate that the simplifications made are acceptable from a practical standpoint. Further, the theory provides the necessary corrections for the rare instances where the modal coupling must be considered.

If we make the simplification that the nonlinear resistance term $kF(\bar{w})$ can be replaced by the term K Equation (A.16) becomes

$$\begin{aligned} KL(\bar{u}) + K(\bar{u}) + c_1 \rho \bar{n} \dot{\bar{u}} \cdot \bar{n} + c_2 \rho \bar{l} \dot{\bar{u}} \cdot \bar{l} + m \ddot{\bar{u}} \\ = \bar{n} \cdot \bar{p} + k \bar{z} + c_1 \rho \bar{n} \dot{\bar{z}} \cdot \bar{n} + c_2 \rho \bar{l} \dot{\bar{z}} \cdot \bar{l} \end{aligned} \quad (A.53)$$

We now define two vectors $\dot{\bar{\psi}}_u$ and $\dot{\bar{\psi}}_z$

$$\text{where} \quad \dot{\bar{\psi}}_u = \frac{c_1}{c} \bar{n} \dot{\bar{u}} \cdot \bar{n} + \frac{c_2}{c} \bar{l} \dot{\bar{u}} \cdot \bar{l} - \dot{\bar{u}} \quad (A.54)$$

and

$$\dot{\bar{\psi}}_z = \frac{c_1}{c} \bar{n} \dot{\bar{z}} \cdot \bar{n} + \frac{c_2}{c} \bar{l} \dot{\bar{z}} \cdot \bar{l} - \dot{\bar{z}} \quad (A.55)$$

Referring to Figure A.1 we see that $\rho c \dot{\psi}_u$ and $\rho c \dot{\psi}_z$ are the vector differences between Equation (A.18) and (A.19) and the accurate Equation (A.53).

Making this substitution and shifting all correction terms to the right side of the equal sign, Equation (A.53) becomes

$$DL(\bar{u}) + K\bar{u} + c\rho\ddot{u} + m\ddot{u} = \bar{n} \cdot \bar{p} + K\bar{z} + c\rho\dot{z} + c\rho\dot{\psi}_z - c\rho\dot{\psi}_u \quad (A.56)$$

$$DL(\bar{u}) + K\bar{u} + c\rho\ddot{u} + m\ddot{u} = \bar{p}_1 + c\rho(\dot{\psi}_z - \dot{\psi}_u) \quad (A.57)$$

Since $\dot{\psi}_z$ is defined in terms of the input parameters it is immediately computable so we can simplify the appearance of Equation (A.57) slightly by defining

$$\bar{p}_1' = \bar{p}_1 + c\rho\dot{\psi}_z \quad (A.58)$$

Then

$$DL(\bar{u}) + K(\bar{u}) + c\rho\ddot{u} + m\ddot{u} = \bar{p}_1' - c\rho\dot{\psi}_u \quad (A.59)$$

Equation (A.59) is of the same form as Equation (A.18) with the $\dot{\psi}_u$ term added.

$$\text{Define } \tau_i' = \frac{1}{N_i} \int_A \bar{p}_1' \cdot \bar{\phi}_i \, dA \quad (A.60)$$

Then

$$\bar{p}_1' = \sum_{i=1}^{i=\infty} \tau_i' \bar{\phi}_i \quad (A.61)$$

Substitute Equations (A.6), (A.23), (A.54) and (A.61) into Equation (A.59).

Divide through by m . The result is

$$\sum_{i=1}^{i=\infty} \left[\ddot{\bar{u}} + \frac{c\rho}{m} \dot{\bar{u}} + \left(\omega_i^2 + \frac{K}{m} \right) \bar{u} \right] \bar{\phi}_i = \sum_{i=1}^{i=\infty} \tau_i' \bar{\phi}_i - \sum_{i=1}^{i=\infty} \frac{c\rho}{m} \left[\frac{c_1}{c} \bar{n} \cdot \bar{\phi}_i + \frac{c_2}{c} \bar{l} \cdot \bar{\phi}_i - \bar{\phi}_i \right] \dot{\bar{u}} \quad (A.62)$$

Equations (A.66) can be solved by successive approximations. At least five conclusions can be drawn from Equations (A.65) and (A.66).

1. The coupling factors remove energy from each mode and deliver it to all other modes.
2. The coupling between modes is a function of the lateral (as opposed to normal) motions of the modes. (The amplitudes of these are invariably small fractions of the normal components of motion.)
3. The numerical values of the factors within the brackets are small and decrease rapidly with increasing modal index. The values are the largest for right circular cylinders. Even for this case the coupling factor between the first and second deformational modes is less than 3%.
4. For the \dot{T}_j monotonically approaching zero the coupling of energy to other modes is very small (less than 1% total for the first 10 modes).
5. If damping ($\frac{\rho c}{m}$) is very small and if the T_i are approximately cyclic, over a period of time considerably energy can be interchanged between modes.

We conclude therefore that the simplification introduced in the previous subsections will not materially affect computed results for the heavily damped underground structures.

A development similar to the above can be carried out when the mass of the structure varies from point to point.

A.6 Natural Frequency

In order to use the material presented in this chapter it is necessary to know or determine the geometries of the normal modes $\bar{\phi}_1$ and the associated natural frequencies.

In theory these can be obtained by solution of Equation (A.6) together with the boundary equations

$$DL(\bar{\phi}_1) = m\omega_1^2 \bar{\phi}_1 \quad (A.6)$$

$$B_n(\bar{\phi}_1) = 0 \quad (n = 1, 2, \dots)$$

These equations are deceptively simple. Actually the operator $L()$ may be a complex differential expression and in fact, since actual numerical work must generally be carried out for the vector functions in terms of their components Equation (A.6) generally must be replaced by two or three scalar equations that are interdependent. The boundary equations are similarly multiplied in number.

We are fortunate in that most of the structure types of interest have already been subjected to such analysis and as a result the frequencies and modal geometries (generally, the components of the modes) are known.

If a structure having geometry significantly different than those for which modal data exists must be analyzed by the normal mode method the modal geometries and frequencies can be determined by approximate methods. The determination need not be highly accurate.

APPENDIX B

A NUMERICAL METHOD OF SOLUTION OF THE RESPONSE EQUATION

A method for solving equations of the form

$$\frac{\ddot{T}}{\Omega^2} + \frac{2\delta}{\Omega} \dot{T} + T = \hat{\tau} \quad (\text{B.1})$$

is desired (Note $\hat{\tau}$ is equivalent to τ/Ω^2 of Section 5 and Appendix A. In this appendix it is presumed to be a known function of time.

We have the initial conditions that

$$\begin{aligned} T(0) &= 0 \\ \dot{T}(0) &= 0 \\ \hat{\tau}(0) &= 0 \end{aligned} \quad (\text{B.2})$$

Integrating once

$$\frac{\dot{T}}{\Omega^2} + \frac{2\delta}{\Omega} T + \int_0^T T \, dt = \int_0^t \hat{\tau} \, dt \quad (\text{B.3})$$

Now suppose that the time axis were divided into a number of equal increments Δt . We order the increments from zero to m with zero at the origin. Also we denote the values of T and $\hat{\tau}$ at the end of the n th increment by T_n and $\hat{\tau}_n$. With these definitions we can approximate Equation (B.3) by

$$\frac{T_{n+1} - T_{n-1}}{2\Omega^2 \Delta t} + \frac{2\delta T_n}{\Omega} + \Delta t \left[\frac{T_1}{4} + \sum_{i=1}^{i=n} T_i \right] = \Delta t \left[\frac{\hat{\tau}_1}{4} + \sum_{i=1}^{i=n} \hat{\tau}_i \right] \quad (\text{B.4})$$

If we denote

$$\Omega \Delta t = \Delta s \quad (B.5)$$

we have for all n greater than zero

$$T_{n+1} = \frac{(\Delta s)^2}{2} (\hat{\tau}_1 - T_1) + 2(\Delta s)^2 \left[\sum_{i=1}^{i=n} \hat{\tau}_i - \sum_{i=1}^{i=n} T_i \right] - 4\delta \Delta s T_n + T_{n-1} \quad (B.6)$$

For $n = 0$ we obtain for T_1

$$T_1 = \frac{\hat{\tau}_1 (\Delta s)^2}{(\Delta s)^2 + 4\delta(\Delta s) + 2} \quad (B.7)$$

Equation (B.6) can be simplified for computation

Denote

$$C_{n+1} = T_{n+1} - T_n \quad (B.8)$$

then

$$C_{n+1} = 2(\Delta s)^2 [\hat{\tau}_n - T_n] - (4\delta \Delta s + 1)(T_n - T_{n-1}) + (T_{n-1} - T_{n-2}) \quad (B.9)$$

This can be rewritten

$$C_{n+1} = 2(\Delta s)^2 [\hat{\tau}_n - \hat{T}_n] - (4\delta \Delta s + 1) C_n + C_{n-1} \quad (B.10)$$

In this scheme

$$c_1 = T_1 = \frac{\hat{\tau}_1 (\Delta s)^2}{(\Delta s)^2 + 4\delta (\Delta s) + 2} \quad (B.11)$$

$$c_2 = \frac{5}{2} (\Delta s)^2 (\hat{\tau}_1 - c_1) - (4\delta \Delta s + 1) c_1 \quad (B.12)$$

Table B.1 shows one setup for the computations.

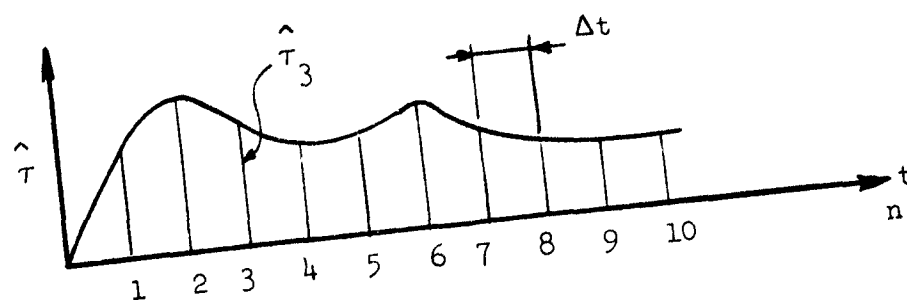


TABLE B.1
NUMERICAL SOLUTION OF $\frac{\ddot{T}}{\Omega^2} + \frac{2\delta}{\Omega} \dot{T} + T = \hat{\tau}$

n	$\hat{\tau}_n$	T_n	C_n	BC_n	$C_n - 1BC_n$	$A(\hat{\tau}_n - T_n)$
1			C_1^*			
2			C_2^*			
3						
4						
5		p	q			
6	i	j	k → l		m	n
7		s	r			
8						

$j = p + k$
 $l = Bk$
 $m = q - l$
 $n = A(i - j)$
 $r = n + m$
 $s = j + r$

$$A = 2(\Delta s)^2 \quad \Delta s = \Omega \Delta t$$

$$B = (4\delta \Delta s + 1)$$

* Compute C_1 and C_2 from

$$C_1 = \frac{\hat{\tau}_1 (\Delta s)^2}{(\Delta s)^2 + 4\delta (\Delta s) + 2}$$

$$C_2 = \frac{5}{2} (\Delta s)^2 (\hat{\tau}_1 - C_1) - (4\delta \Delta s + 1) C_1$$

$$C_2 = \frac{5}{4} A (\hat{\tau}_1 - C_1) - BC_1$$

REFERENCES

1. American Machine & Foundry Co., Mechanics Research Division, "Site Hardening for Aerodynamic Weapon Systems", Vol. II, Part 3, Section 4.5.3.2 WADD Technical Report 60-219 Volume II, Part 3 Aug. 1960 (Secret).
2. Brode, H.L., "Weapons Effects for Protective Design", Rand Corporation Document P-1951, March 31, 1960.
3. Kolsky, H., "Stress Waves in Solids", 1953, Oxford at the Clarendon Press.
4. Muskat, M., and Meres, M.W., "Reflection and Transmission Coefficients for Plane Waves in Elastic Media", Geophysics, Vol. 5, pp. 115-148, 1940.
5. Neidhardt, G.L. and Sasaki, F.T., "Inertial Test Table is Stable to 10^{-6} g" Space/Aeronautics, Oct. 1961.
6. Newmark, N.M. & Haultiwanger, J.D., "Principles and Practices for Design of Hardened Structures", Dec. 1962, AFSWC, TDR-62-138.
7. Ralph M. Parsons Co., "A Guide for the Design of Shock Isolation Systems for Underground Protective Structures", Dec. 1962, AFSWC-TDR-62-64.
8. Rojansky, V., "Gyrograms for Simple Harmonic Systems Subjected to External Forces", Journal of Applied Physics, Volume 19, March 1948, p297. (Also see Ref. 13)
9. Sauer, F. M., "Ground Motions Produced by Above Ground Nuclear Explosions", April 1959, AFSWC, TR-59-71 (Secret).
10. Weiner, R.S., "Deduction of Shock Testing Methods and Facilities Criteria", December 1962, Defense Atomic Support Agency, DASA 1328.
11. Whitman, R.V., "Nuclear Geophysics", Defense Atomic Support Agency, DASA - 1285 (11) 3203 (11) Draft.
12. Wilson, S.D. and Sibley, E.A., "Ground Displacements Resulting from Air Blast Loading", Proceedings of ASCE Soil Mechanics and Foundation Division, December 1962, Paper No. 3346.
13. Fuchs, H.O., "Spiral Diagrams to Solve Vibration Damping Problems", Product Engineering, August 1936, p. 294.

DISTRIBUTION

No. cys

HEADQUARTERS USAF

3	Hq USAF (AFOCE), Wash, DC 20330
1	Hq USAF (AFRDP), Wash, DC 20330
1	Hq USAF (AFRNE-A, Maj Griesmer), Wash, DC 20330
1	Hq USAF (AFTAC), Wash, DC 20330
1	USAF Dep, The Inspector General (AFIDI), Norton AFB, Calif 92409
1	USAF Directorate of Nuclear Safety (AFINS), Kirtland AFB, NM 87117

MAJOR AIR COMMANDS

AFSC, Andrews AFB, Wash, DC 20331

1	(SCT)
1	(SCLT)
1	(SCMC)
2	TAC, ATTN: Director of Civil Engineering, Langley AFB, Va 23365
2	SAC, ATTN: Director of Civil Engineering, Offut AFB, Nebr 68113
2	ADC, ATTN: Director of Civil Engineering, Ent AFB, Colorado Springs, Colo 80912
1	AUL, Maxwell AFB Ala 36112
1	USAFIT, Wright-Patterson AFB, Ohio 45433
1	USAFE, ATTN: Director of Civil Engineering, APO 633, New York, NY
1	PACAF, ATTN: Director of Civil Engineering, Camp Smith, Hawaii

AFSC ORGANIZATIONS

1	AFSC Scientific and Technical Liaison Office, Research and Technology Division (AFUPO), Los Angeles, Calif 90045
	ASD, Wright-Patterson AFB, Ohio 45433
2	(SEPIR)
2	(ASAMC)
	RTD, Bolling AFB, Wash, DC 20332
1	(RTN)
1	(RTN-W, Lt Col Munyon)
1	(RTS)

DISTRIBUTION (cont'd)

No. cys

	BSD, Norton AFB, Calif 92409
1	(BSR)
1	(BSRA)
2	(BSSF)
2	(Document Library)
2	SSD (SSN), AF Unit Post Office, Los Angeles, Calif 90045
	ESD, L. G. Hanscom Fld, Bedford, Mass 01731
3	(ESTI)
1	(ESFD)
1	AF Msl Dev Cen (RRRT), Holloman AFB, NM 88330
1	6593 Test Group (Development), Edwards AFB, Calif 93523
1	AFMTC (MU-135, Tech Library), Patrick AFB, Fla 32925
1	APGC (PGBAP-1), Eglin AFB, Fla 32542
	RADC, Griffiss AFB, NY 13442
2	(Document Library)
1	(EMEAM)
1	AEDC (AEOL), Arnold AFS, Tenn 37389
KIRTLAND AFB ORGANIZATIONS	
	AFSWC, Kirtland AFB, NM 87117
1	(SWEH)
1	(SWT)
	AFWL, Kirtland AFB, NM 87117
20	(WLIL)
2	(WLR)
10	(WLRC)
1	ADC (ADSWO), Special Weapons Office, Kirtland AFB, NM 87117
1	SAC Res Rep (SACLO), AFSWC, Kirtland AFB, NM 87117
1	TAC Liaison Office (TACLO-S), AFSWC, Kirtland AFB, NM 87117
OTHER AIR FORCE AGENCIES	
1	USAF Engineering Liaison Office, APO 125, New York, NY
1	AFOAR, Bldg T-D, Wash, DC 20333
1	AFOSR, Bldg T-D, Wash, DC 20333

DISTRIBUTION (cont'd)

No. cys

- 2 Director, USAF Project RAND, via: Air Force Liaison Office,
The RAND Corporation, 1700 Main Street, Santa Monica, Calif
90406

ARMY ACTIVITIES

- 1 Chief of Research and Development, Department of the Army
(Special Weapons and Air Defense Division), Wash, DC 20310
- 1 Commanding Officer, US Army Combat Developments Command,
Nuclear Group (USACDCNG), ATTN: Top Secret Control Officer
Ft Bliss, Tex 79916
- 1 Director, Ballistic Research Laboratories (Library), Aberdeen
Proving Ground, Md 21005
- 1 US Army Research Office, ATTN: Lt Gregory D. Atmore, Box
CM, Duke Station, Durham, NC
- 1 Hq US Army Air Defense Command (ADGCB), Ent AFB, Colo
80912
- 1 President, US Army Air Defense Board, Ft Bliss, Tex 79916
- 2 Chief of Engineers (ENGMC-EM), Department of the Army,
Wash, DC 20315
- 1 Director, Army Research Office, 3045 Columbia Pike,
Arlington, Va 22204
- 4 Director, US Army Waterways Experiment Sta (WESRL), P. O.
Box 631, Vicksburg, Miss 39181
- 2 Director, US Army Engineer Research and Development
Laboratories, ATTN: STINFO Branch, Ft Belvoir, Va

NAVY ACTIVITIES

- 1 Chief of Naval Research, Department of the Navy, Wash, DC
20390
- 1 Chief, Bureau of Naval Weapons, RRNU, Department of the Navy,
Wash 25, DC
- 2 Bureau of Yards and Docks, Department of the Navy, Code 22.102,
(Branch Manager, Code 42.330), Wash 25, DC
- 1 Commanding Officer, Naval Research Laboratory, Wash, DC
20390
- 1 Superintendent, US Naval Postgraduate School, ATTN: George R.
Lockett, Monterey, Calif
- 4 Commanding Officer and Director, Naval Civil Engineering
Laboratory, Port Hueneme, Calif

DISTRIBUTION (cont'd)

No. cys

Stanford Research Institute, 333 Ravens Wood, Menlo Park, Calif
1 (Mr. Ernie Chilton)
1 (Mr. F. N. Sauer)
1 (Mr. G. R. Fowles)
1 Portland Cement Association, Structural Development Section, ATTN:
Eivind Hognestad, 33 W. Grand Ave, Chicago, Ill
1 Agbabian-Jacobsen & Associates, ATTN: Drs. M. S. Agbabian and
Lydik S. Jacobsen, 8939 S. Sepulveda Blvd, Los Angeles 45, Calif
Bell Telephone Laboratories, Whippany, NY
1 (Mr. John Foss)
1 (Mr. Robert Crawford)
1 Allied Research Associates, ATTN: Mr. David C. Knodel, 43
Leon St, Boston, Mass
1 MITRON Research and Development Corp, ATTN: Dr. Maurice
Gertel, 899 Main St, Waltham, Mass
1 Barry Controls, Inc., ATTN: Mr. Richard Cavanaugh, 1400
Flower St, Glendale, Calif
1 Southwest Research Institute, ATTN: Mr. Gale Nevill, 8500
Culebra Road, San Antonio 6, Tex
1 Paul Weidlinger Associates, ATTN: Mr. Paul Weidlinger, 777
Third Avenue, New York, NY 10017
1 Shannon and Wilson, ATTN: Mr. Stanley D. Wilson, 1105 N. 38th
St, Seattle 3, Wash
1 The MITRE Corp, ATTN: Mr. Warren McCabe, P. O. Box 208,
Bedford, Mass
1 Space Technology Labs, Inc., Engineering Mechanics Dept, ATTN:
Dr. Millard V. Barton, P. O. Box 95001, Los Angeles 45, Calif
1 Northrop-Ventura Corp, ATTN: Dr. J. G. Trulio, 1515 Rancho
Conejo Blvd, Newbury Park, Calif
1 Physics International Co., ATTN: Dr. C. S. Godfrey, 2229 Fourth
Street, Berkeley 10, Calif
1 West Virginia University, Dept of Civil Engineering, ATTN: Dr.
J. H. Schaub, Morgantown, WVa
1 North Carolina State University, Dept of Civil Engineering, ATTN:
Dr. R. E. Fadum, Raleigh, NC
20 University of Illinois, ATTN: Dr. Nathan M. Newmark, 207 Talbot
Laboratory, Urbana, Ill

DISTRIBUTION (cont'd)

No. cys

California Institute of Technology, Dept of Engineering, Pasadena,
Calif

1 (Prof. C. E. Crede)

1 (Dr. Seed)

1 University of Florida, Dept of Civil Engineering, ATTN: Mr. Frank
Richardt, Gainesville, Fla

1 Colorado School of Mines, ATTN: Mr. Dave C. Card, Golden, Colo

1 Grumman Aircraft Engineering Corp, ATTN: Dr. Hyman R. Garnet,
Bethpage, NY

1 South Dakota School of Mines and Technology, ATTN: Mr. Edwin H.
Oshier, Rapid City, SD

1 United Electrodynamics, Inc., ATTN: Mr. Ted Winston, 200
Allendale Road, Pasadena, Calif

1 Iowa State University, Dept of Theoretical and Applied Mechanics,
ATTN: Mr. Glen Murphy, Ames, Ia

1 Princeton University, Dept of Civil Engineering, Princeton, NJ

IIT Research Institute, 3422 S. Dearborn St, Chicago 15, Ill

1 (Dr. Eugene Seven)

1 (Dr. Eben Vey)

1 (Dr. Charles Miller)

1 (Dr. T. H. Schiffman)

1 Massachusetts Institute of Technology, Dept of Civil and Sanitary
Engineering, ATTN: Dr. Robert V. Whitman, 77 Massachusetts
Ave, Cambridge 39, Mass

1 Massachusetts Institute of Technology, Lincoln Laboratory
Document Library, P. O. Box 73, Lexington, Mass 02173

1 University of Notre Dame, Dept of Civil Engineering, ATTN: Dr.
Harry Saxe, Notre Dame, Ind

1 Purdue University, Civil Engineering Dept, ATTN: Prof. G. A.
Leonards, Lafayette, Ind

1 Lockheed Missiles and Space Co., Technical Information Center,
ATTN: W. A. Kozumplik, 3251 Hanover St, Palo Alto, Calif

1 Livermore Radiation Laboratory, Plowshare Div, L 43, ATTN:
Capt Lewis Cauthen, P. O. Box 808, Livermore, Calif

1 The Boeing Co., ATTN: Mr. Ror Carleson, Suite 802, First
National Bank Bldg, Albuquerque, New Mexico

DISTRIBUTION (cont'd)

No. cys

- 1 St Louis University, Institute of Technology, ATTN: Dr. Carl Kisslinger, 3621 Olive St, St Louis 8, Mo
- 1 University of Michigan, Dept of Civil Engineering, ATTN: Mr. Frank E. Richardt, Ann Arbor, Mich
- 1 University of California, College of Engineering, ATTN: Prof. Martin Duke, Los Angeles, Calif
- 1 University of Washington, ATTN: Dr. I. M. Fyfe, Seattle 5, Wash
- 1 Massachusetts Institute of Technology, ATTN: Prof J. P. DenHartog, Cambridge 39, Mass
- 1 Westinghouse Research Laboratory, ATTN: Dr. E. G. Fischer, Pittsburgh, Pa
- 1 Pennsylvania State University, ATTN: Dr. Snowden, State College, Pa
- 1 Sandia Corporation, Underground Physics Div, ATTN: Mr. Luke J. Vortman, Sandia Base, NM 87115
- 1 National Academy of Sciences, Advisory Committee on Civil Defense, ATTN: Mr. Richard Parks, 2101 Constitution Ave NW, Wash, DC 20418
- 1 Mechanics Research, Inc., ATTN: Dr. Robert H. Anderson, 540 Aero Space Center, 650 N. Sepulveda Blvd, El Segundo, Calif
- 1 Official Record Copy (Lt J. F. Flory, WLRC)